

**UCLA**

**UCLA Electronic Theses and Dissertations**

**Title**

Phase-Amplitude Cross-Frequency Coupling in the Globus Pallidus Internus and Motor Cortex of Patients with Parkinson's Disease

**Permalink**

<https://escholarship.org/uc/item/57c538sn>

**Author**

Tsiokos, Christos

**Publication Date**

2013

Peer reviewed|Thesis/dissertation

UNIVERSITY OF CALIFORNIA

Los Angeles

Phase-Amplitude Cross-Frequency Coupling in the Globus Pallidus Internus and Motor Cortex  
of Patients with Parkinson's Disease

A dissertation submitted in partial satisfaction of the requirements for the degree Doctor of  
Philosophy in Biomedical Engineering

by

Christos Tsiokos

2013

© Copyright by

Christos Tsiokos

2013

## ABSTRACT OF THE DISSERTATION

Phase-Amplitude Cross-Frequency Coupling in the Globus Pallidus Internus and Motor Cortex  
of Patients with Parkinson's Disease

by

Christos Tsiokos

Doctor of Philosophy in Biomedical Engineering

University of California, Los Angeles, 2013

Professor Nader Pouratian, Chair

Different models of the cortico-basal ganglia thalamocortical circuit are currently in existence, pointing to an incomplete understanding of those nuclei. Decades long research efforts have established the presence of oscillations in the basal ganglia and their link to functional and pathological states. More recently, hierarchical relations between those oscillations have also been shown to be functionally relevant. Phase-amplitude cross frequency coupling (PACFC), in particular, has been shown to exist within and between the human subthalamic nucleus (STN) and motor areas of the cortex. In our study we report high levels of PACFC in the human GPi of patients with Parkinson's disease (PD) and show its high correlation to local spectral power as well as coherence across GPi and motor cortex. Cross-site bidirectional PACFC was also shown to exist between the two sites in a small number of subjects. Contralateral finger movement seemed to significantly decrease coupling only in some subjects, possibly manifesting a deficiency in the

diseased BG. The angle of modulation was about 28% the period of the slow oscillation and one subject had unusually high coupling (z-score = 148). The coupling was the strongest for the beta-gamma band pair, while there were also beta – (200-300 Hz) and theta – beta coupling to a lesser extent in a subset of subjects. The findings mark advances in our understanding of a nucleus that has received little attention compared to the STN, as well as its relation to the motor cortex.

The dissertation of Christos Tsiokos is approved.

Tetsuya Iwasaki

Dejan Markovic

Xiao Hu

Nader Pouratian, Committee Chair

University of California, Los Angeles

2013

To Mrs. Chrisoula Tsiokou, Mr. Michael Tsiokos, Ms. Aleksandra Mstowska, all the patients who volunteered for our experiments, and all others who helped me, I sincerely dedicate this work.

Christos Tsiokos

# Table of contents

Table of contents.....	vi
List of figures.....	vii
List of tables.....	viii
1. Motivation and goals.....	1
1.1 Overview.....	1
1.2. Association between oscillations in the basal ganglia and PD.....	3
1.3. Current treatments for PD .....	3
1.4. Relation of phase-amplitude cross-frequency coupling to disease .....	5
2. Experimental design.....	8
2.1. Overview.....	8
2.2. 200-300 Hz oscillations in the GPi .....	10
2.3. PACFC in GPi and motor cortex .....	18
3. Experimental outcome .....	27
3.1. 200-300 Hz oscillations in the GPi .....	27
3.2. PACFC in GPi and motor cortex .....	37
4. Discussion.....	54
4.1. 200 – 300 Hz oscillations in the GPi.....	54
4.2. PACFC in GPi and motor cortex .....	58
5. Future directions .....	64
5.1. GPi features in a broader context of tasks and brain nuclei.....	64
5.2 Basal ganglia modeling for closed-loop DBS.....	65
5.3 Incorporating PACFC into closed-loop DBS.....	67
6. Conclusion .....	70
7. Appendices.....	72
7.1 PACFC algorithm .....	72
7.2 PACFC algorithm implementation .....	82
5.2. PACFC grid features.....	93
7.3. Windowed spectra and signal power .....	95
7.4. Time-frequency representation in real time .....	105
7.5. Ring buffer optimized for read operations.....	113



8. Bibliography.....	116
----------------------	-----

## List of figures

Figure 1. ....	2
Figure 2. ....	8
Figure 3. ....	8
Figure 4. ....	13
Figure 5. ....	16
Figure 6. ....	27
Figure 7. ....	31
Figure 8. ....	32
Figure 9. ....	33
Figure 10. ....	34
Figure 11. ....	35
Figure 12. ....	36
Figure 13. ....	39
Figure 14. ....	40
Figure 15. ....	41
Figure 16. ....	43
Figure 17. ....	45
Figure 18. ....	46
Figure 19. ....	48
Figure 20. ....	49
Figure 21. ....	50
Figure 22. ....	52
Figure 23. ....	76
Figure 24. ....	77
Figure 25. ....	81
Figure 26. ....	105
Figure 27. ....	106
Figure 28. ....	113
Figure 29. ....	115
Figure 30. ....	115

## List of tables

Table 1. ....	10
Table 2. ....	12
Table 3. ....	45

## Acknowledgments

I would like to thank Dr. Pamela Hurley and Dr. Linda L. McCabe for their guidance and support during my studies at UCLA. I am also grateful to the graduate division for awarding me with the dissertation year fellowship. This work would not have been made possible without the patients' consent and Dr. Pouratian's surgical team. Dr. Pouratian's role in this work must be distinguished as it was central to the reported discoveries and the associated advance in the field of neurophysiology. I also acknowledge all members of the committee for their advice and evaluation at various stages of the dissertation.

## Vita

2007            B.S. Electrical and Computer Engineering  
2007            B.S. Biochemistry and Molecular Biology  
2012            M.S. Biomedical Engineering

## Publications and Presentations

A. O. Hebb, J. J. Zhang, M. H. Mahoor, C. Tsiokos, C. Matlack, H.J Chizeck, N. Pouratian. Creating the feedback loop: Closed Loop Neurostimulation. Neurosurgery Clinics of North America. Advances in Neuromodulation: From Periphery to Brain (2013).

C. Tsiokos, X. Hu, N. Pouratian. 200-300 Hz movement modulated oscillations in the internal globus pallidus of patients with Parkinson's Disease. Neurobiology of Disease 54 (2013) 464-474.

C. Tsiokos. LFPs in the GPi of PD patients contain increased high frequency (200-300 Hz) power. American Association of Neurological Surgeons, Annual Scientific Meeting April 14-18, (2012)

C. Tsiokos, X. Hu, N. Pouratian. Biomarkers for use in closed-loop deep brain stimulation for Parkinson's disease. UCLA Henry Samueli School of Engineering and Applied Science Tech Forum (2012).

A. O. Fung, C. Tsiokos, O. Paydar, L. H. Chen, S. Jin, Y. Wang, J. W. Judy. Electrochemical Properties and Myocyte Interaction of Carbon Nanotube Microelectrodes. Nano Letters (2010), 10(11), pp 4321-4327

# 1. Motivation and goals

## 1.1 Overview

Parkinson's disease (PD) is a neurodegenerative disease that affects about 7-10 million people worldwide and one million Americans (Parkinson's disease Foundation, 2012). Cardinal signs of PD are motor deficits (rest tremor, rigidity and bradykinesia) as well as cognitive and emotional impairments (Rivlin-Etzion, M., et al. 2006). Treatment for PD is typically accomplished through administration of levodopa, a dopamine derivative, or deep brain stimulation (DBS) of basal ganglia (BG) nuclei for advanced or drug resistant PD. Despite the relative effectiveness of these treatments an incomplete understanding of how the BG function, imposes considerable limits on further improvements. The focus of our research was to shed more light on dynamic electrophysiologic relationships within the BG in order to pave the way for future studies that will adopt a relatively new paradigm, closed-loop DBS. In particular, we tested the hypothesis that certain electrophysiological biomarkers can be observed in an output nucleus of the BG, the Globus Pallidus Internus (GPi) and the motor cortex, that are relevant to the pathophysiology of PD. These biomarkers could have utility in future studies toward the development of a DBS system with feedback control. Our findings indicated that oscillations in at least two spectral bands are present in the GPi of patients with PD. We also identified phase-amplitude cross-frequency coupling (PACFC), the amplitude modulation of fast oscillations by the phase of slower ones, both within the GPi and between GPi and motor cortex. The changes in the spectrum and the coupling among different oscillations are likely to encode information about the functional state of the BG. Applying them in the largely unexplored field of closed-loop DBS

systems presents an opportunity for groundbreaking work that redefines how PD patients receive treatment so that it is more effective and decreases their dependence on frequent calibrations.

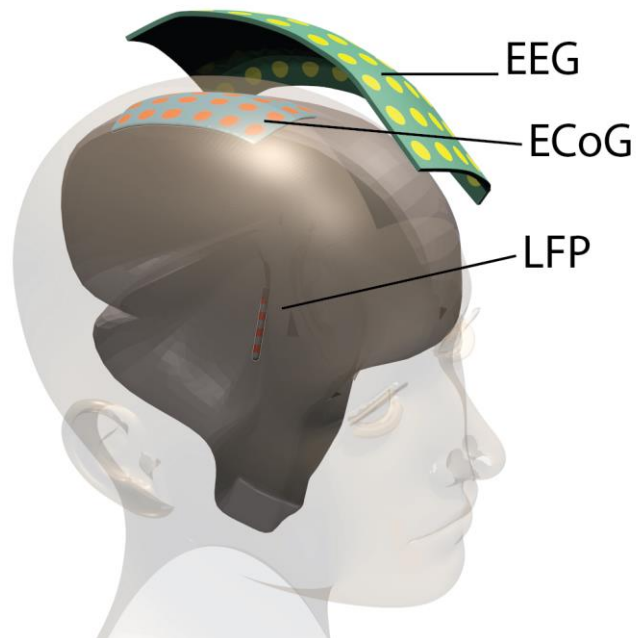


Figure 1.

Three types of electrodes used in neuro-electrophysiological studies of aggregate activity of neuronal populations. Electroencephalography (EEG) is non-invasive as an electrode grid is overlaid over the skin. The signal 's resolution is poor compared to the other methods, as there is a greater distance between electrodes and the signal source (cortex) and the dura and skull act as low pass filters putting an upper limit in the observable range of spectral power to about 150 Hz. Electrocorticography (ECoG) is performed with subdural electrode grids and provides superior resolution and a smaller signal to noise ratio. In our study we used an 8-electrode strip approximately centered over the motor cortex. Local field potentials (LFPs) sometimes are used synonymously with EEG and ECoG signals. However, here we denote as LFPs the signals acquired from deep brain nuclei using a lead that usually has four macro-electrodes. In our study such a lead was placed at the GPi of patients with PD for therapeutic deep brain stimulation and when informed consent was provided the lead was used for an intra-operative recording during a 10-20 minute period. This recording was concurrent with the the ECoG recording allowing us to examine the coherence and cross-frequency coupling across between the GPi and motor cortex.

## 1.2. Association between oscillations in the basal ganglia and PD

The progressive impairment of motor skills due to dopamine depletion in the BG is one of the most prominent pathological symptoms of PD. At an advanced stage or in drug-resistant types of PD, DBS of BG nuclei such as the GPi or Subthalamic Nucleus (STN) can provide some alleviation. These nuclei have been found to contain abnormal oscillatory activity due to synchronized firing of neuronal populations (Brown, P. 2007, Giannicola, G. et al. 2010).

In humans, the synchronization seems to occur mostly in the beta band (13-30Hz), which is higher during PD symptoms and lower with the administration of levodopa (Brown, P. 2001), signifying an association between oscillatory activity and the pathology of PD. It has been suggested that the neuronal synchronization blocks the normal function of the BG by not allowing information to be processed or transmitted effectively in the motor control networks. Additionally, recent findings suggest that cross-frequency coupling has been observed in the STN during the pathological state of a patient with PD (López-Azcárate, J. et al. 2010).

## 1.3. Current treatments for PD

Open-loop DBS has been successfully used to ameliorate symptoms of PD patients since 1997 (Benabid, A. L. 2003). The success of this method has its roots on experimentation rather than the understanding of the cortico-basal ganglia circuits in such a depth that would have allowed reverse engineering their mechanisms to replicate them artificially through high frequency stimulation. A variety of models of how DBS brings about a beneficial outcome and models of basal ganglia functionality are currently being debated (Leblois, A. et al. 2006; Bernsz, S.,

Sejnowskil, TJ 2010; Da Cunha, et al. 2009; Ryan, L.J. 2000; Gillies, A. Willshaw, D. 2004; Bergman, H. 1998; Sridharan, D. 2006).

As a result of dopaminergic depletion, the afflicted basal ganglia are characterized by radical changes at the single neuron level as well as the systems level. Neuronal firing patterns change significantly in animal models of PD (Cruz, A.V. et al. 2009). In the internal part of the human globus pallidus neuronal activity has been found to be synchronized to local field potentials in patients with dystonia (Chen, C.C, et al. 2006), while in patients with PD neurons with 4-6 Hz tremor frequency activity have been identified (Hutchison, E.D. et al. 1996). The oscillatory activity observed in LFPs is believed to stem from the altered firing patterns of neuronal ensembles and seems to be exaggerated in motor disorders of the basal ganglia.

A hypothesis is that DBS can alleviate PD symptoms by imposing a different oscillation to the network and reducing the effect of the harmful oscillations (Brown P. 2004). Similarly, the coupling of frequencies in the STN or GPi might be affected, and perhaps abolished, by DBS. The DBS electrode contacts are driven by a pulse generator that delivers a high frequency pulse (120-200Hz) which diffuses through a volume of tissue and causes the membrane potential of cells to oscillate. The collective and widespread changes in the affected neuronal population turn out to be beneficial to the patient in most cases, although the reasons have yet to be discovered.

Neurosurgical lesioning or high frequency stimulation of the GPi or STN yields a somewhat surprising amelioration of disease symptoms. The effectiveness of those methods without utilizing any information about the system they are affecting gives rise to the notion of a robust neuronal network able to retain partial functionality in the absence of sufficient dopaminergic innervation. An optimistic view is that the present therapeutic methods are not restoring basal ganglia functionality to the full extent they can attain for PD patients due to the



static approach of those interventions in an inherently dynamic system. It is therefore compelling to seek a treatment that could make the most out of the “surviving” functionality in the BG.

A less optimistic view is that the true extent of damage to the basal ganglia is attributed to irreversible loss of neuronal circuitry that is involved in highly specialized information processing such as one necessary to represent sequences of actions. In that case, restoring the rhythms needed for integration of processing in a dynamic fashion might not present an advantage compared to current open-loop DBS methods, since the components of the neuronal network would continue generating faulty outputs and to comprise the primary cause of the symptoms.

## 1.4. Relation of phase-amplitude cross-frequency coupling to disease

Given the perceived physiological role of BG oscillations, it is proposed that disruptions to normal oscillatory activity may be a biomarker of disease, whose understanding could lead to better treatment of movement disorders such as Parkinson’s disease (PD) and dystonia. Chronic dopaminergic depletion in the BG is associated with a pronounced amplification of beta power in the LFPs from the motor system (N. Mallet, et al. 2008, A. Cruz 2009), while oscillations in the gamma range which are usually present during normal execution of movement are attenuated in the subthalamic nucleus (STN) (Foffani, et al. 2005). These gamma oscillations are enhanced in the cortico-basal ganglia thalamo-cortical circuit after restoration of dopaminergic activity (P. Brown 2003). Observations from single neuron recordings (J Soares, et al. 2004, P Gatev, T Wichmann, 2008) suggest the abnormal LFP synchronization reflects abnormal neuron firing patterns, with altered bursting activity, firing rate and concurrency (R Levy, et al. 2002) among neighboring and distant neurons.

While earlier work has often focused on studying individual bands of activity, there is increasing interest in how oscillations in distinct bands relate to each other through non-linear interactions. In particular, the phase of slower oscillations in the theta, alpha, and beta band modulate the amplitude of faster rhythms in the beta, gamma and very high gamma ranges (R. Canolty, et al. 2006, A. Tort 2008, J. Lopez-Azcarate, et al. 2010). This phenomenon, called phase-amplitude cross frequency coupling (PACFC) is thought to be intimately related to the pathophysiology of disease not only because coupling is seen between frequency ranges implicated in the pathophysiology of PD, but also because coupling patterns change with pathological state. Specifically, therapeutic STN stimulation reduces the magnitude of coupling between beta-phase and gamma-amplitude (C. de Hemptinne, et al. 2013). The same study showed that PACFC in the motor cortex was exaggerated in PD patients compared to patients with epilepsy who did not have a movement disorder. In a separate study it was shown that in the STN of patients with PD, PACFC between the beta band and very high gamma oscillations at around 300Hz is significantly reduced with dopaminergic medication (J. Lopez-Azcarate, et al. 2010).

Taken together, these findings favor the view that PACFC plays an important role as a mechanism for information processing in the motor network. A literature review, however, reveals that analysis of PACFC in the BG is sparse compared to more traditional methods such as measuring spectral power and coherence. In this manuscript, we present previously undocumented PACFC in the human GPi, the major output nucleus of the basal ganglia. PACFC was identified between three distinct band pairs: beta-gamma, beta – very high gamma (200 – 300 Hz) and theta – beta. In addition, our results point to coupling being very strong in the GPi, with one subject showing a magnitude (z-score = 148) not previously reported in studies using similar algorithms.

In addition, PACFC was found to be highly correlated with coherence between the motor cortex and GPi, and was observed across those two structures, suggesting it may be a key mechanism of information integration across the entire cortico-basal ganglia loop. Our findings complement prior analyses in the STN, a nucleus that has historically been more accessible and evaluated.

## 2. Experimental design

### 2.1. Overview

The present study aimed to build on existing knowledge about the BG networks and their role in PD by leveraging the advent of recently reported electrophysiological signatures and recordings from the human GPi, as opposed to the STN, a more typical target for DBS.

The same electrodes used for stimulation can also be used for recording of local field potentials (LFPs) [5] which correspond to the aggregate firing of neuronal populations. Upon examination of spectra in time-frequency plots we have observed a new feature, a significantly increased high-frequency (200-300Hz) oscillation in the GPi (Figure 2). Similar activity has been reported in the STN with the administration of dopamine (Foffani, G. et al. 2003). Since our recordings came from patients who had not been administered dopamine the night before surgery, the high-frequency band might play a different functional role in the GPi compared to the STN.

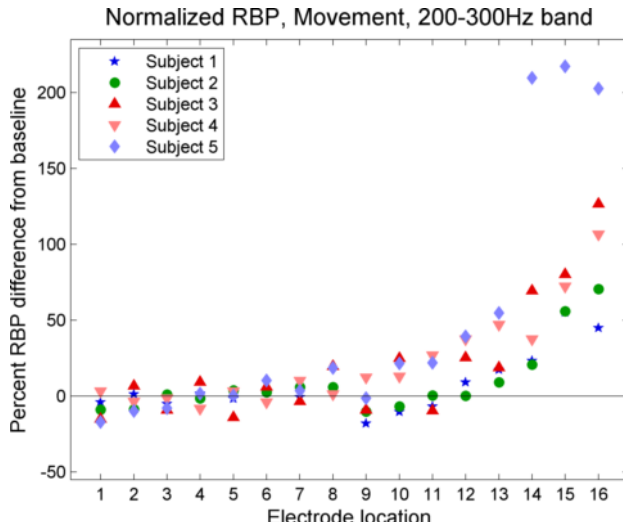


Figure 2.

The relative band power (RBP) of 200-300Hz is increased at GPi locations (~ 15-16) compared to more distant locations.

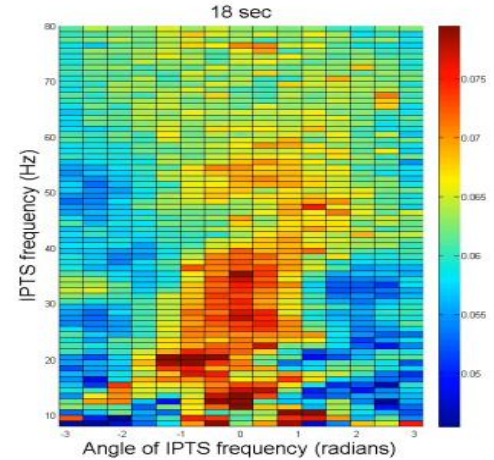


Figure 3.

The time series of the instantaneous phase (IPTS) of beta and low gamma band oscillations has a phase that modulates the amplitude of a 200Hz component. At 0 radians that amplitude has a maximum while it is minimum at around  $\pi$  radians. The effect is called CFC.

To focus on a more detailed aspect of the generally accepted high oscillatory activity in PD patients we also examined the extent of phase-to-amplitude cross-frequency coupling (CFC) (Figure 3). This feature has been detected across several areas of the central nervous system such as the human neocortex, and STN. It reports the extent of amplitude modulation of fast oscillations by the phase of slower oscillations. Preliminary findings indicated that CFC takes place in the GPi of PD patients in a highly dynamic manner. Also, although CFC has been explored extensively within structures, to date, only one report (de Hemptinne, et al. 2013) has examined CFC between structurally connected tissues. Our unique data set enabled us to explore the coupling of electrophysiological activity between the GP and motor cortex to uncover additional pathophysiological biomarkers of disease. Since activity in the basal ganglia has been found to be coherent with neurons in the sensory-motor cortex we also examined CFC between the GPi and cortex.

In addition to the spectral and CFC analysis we looked at the coherence between oscillations in the GPi and the motor cortex to obtain information on the activity of a well-established anatomical network, the cortex – BG – thalamus – cortex loop. Finally, we looked at correlations between PACFC and coherence and PACFC and power.

## 2.2. 200-300 Hz oscillations in the GPi

### 2.2.1. Subjects

Seven subjects (table 1) with PD symptoms undergoing DBS implantation on the right GPi participated in the study after having provided informed consent approved by the internal review board at the University of California, Los Angeles.

Table 1. Subjects in this study. Subjects 1 and 6 could not be present for Off UPDRS because they were severely affected by symptoms. Subject 4 could not be tested for On UPDRS due to intolerance to medication.

<b>Subject</b>	<b>Age</b>	<b>Sex</b>	<b>MDS-UPDRS PIII, Off/On</b>	<b>Disease duration (years)</b>
1	62	F	52/27	25
2	69	F	33/9	12
3	64	M	NA/21	12
4	60	M	30/NA	10
5	40	M	56/42	5
6	71	M	NA/23	13
7	72	M	46/9	15

### 2.2.2. Recording procedures

LFP recordings from the last 24mm of the DBS lead trajectory of implantation, which included the GPi, were obtained from the lead's four ring electrode contacts (Medtronic, Model 3387, length 1.5mm, inter-contact distance 1.5mm). Signal acquisition was performed using BCI2000 v6.2 through a connection of the DBS lead to an amplifier (g.Tec, g.USBamp 2.0). The recording was performed at a sampling rate of 2400 Hz and online high-pass filtering above 0.1

Hz. Concurrent recordings from a data glove (5DT data glove 5 Ultra) worn by the patient on the hand contralateral to the DBS lead were obtained at a slower effective sampling rate, which was oversampled at 2400 Hz by BCI2000 using stair step interpolation. Scalp ground and reference were used. Amplifier potential equalization was provided by an ECG lead attached to each patient's left shoulder.

Once target coordinates were determined based on standard clinical methods, including indirect and direct (image-guided) targeting, microelectrode recordings, and intraoperative fluoroscopy, the DBS lead was advanced to target (average distance anterior to mid-commissural point: 19.82mm, and interior to AC-PC plane: 4.61 mm) in four incremental steps, beginning initially at a point 13.5 mm from target with subsequent advances as illustrated in Figure 4. This provided LFP recordings from a 24 mm span of the trajectory with non-overlapping interleaving recordings. At each position, signals were recorded during 60 seconds of rest and 60 seconds of self-paced contralateral hand movement (hand opening and closing, Table 2). Thirty to 60 seconds was allowed between each recording position to allow advancing of the electrode. In each case, the electrode was advanced using the Alpha Omega microdrive system.

Table 2. Intra-operative recording protocol. Rest (R1, R2, R3, R4), movement (M1, M2, M3, M4), and lead location transition (T1, T2, T3) phases were alternated in order to obtain recordings for 16 locations evenly spread along a 24mm trajectory ending at the GPi.

<b>Phase</b>	<b>Duration</b>	<b>DBS location</b>	<b>Hand movement</b>
R1	60 sec	1, 3, 5, 7	no
M1	60 sec	1, 3, 5, 7	yes
T1	60 sec	(transition)	-
R2	60 sec	2, 4, 6, 8	no
M2	60 sec	2, 4, 6, 8	yes
T2	60 sec	(transition)	-
R3	60 sec	9, 11, 13, 15	no
M3	60 sec	9, 11, 13, 15	yes
T3	60 sec	(transition)	-
R4	60 sec	10, 12, 14, 16	no
M4	60 sec	10, 12, 14, 16	yes



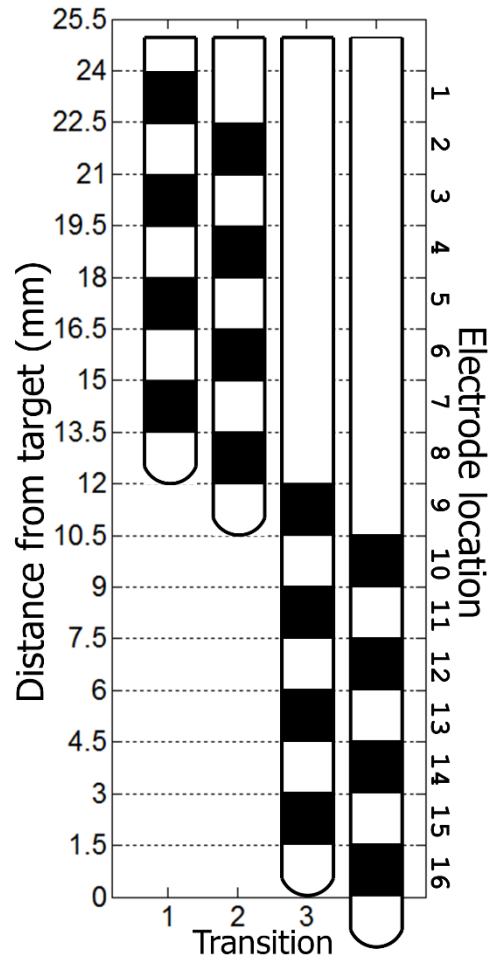


Figure 2.

Advancement of DBS lead to target. The lead was advanced four times such that its most distal electrode contact was 13.5 mm, 12 mm, 1.5 mm and 0 mm away from target. This protocol ensured recordings took place in every part of the last 2.4 cm along the path used to implant the lead. The most dorsal location was named location 1, while the most ventral location 16. Locations 15 and 16 were considered to be in the GPi, the target nucleus for stimulation.

### 2.2.3. *Signal pre-processing*

All computational procedures were performed in Matlab v.7.10.0 ([www.mathworks.com](http://www.mathworks.com)). The original monopolar signal recordings (MON) were re-referenced offline to generate the equivalent time series for a bipolar (BIP) and a common average referenced (CAR) configuration. Bipolar signals were generated by subtracting signals from adjacent pairs of contacts at each recording position. For CAR, the common average reference of all four electrodes at each recording position was subtracted from the recordings of each contact in that recording position. Because noise characteristics were different among the three configurations, procedures to remove noise were separate.

In the MON configuration data was filtered using a 2 Hz high pass Chebyshev II filter (filter order  $n=18$ ) implemented as a second order sections direct form II structure using double precision arithmetic. The signals were then notch filtered at 60 Hz (Butterworth,  $n=8$ , quality factor  $Q = 50$ ) in order to remove line noise. The phase of the oscillations in the processed signals was preserved (zero-phase filtering) by filtering first in a forward fashion and then in the reverse direction (Gustafsson, 1996). Periods during which the power spectra had abnormally high values and a pattern with excessive presence of harmonics, accompanied by a time series with high rates of voltage change measured by the first derivative, were spliced out from the signal and not included in the analysis (26, 2, 4.8, 6, 3.3, 38.7 and 0 sec. total duration in the 1<sup>st</sup>-7<sup>th</sup> subject respectively during ~480 sec. of rest and movement recordings per subject). In addition, sudden DC shifts in the signal of the 1<sup>st</sup> and 7<sup>th</sup> subject possibly caused by internal adjustments of the amplifier were also spliced out with almost negligible amount of signal loss, in the range of 3-32 msec. per DC shift. All splicing was done in an automated manner and subsequently inspected to ensure proper removal of segments with high signal-to-noise ratio. For subject 6, recordings at target were free of artifacts, whereas several locations proximal to it had significant signal

contamination. Therefore, only a 23 second recording was considered to extract baseline activity in the metric Relative Band Power mentioned later and the analysis for that subject was limited to only the MON and CAR configurations.

Signals from the CAR and BIP configurations, were filtered as in MON. Re-referencing removed the seconds-long spectral perturbations (except for the 6<sup>th</sup> subject) seen in MON. Any sudden DC shifts were spliced out while keeping the signal loss minimal (CAR: 160, 26 msec. for 1<sup>st</sup> and 5<sup>th</sup> subjects respectively; BIP: 245, 125, 67 msec. for the 1st, 3rd and 5th subjects respectively).

#### *2.2.4 Data analysis*

**Peak extraction.** Besides block design, to ensure proper differentiation of rest vs. movement, movement phases were confirmed based on signals generated from the data glove. The signals were remapped with respect to location and phase type: rest (R), movement (M), and transition (T) (Table 2, Figure 5). Location 1 was designated as the most dorsal (furthest from target), while location 16 or 12 (BIP) as the target site.

For each time segment we obtained the power spectral density using the multitaper method implemented in Matlab signal processing toolbox (time-bandwidth product  $NW = 9$ , number of leading tapers  $K = 17$ ) and time-frequency representations (TFR) using both a custom Matlab script ( $NW = 6$ ,  $K = 11$ , moving window size = 6 sec. and step = 6 sec.) and the chronux toolbox (v.2.00) ( $NW = 3$ ,  $K = 5$ , moving window size = 6 sec. and step = 0.5 sec). The range of frequencies for all spectral estimates was 2-1000 Hz and all the resulting data was log transformed.

To extract peak parameters in the 200-300Hz range we used the curve fitting toolbox from Matlab. We first fitted a power law in each spectrum using only the ranges 55-130 Hz and 400-700 Hz (Figure 5A) to reduce the effect of spectral peaks on the model, and then subtracted the

fitted curve from the spectrum. A Gaussian curve was then fitted (nonlinear least squares with bisquare robust method, Figure 5B) to the part of the resulting data that corresponded to the 100-350 Hz range. All fitting was verified individually and in cases where a clear peak was not obvious, the fitted curve height was set to zero and the center frequency and bandwidth were ignored. In those cases the height was small and the bandwidth large, reflecting the mismatch between the power law and the actual data rather than an underlying peak.

To observe the evolution of peak parameter values from the rest to the movement condition we obtained TFRs with finer time resolution ( $NW = 2$ ,  $K = 3$ , moving window size = 1 sec. and step = 0.1 sec.). From those, we calculated the average band power in a frequency range with center and bandwidth that was obtained as an average of the centers and bandwidths between rest and movement. The band power was then plotted against time.

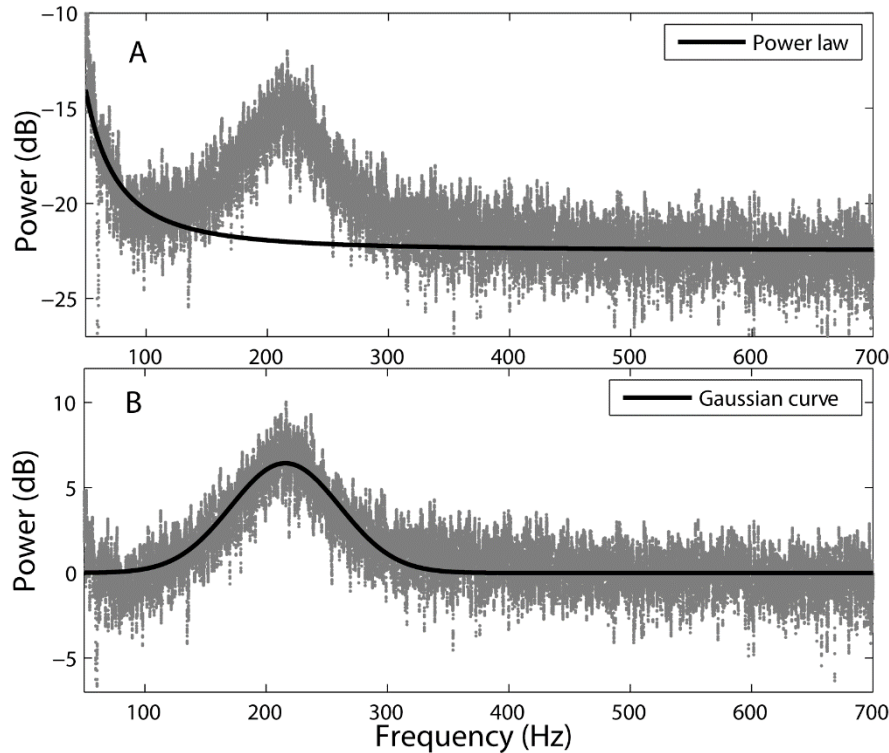


Figure 3.

Peak extraction at 200-300 Hz. (A) The power law (black) was fitted to spectra (subject 2, location 15, CAR) in frequencies that had minimal or no spectral peaks (55-130 Hz and 400-700 Hz). (B) A Gaussian curve (black) was fitted to spectra (100-350 Hz) from which the power law had been subtracted (gray).

**Relative Band Power.** Because increases in  $\beta$  power could not be described by Gaussian peaks accurately, we measured activity in low  $\beta$  (12-20 Hz) and high  $\beta$  (20-35 Hz) using the summary statistic Relative Band Power ( $RBP_{low\_beta}$ ,  $RBP_{high\_beta}$ ), calculated as a log-transformed average band power normalized with respect to the 600-1000Hz band, which served as a reference because it followed the power law and did not show significant peaks in any part of the recordings (equation 1). This method is similar to that previously described by Foffani, et al. (2006).

$$RBP = 10 \log_{10} ((a+b)/b) \quad (1)$$

In (1),  $a$  is the mean power of the band of interest and  $b$  is the mean power of the reference band (600-1000Hz). We also measured this statistic for the 200-300 Hz band,  $RBP_{200-300Hz}$ , in addition to the peak analysis in order to verify our results. This statistic was reported as a percent difference from baseline, with baseline defined as the average RBP from the most proximal locations (1-8 for MON and CAR; 1-6 for BIP).

**Statistical analysis.** The analysis involved an inter-subject design from which we could make inferences about the underlying population, as well as an intra-subject design in which the results were relevant to each subject. Because not all the selected statistics had normal distributions and the sample sizes were relatively small ( $n=7$  for inter-subject,  $n \sim 10$  for intra-subject), we used only non-parametric tests (one-sided, single or paired sample, Wilcoxon signed rank test) for all three configurations: MON, CAR and BIP.

In the inter-subject design we tested the null hypotheses that peak height in the 200-300 Hz band is greater than zero at the GPi of patients with PD, and that the peak height increases and the bandwidth decreases during movement. We also tested the null hypothesis that the center

frequency differs between rest and movement using paired-sample tests. In the intra-subject design, we considered 6 second non-overlapping windows for the ~60 second rest and movement phases to test the same null hypotheses. Moreover, we tested the hypothesis that there is increased low  $\beta$  (12-20Hz) and high  $\beta$  (20-35Hz) band activity at and near the GPi compared to recordings made outside of the GPi target region.

## 2.3. PACFC in GPi and motor cortex

### 2.3.1) *Subjects*

Ten subjects with PD symptoms undergoing unilateral (subjects 1, 2, 3, 4, 5, 7) and bilateral (9, 10, 11) DBS implantation participated in the study. All subjects provided informed consent approved by the institutional review board at the University of California, Los Angeles.

### 2.3.2) *Recording procedures*

LFP recordings in the GPi were obtained for all subjects from the lead's four ring electrode contacts (Medtronic, Model 3387, length 1.5mm, inter-contact distance 1.5mm) at their target coordinates for therapeutic stimulation. Data from additional locations along the last 24mm of the DBS lead trajectory were also obtained for subjects 1-5 and 7 (Christos Tsiokos, et al. 2013, Figure 1).

Unilateral LFP recordings in the Motor Cortex of the right hemisphere were obtained using a subdural electrocorticographic strip with eight contacts, for all subjects except 2 and 9. The strip was positioned such that the contacts in the middle had a higher chance of covering the area that responds to finger movement. Signal acquisition was performed using BCI2000 v2 or v3 connected to an amplifier (g.Tec, g.USBamp 2.0). The sampling rate was 2400 Hz with a 0.1Hz-1000Hz band pass filter.

A data glove (5DT data glove 5 Ultra) worn by the patient on the hand contralateral to the Ecog strip provided concurrent recordings at a slower effective sampling rate which was oversampled at 2400 Hz by BCI2000 using stair step interpolation. For subjects 9, 10 and 11 ipsilateral finger movements were also performed. Because for those subjects bilateral GPi recordings were obtained, right hand movements were contralateral to the left GPi. A ground and reference connection to the scalp were used. In addition an amplifier potential equalization ECG lead was attached to the patient's left shoulder. A description of how the target coordinates for the GPi lead implantation were obtained is provided elsewhere (Christos Tsiokos, et al. 2013).

### *2.3.3) Time series pre-processing*

Recorded signals were pre-processed in order to exclude time segments with artefacts as described previously (Christos Tsiokos, et al. 2013). Those primarily featured power spectra with abnormally high values, excessive harmonics and time series with high rates of voltage change. All time epochs with artefact in any contact were removed prior to analysis. Only a monopolar (MON) electrode configuration and bipolar montage (BIP) were considered.

#### *2.3.4) Spectral analysis and coherence*

The spectral analysis performed on the LFPs from the GPi and motor cortex has a dual purpose: 1) the discovery of sites in the motor cortex with movement related spectral power changes, 2) to ascertain the presence of oscillations in the frequency ranges examined in the PACFC analysis.

Spectra were obtained from each subject by applying six second, non-overlapping windows in time series corresponding to either the rest or movement condition. In each experimental block, which lasted about 60 seconds, the signals were normalized such that their mean was equal to zero and standard deviation to one. We used the multitapering method ( $NW = 4$ ) in each window, as well as Welch's periodogram (2048 samples per window with 50% overlap) in order to verify the results. The average band power for the theta (4 – 8 Hz), alpha (8-12 Hz), low beta (12 – 20 Hz), high beta (20 – 35 Hz), low gamma (35 – 80 Hz), high gamma (80 – 150 Hz), and very high gamma (150 – 300 Hz), were calculated for each window. These values were used to estimate the standard deviation around the average band power for rest and for movement, as well as to examine the temporal correlation between fluctuations in power and other metrics such as PACFC. In the case of motor cortex LFPs they were used to find the electrode contacts that showed the greatest movement-related changes in spectral power. In general, beta band was chosen to determine the movement-responsive-sites (MRSs) because it was the most consistent among subjects. While gamma band changes were seen, given the very focal nature of gamma band activations and the fact that strip electrodes were used for this analysis, movement-related changes in gamma spectral power were not consistently observed across all subjects. A third metric for estimating band power was obtained as the mean squared amplitudes of the time series obtained after filtering the signals through a band pass filter (filter order = 8, Chebyshev I, second order section, direct form II)



keeping only frequencies in the corresponding range. Noise in harmonics of the 60 Hz line noise that had not been removed previously was rejected using a notch filter (filter order = 6, Quality factor = 60, Butterworth, second-order sections, direct form II). For each subject, the MRS was chosen to be the contact with maximum beta band power suppression. The three metrics we described led to the same selection of contacts almost invariably. A requirement was that the reduction in beta band power was significant using a non-parametric test (Kolmogorov's two-sample one-sided).

The magnitude squared coherence was obtained for the range of frequencies 0 – 350 Hz and is henceforth referred to simply as coherence. It was calculated for entire experimental blocks (~60 seconds) as well as by windowing. The window length and step were the same as for PACFC, and the signals were first truncated by 2 percent at the beginning and end of the series, as was done for PACFC, thereby aligning PACFC windows with those of coherence.

To find the correlation between GPi PACFC and GPi – motor cortex coherence, from the candidate locations in the GPi (10-12 in BIP), the one with the greatest magnitude PACFC was selected. Time series of power in all bands of interest were extracted from those same locations, while for coherence the motor cortex sites with the highest coherence values (which were also at or near MRSs) in the high-beta band were used.

### *2.3.5) Phase-to-amplitude cross-frequency coupling*

The method used to extract phase-to-amplitude cross frequency coupling is based on the Kullback-Liebler based modulation index described previously (Canolty, et al. 2010, Tort, et al. 2010). In summary, two frequency components were extracted through IIR zero-phase filtering

(without phase distortion) (Gustafsson, 1996) from one or two LFP signals, with the later suitable for examining PACFC across structures. The instantaneous phase time series (IPS) of one component, and the instantaneous amplitude time series (IAS) of the other component were obtained through a Hilbert transformation that provides the analytic signal. IPS was always chosen to have a lower frequency than IAS. IPS values ranged from  $-\pi$  to  $\pi$  and were allocated into 16 bins of equal width along that range. For each bin the corresponding (concurrent) IAS values were obtained and the mean bin value was calculated. All values were normalized such that their sum was equal to one. That way the mean values of the 16 bins could be viewed as a distribution. Then, they were compared to a uniform distribution by measuring the relative entropy between the two. The resulting value was divided by the highest possible entropy that could be attained, which is  $\log(16)$ . Values closer to zero reflected a lack of PACFC while those closer to one its presence.

The method just described has the drawback that it is frequency dependent. Electrophysiological recordings reveal an exponential decay of the PACFC estimation as the center frequency of IPS increases. In addition, the metric does not provide any information about statistical significance. To address these issues, one approach is to create surrogate data from the same IPS and IAS that lack cross-frequency coupling but retain their other statistical properties. This is attained by circularly shifting one of them in time by a minimum amount (20 percent of the length of the time series segment under consideration) and then recalculating PACFC between the out-of-sync series. In our experiments we used 60 surrogates for each IAS-IPS pair and then a z-score approximation was obtained for the PACFC of the synced IPS and IAS in relation to the population of the surrogates. Due to the large number of tests performed relatively high z-scores were likely to be observed by chance. Therefore results from single IAS-IPS pairs were not reported in this study. Instead averages across frequency ranges were considered. Selecting more

than 60 surrogates would have led to decreased variability in the z-score estimates in the expense of computational time. However, since the z-score results were averaged over frequency ranges and neighboring IPS-IAS pairs covered largely overlapping parts of the spectrum, the effect of that variability was reduced and the selected number of surrogates was deemed satisfactory with a resolution of 1 Hz.

The PACFC algorithm was performed for the range of frequency components for IPS 2-35 Hz in 1 Hz steps and 4 Hz bandwidth, and for IAS 3 – 250 Hz in 1 Hz steps and 6 Hz bandwidth. The relatively large bandwidth in IPS allowed for greater variability in the period of the signal. This sacrificed some precision in exchange for increased sensitivity, as it made it less likely that coupling in the surrogate data would occur by chance. The bandwidth selected might account for the very high z-score observed in subject 2. A larger bandwidth was selected for IAS to accommodate for the increased spectral leakage of the LFPs in faster oscillations.

In the intra-subject experiments, non-overlapping, consecutive and rectangular windows 6 seconds long were applied to the filtered data to obtain the time-evolution of PACFC and also to acquire samples that were approximately independent and identically distributed. The windowing was performed in the same manner as in the spectral and coherence analysis in order to obtain temporal correlations.

To minimize the effect of filtering on the edge of the time series, all data were filtered prior to any windowing operations. Two percent from the beginning and two percent from the end of the time series were discarded.

The computation of PACFC over a range of IPS and IAS components yielded a map in which IPS-IAS pairs corresponded to a z-score. The map did not include pairs in which the center

frequency of the IAS component was lower than that of the IPS, as that measure does not reflect the frequency coupling under examination.

When coupling was identified, three features were extracted from the z-score maps: 1) the center of gravity of the 2D plane specified by the IAS and IPS frequencies with z-scores viewed as density values, 2) the peak z-score defined as the average value in a small area (3 Hz – 6 Hz) centered at the center of gravity, and 4) the phase of the IPS component at which IAS peaked. A non-parametric approach in feature extraction was taken because peak characterization using a bivariate normal distribution did not yield a good fit with the z-scores in the plane. One probable cause is the variability in modulating and modulated frequencies between the coupled bands. On aggregate, such variability can lead to areas in the z-score map that are distinctly higher than controls but with a complex shape. Moreover, the non-parametric approach eliminated dependency on assumptions that the data comes from a particular model.

In order to extract the phase from IPS corresponding to the peak of IAS, which we refer to as preferred phase, we considered the distributions of the PACFC algorithm explained earlier. The weights of the distribution were used as amplitudes of a complex number, while the center phase of each bin (e.g.  $11.25^\circ$  for the first bin) constituted the phase of the complex number. This approach is similar to an alternative method for calculating PACFC referred to as mean vector length modulation index by Canolty, et al. (2010) which was not used in this study due to its decreased sensitivity in some circumstances, such as when the modulated oscillation contains more than one peaks within a cycle of the modulating component. In addition, when the length of the signals examined is not an integer value of the cycles of IAS, the mean vector length modulation index introduces bias from the remainder, which becomes more significant in small segments such as those lasting only 6 seconds and might contain only a few cycles. In this study, the preferred

phase was obtained simply by adding the 16 complex numbers and extracting the phase of the resulting vector.

### *2.3.6) Statistical analysis*

Both inter-subject and intra-subject analyses were performed. The inter-subject analysis was best suited for reporting average PACFC activity in each subject for a given band pair and condition. The intra-subject analysis was performed by windowing the data (6 seconds, no overlap) and offered us the ability to look at dynamic changes in PACFC, albeit at the cost of a reduced strength of detection, which was about one order of magnitude less.

In the inter-subject analysis, paired-sample one-sided Wilcoxon's signed rank tests were performed to compare PACFC at the GPi and baseline values obtained from locations 1-8 in MON in those subjects for which the baseline data was available (subjects 1-7). The same method was used for the motor cortex, but this time comparing PACFC of MRSs to that of sites separated from the MRSs by at least 2 contacts on the electrode strip. Two sample non-parametric (Kolmogorov-Smirnov) tests were performed to compare the rest and movement conditions. Since oftentimes multiple experimental blocks within a subject corresponded to the same location and condition, the samples were often the result of an arithmetic mean of results obtained from equivalent blocks. The tests were non-parametric due to the limited number of subjects precluding us from determining whether the data followed a particular distribution. The results were interpreted as representing electrophysiological markers in the population of Parkinson's disease patients.

In the intra-subject analysis samples were obtained from non-overlapping windows. The number of samples was limited by the length of the window, six seconds, which allowed for

approximately 10 samples per block. Thus we performed non-parametric tests (Kolmogorov-Smirnov). The window length was not lowered to avoid excessive noise in the PACFC measure. The results were interpreted as representing electrophysiological markers only for each individual patient.

To examine the relation of PACFC to coherence and between the GPi and motor cortex the correlation between the windowed PACFC series and coherence values was found. Similarly, we calculated the correlation between the PACFC series and the power of the bands involved in the coupling.

### 3. Experimental outcome

#### 3.1. 200-300 Hz oscillations in the GPi

The power in the 200-300 Hz band demonstrated a clear and consistent increase in power across all subjects at recording sites at and close to the GPi target (Figure 6), particularly after the second electrode position transition (T2, Table 2). A similar pattern of increased power was seen in the beta band at and close to the GPi target (Figure 6). Subsequent analyses focus on characterizing this previously undescribed GPi very high gamma band activity in patients with PD and verifying the presence of  $\beta$  band activity that has been previously described.

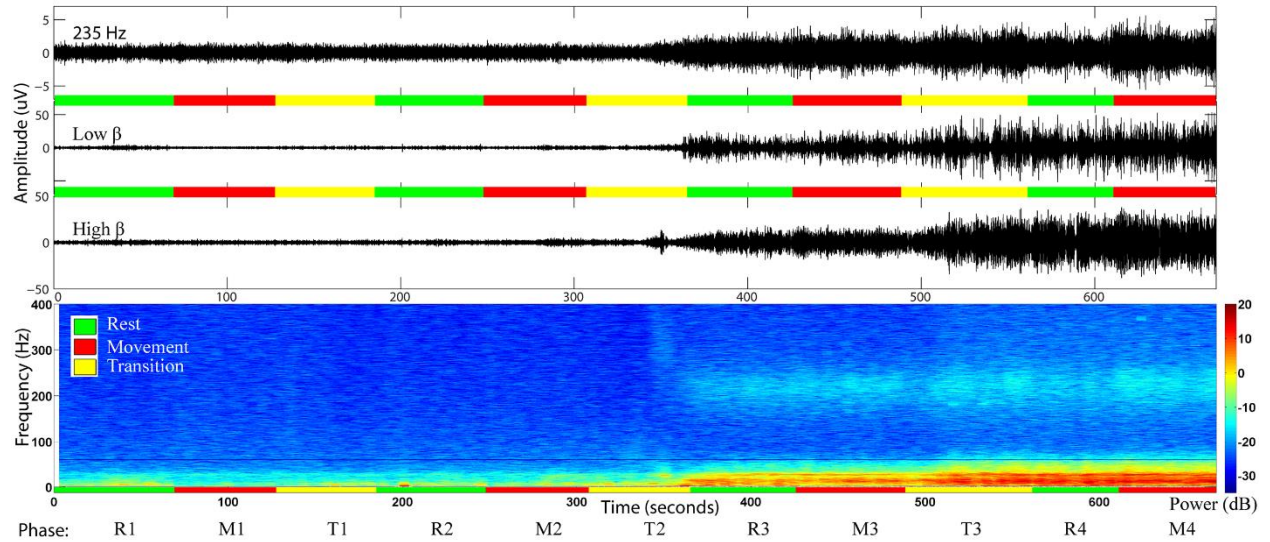


Figure 4.

Time series (top) and time frequency representation (TFR) (bottom), of the recording from the most distal electrode contact of the lead in subject 2. According to the recording protocol this electrode covered locations 7, 8, 15 and 16. The green, red and yellow horizontal lines correspond to rest, movement and lead transition phases respectively. After the second transition the electrode was advanced to location 15 and a noticeable increase in power near 200 Hz appeared. Starting with the third transition the electrode contact reached location 16 and a further increase in the power of the higher frequencies was observed. Careful inspection also reveals that finger movement further increased the power near 200 Hz compared to rest.

### *3.1.1. 200-300 Hz power in the GPi*

#### *Rest Condition.*

200-300 Hz power was first measured with the  $RBP_{200-300\text{Hz}}$  index, which confirmed our initial hypothesis that power in that range increases near target.  $RBP_{200-300\text{Hz}}$  in the GPi (locations 15 and 16) was higher than baseline (MON, CAR: locations 1-8) in all subjects regardless of referencing configuration (Figure 7 A, B) (percent difference in MON:  $22.22 \pm 19.77 \%$ ,  $p=0.0079$  for location 15 and  $17.1 \pm 14.0 \%$ ,  $p=0.023$  for location 16).

We then proceeded to further characterize the very high gamma band power increase by characterizing peak parameters in further detail. In the inter-subject analysis, peaks in the 200-300Hz band were only detected after the second electrode transition, corresponding to recordings from within the globus pallidus. Even within the globus pallidus, the consistency with which peaks were detected across subjects increased with increasingly ventral recordings (i.e., positions 15 and 16, Figure 8 A-C, Figure 9). Moreover, the heights (or associated power) of these peaks were greatest at the most ventral recording sites (near target) within the GPi (MON:  $3.7 \pm 2.0$  dB at location 15 and  $3.5 \pm 1.6$  at location 16, MON: one-sample, one-sided, Wilcoxon Signed Rank,  $p<0.0079$ , Figure 8A). The center frequency at the most distal location (16 for MON and CAR) was  $237.6 \pm 16.0$  Hz for MON,  $235.2 \pm 17.2$  Hz for CAR and  $230.2 \pm 16.7$  Hz for BIP. Finally, the peak's full width at half maximum (FWHM) was  $62.0 \pm 19.2$  Hz (MON),  $59.3 \pm 8.4$  Hz (CAR) and  $59.1 \pm 8.1$  Hz (BIP).

In the intra-subject analysis, peaks in the 200-300Hz band were more frequently identified from 6-second samples from recordings within GPi (locations 15 and 16) than recordings from other locations in the trajectory. Peak height was significantly greater than zero (MON: one-sample, one-sided, Wilcoxon Signed Rank,  $p < 0.016$ ) at both of these most ventral locations.



### *Movement Condition.*

In the inter-subject analysis, the height (or associated power) of the peak in the 200-300Hz band was higher during movement compared to rest (difference in MON:  $0.50 \pm 0.48$  dB at location 15, and  $0.30 \pm 0.80$  at location 16, Figure 10A). Statistical significance depended on location (paired-sample, one-sided Wilcoxon Signed Rank,  $p = 0.023$  and  $p = 0.23$  for locations 15 and 16 respectively). The equivalent results in CAR ( $0.36 \pm 0.45$  dB,  $p=0.055$  and  $0.64 \pm 0.61$ ,  $p=0.0078$  for locations 15 and 16) and BIP ( $0.64 \pm 0.55$ ,  $p=0.016$  for location 12 [corresponding to the most ventral recording site]) suggest that movement increased the peak height near and at target.

The FWHM of the peak in the 200-300Hz band decreased during movement compared to rest (MON:  $-13.0 \pm -8.5$  Hz and  $-21.2 \pm -14.1$  Hz at locations 15 and 16 respectively, Figure 10G). The results were significant for both locations in any electrode configuration (paired-sampled, one-sided Wilcoxon Signed Rank,  $p < 0.023$ ) with one exception that approached significance (location 12 in BIP,  $p = 0.055$ ).

The center frequency of the peak was not movement-modulated, with the difference between the two conditions in the peak center being near zero (MON:  $-1.1 \pm -6.1$  Hz and  $1.5 \pm -3.9$  Hz at locations 15 and 16, Figure 10D).

An observation of how the peak height changes during rest and movement using a moving windows of size 1 second and step size 0.1 seconds revealed that in subjects in which movement modulation was found, the increase in height was not a transient response, but rather persisted throughout the duration of the movement (Figure 11).

In the intra-subject analysis, the height of the peak was significantly higher during movement in at least one of the locations 15 and 16 in 5 of 7 subjects (MON: t-test,  $p < 0.033$ ). For the same subjects the peak FWHM was significantly reduced in at least one of the two locations (MON: t-test,  $p < 0.022$ ). Differences in the peak center frequencies between movement and rest

were sometimes significant (6 increases and 2 decreases at location 15 and 16,  $p < 0.05$ ) indicating the polarity of the modulation was dependent on the subject.

### *3.1.2. Beta band power in the GPi*

Results for the  $\beta$  band resembled those of the 200-300 Hz band during both rest and movement conditions (Figure 6). Regardless of referencing algorithm (MON, CAR, BIP),  $RBP_{low\_beta}$  and  $RBP_{high\_beta}$  values at distal recording sites (i.e., within the GPi) at rest were significantly greater (approximately 30%, Figure 7 C-F) than those recorded from proximal positions within the trajectory (locations 1-8 for MON and CAR, and 1-6 for BIP) from white matter areas including anterior corona radiata (percent difference from baseline in MON for  $RBP_{low\_beta}$ :  $13.18 \pm 12.8 \%$ ,  $p=0.023$  and  $11.2 \pm 10.2 \%$ ,  $p=0.016$  for locations 15 and 16 respectively). Equivalent results for  $RBP_{high\_beta}$  were significant ( $14.9 \pm 8.9$ ,  $p=0.016$  and  $14.0 \pm 15.4$ ,  $p=0.016$ ).

The low  $\beta$  (12-20 Hz) band power at locations 15 and 16 increased with movement for 4 out of 7 subjects while high  $\beta$  (20-35 Hz) increased in 3 subjects (Figure 12 B-D). These results did not reach significance (percent difference between movement and rest at location 16 for MON:  $56.2 \pm 96.6 \%$ ,  $p=0.11$ , 5 positive values). In the other subjects at least one of the locations showed a decrease in  $\beta$  power with movement.

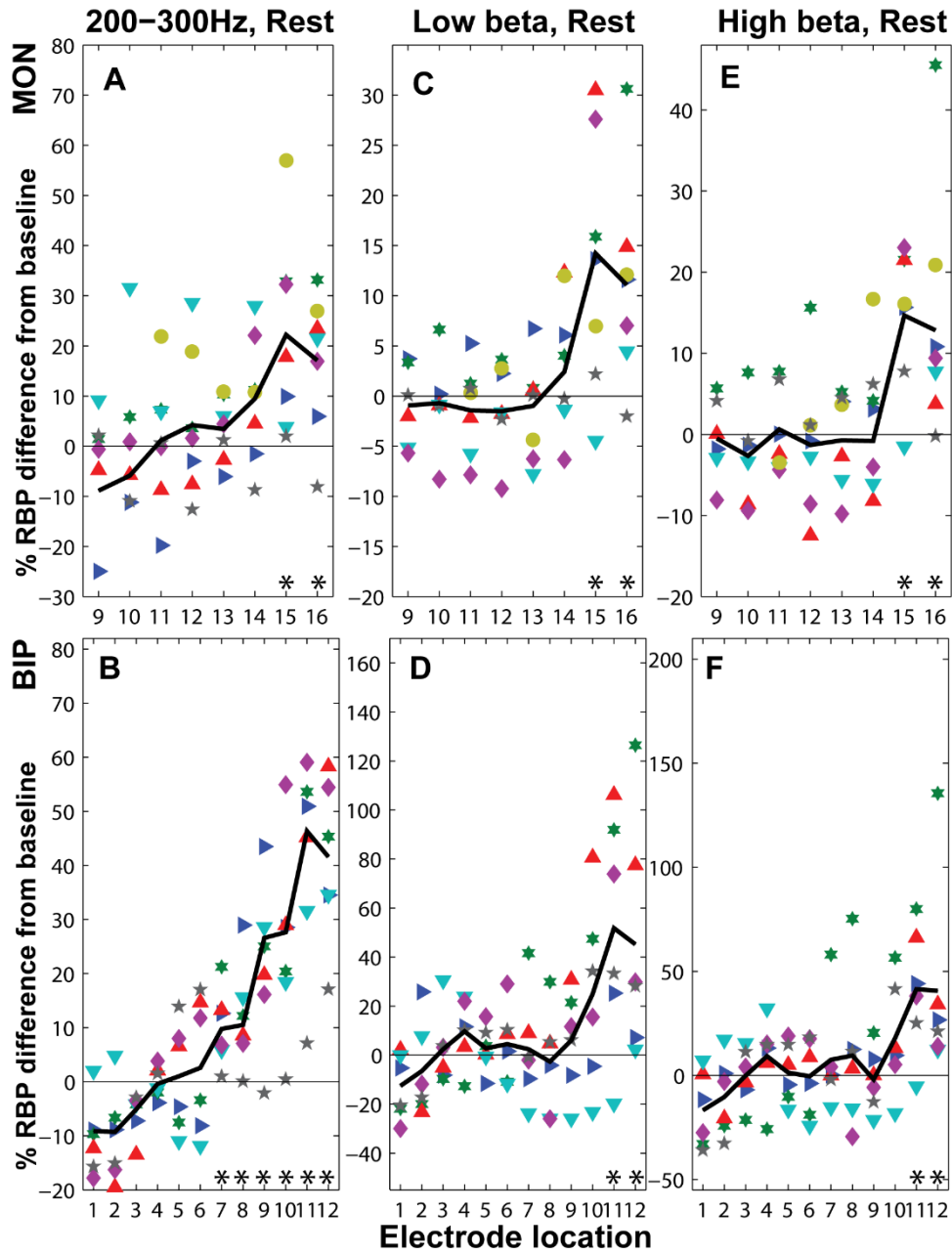


Figure 5.

Relative Band Power (RBP) for the 200-300 Hz, low  $\beta$  (12-20 Hz) and high  $\beta$  (20-35 Hz) in the GPi for all subjects. The percent difference from baseline (locations 1-8 in MON) is denoted for each subject with a different symbol and color. The average RBP<sub>200-300Hz</sub> (black line) (A,B) increased at target, consistent with the observation from a subsequent analysis that the peak height at around 235Hz reached its highest value at target. Both RBP<sub>low  $\beta$</sub>  and RBP<sub>high  $\beta$</sub>  are higher than baseline at the GPi (C-F) (locations 15 and 16 for MON, and 12 for BIP). Values for the 6<sup>th</sup> subject were not considered in the bipolar configuration (B, D, F). Asterisks indicate significance at the 5% level for one-sided non-parametric tests.

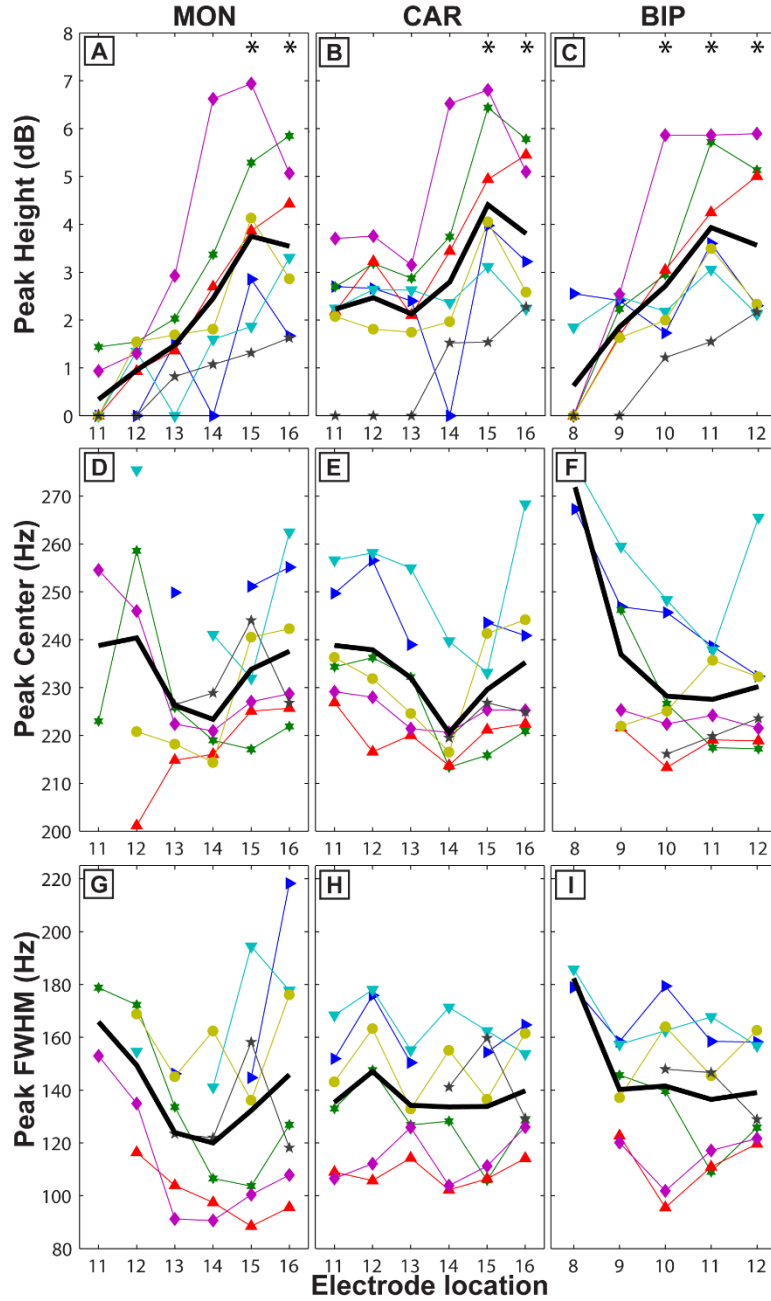


Figure 6.

Peak characteristics at GPi. During rest (A-I) the peak height was greatest at GPi (A-C) with highest average values (black line) reached at location 15. Peaks were detected for all subjects at target, in more proximal locations. The peak centers at location 16 were  $235 \pm 4$  Hz depending on electrode configuration (MON: D; CAR: E; and BIP: F). In D and F there is a tendency for the peak centers to have less variability at the GPi compared to more distal locations (e.g.  $240.4 \pm 29.6$  at location 12 whereas  $233.8 \pm 11.9$  at location 15, D). A comparison between MON and CAR reveals that by subtracting the common average reference from each of the four concurrent recordings (B) the 235 Hz spectral component at the GPi has affected other locations (11-12). Asterisks in A-C indicate that peak height is greater than zero at the 1% significance level using one-sided non-parametric tests.

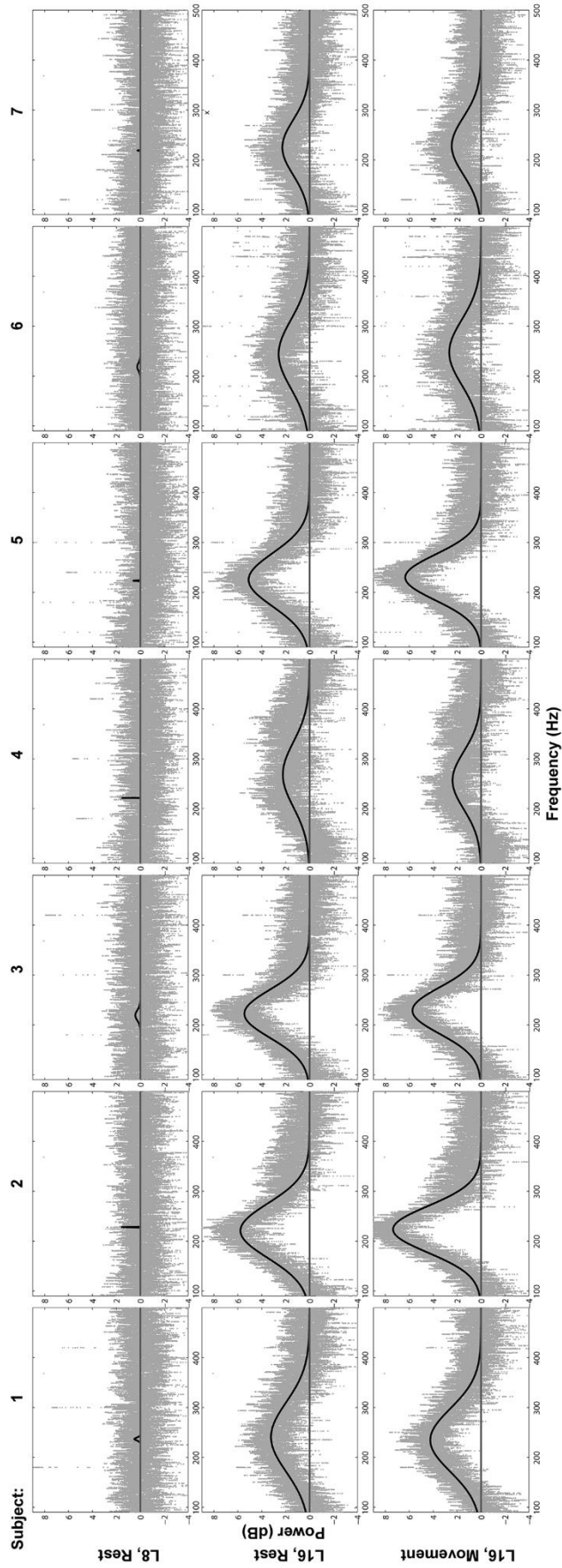


Figure 7.

Peak extraction (CAR). Peaks were not present away from the GPI (e.g. location 8, 1<sup>st</sup> row). At locations 9 and 10 (not illustrated) there was not usually a peak, but if present it was either weak ( $< 1$  dB) or a result of re-referencing using the common average reference and bipolar configurations. At target (location 16) in the rest condition peaks were present for all 7 subjects (2<sup>nd</sup> row). During movement the peak heights were increased by  $\sim 0.7$  dB (Figure 7 B) for all subjects (3<sup>rd</sup> row). In different configurations (MON, BP) not all subjects showed an increase (Figure 7 A, C).

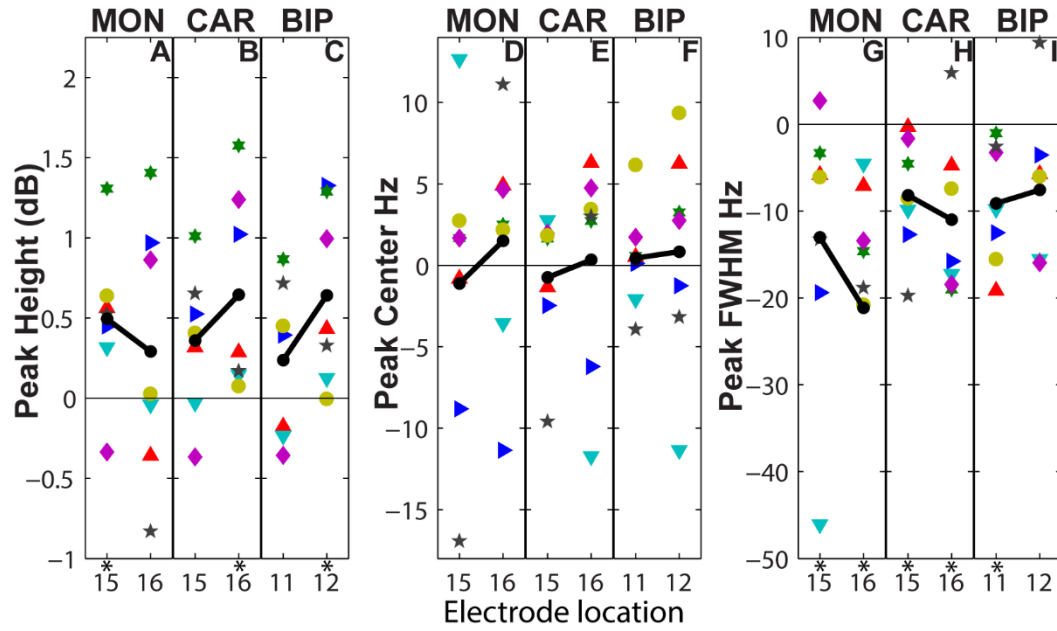


Figure 8.

Effect of voluntary finger movement on peak attributes. Movement caused an increase in average peak height (A-B, black line) of  $\sim 0.4$  dB and decrease in average peak width (G-I, black line) of  $\sim 10$  Hz compared to rest. Movement seemed to modulate the peak center for some subjects by either increasing or decreasing its value (D-F). Asterisks indicate significance at the 5% level with one-sided non-parametric tests.

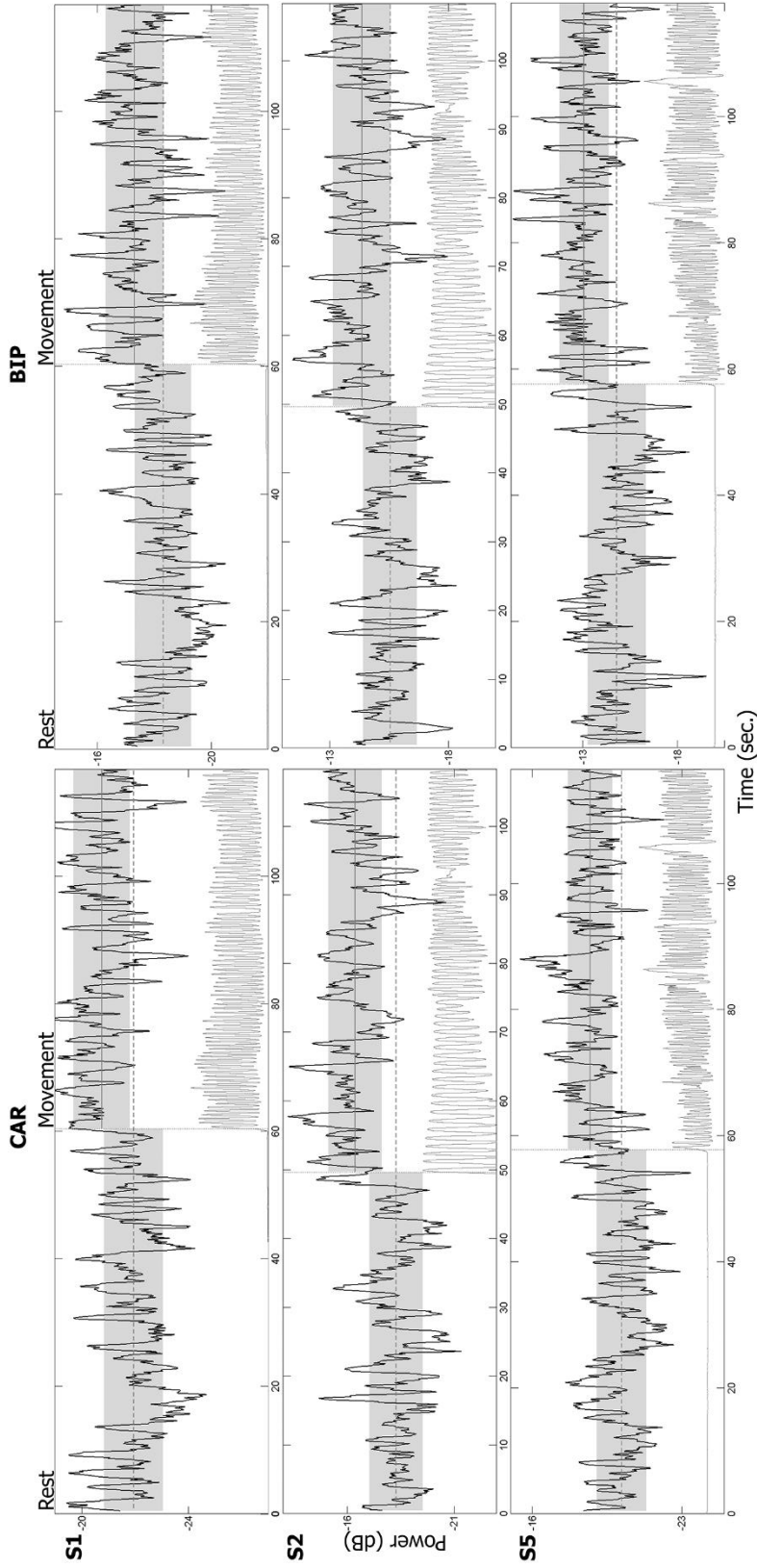


Figure 9.

Sustained increase in 200-300 Hz power during movement. The average values (straight horizontal lines) and standard deviations (top and bottom of shadowed areas) for rest and movement are shown for subjects 1, 2 and 5 at the 1<sup>st</sup>, 2<sup>nd</sup> and 3<sup>rd</sup> rows respectively in two configurations (CAR and BIP). The increase in 200-300 Hz power persisted for as long as the subject was moving their contralateral fingers and did not have a clear transient response. After initiation of movement the band power was higher than the baseline resting average for most of the time.

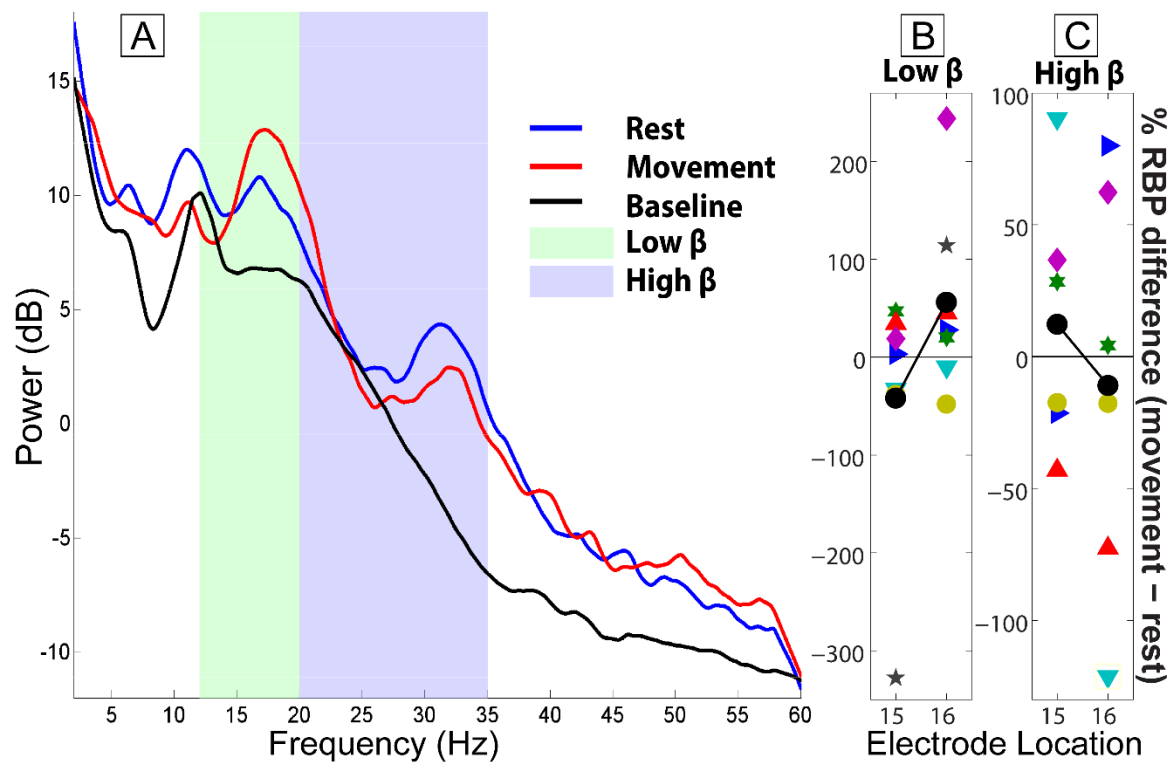


Figure 10.

Low and high  $\beta$  band power for the 5<sup>th</sup> subject at GPI (locations 15 and 16) using a monopolar electrode configuration. The spectra (A) at location 16 were obtained with a multitaper method (NW = 9, K = 17) and smoothed with local regression (linear least squares, 1st degree polynomial model, range of 3Hz). Activity at the low and high  $\beta$  bands in the GPI is higher than baseline (locations 1-8) as evidenced by the spectra (shown only for subject 5) and Figure 4 C-F. The Relative Band Power (RBP) of low and high  $\beta$  band was normalized against a baseline (average RBP of locations 1-8) for movement and rest. The percent differences between the two conditions are shown in B and C for each subject. Average values of those differences (black lines) varied above and below zero depending on electrode configuration (only MON shown) and electrode location. Within subjects a tendency towards increased or decreased  $\beta$  band activity with movement was at times significant but across subjects there was not a significant difference between movement and rest (location 15 and 16 average values from subjects with less than 50 percent and more than -50 percent difference:  $2.76 \pm 34.19$  and  $7.06 \pm 32.73$ ).



## 3.2. PACFC in GPi and motor cortex

Preliminary findings on PACFC in the GPi and motor cortex, the spectral content of both regions and interacting band pairs reported by independent studies (Tort, et al. 2008, Azcarate, et al. 2010, de Hemptinne, et al. 2013) pointed to three types of PACFC coupling: theta and alpha coupled to beta (4 – 12 Hz to 12 – 35 Hz), which for brevity is often referred to as theta-beta coupling, beta coupled to gamma (12 – 35 Hz to 20 – 100 Hz), and beta coupled to very high gamma bands (12-35 Hz to 200 – 300 Hz).

These observations are further explained below starting with the predominant beta-gamma PACFC in the GPi. The spectral content had been examined in a prior study (C Tsiokos, et al. 2013) showing beta and very high gamma band increases at that region. Next, it is shown the motor cortex is also involved in similar coupling, with one important difference being the angle of modulation. Results on coherence, its relation to local PACF, and cross-site PACFC follow, in which temporal correlations between PACFC and the other two metrics are shown to be high in the subset of subjects examined. Limitations in observing PACFC in the intra-subject, windowed analysis led to exclude several subjects from the analysis of temporal correlations. Findings on movement modulated PACFC verified the strong reduction in coupling in the motor cortex during movement, and a lack of significant modulation in the GPi in most of the subjects, possibly as a result of basal ganglia dysfunction.

### 3.2.1) PACFC within the GPi

The most prominent coupling occurred between beta-gamma in all subjects. In the rest condition, subject 2, 3, 5 and 11 had beta-gamma PACFC greater than 12 in the BIP configuration

(Figure 13B). For subject 1 and 4 GPi locations did not exceed 0.95 and 1.52 respectively. For subjects 1-7, for which baseline data was available, GPi z-scores (locations 10-12) were shown to be significantly higher than baseline (  $p$ -value = 0.031). In subjects 9 and 10, for which bilateral GPi data was available, the coupling was stronger in the left and right GPi respectively (z-scores of 3.8 vs 1.3 and 5.2 vs 1.2) possibly indicating a preferred side for PACFC. However, this hypothesis was challenged by the MON data that did not show a consistent polarity. It is worth noting that the MON configuration, despite providing a finer resolution was significantly more likely to be affected by oscillations in distant, unrelated locations and by crosstalk between channels in the ECoG strip and GPi. For subject 11, both left and right GPi showed strong coupling (z-scores 30.10 and 35.58). The highest degree of coupling was seen in the 2<sup>nd</sup> subject (z-score = 147.8).

During rest, there were also strong indicators that beta – very high gamma PACFC was present in the GPi of all subjects (Figure 13E), but its magnitude was substantially smaller compared to beta – gamma PACFC. Nevertheless the GPi beta – very high gamma PACFC was significantly higher than baseline (  $p$ -value = 0.047). Theta-gamma coupling was constrained to shorter frequency ranges compared to the other types of coupling.

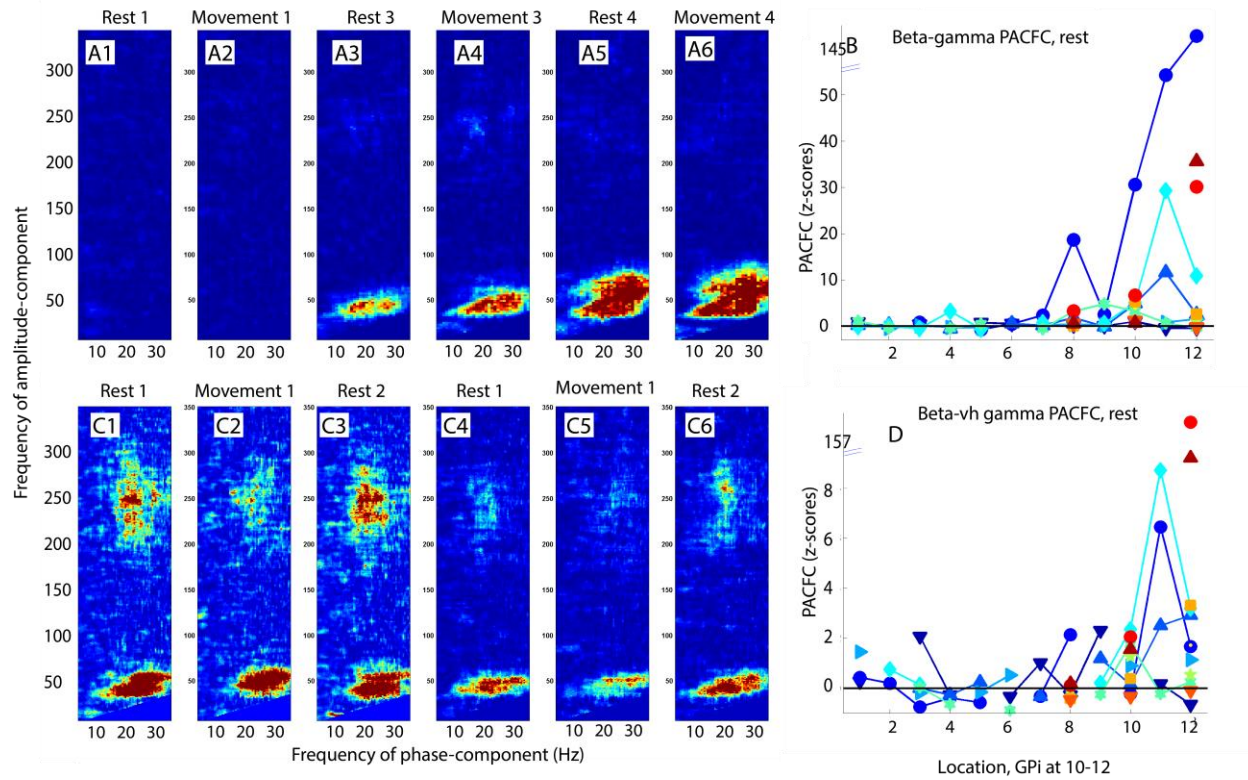


Figure 13.

Phase-amplitude cross frequency coupling (PACFC) in the GPi. Using the same techniques as in the motor cortex to extract the magnitude of PACFC for three band pairs (theta - beta, beta - gamma, beta - very high gamma), PACFC was found to be present in most subjects. A) beta-gamma PACFC for subject 2. From left to right in A1-A6, each picture represents PACFC over a block of about 60 seconds during rest (A1, A3, and A5) and movement (A2, A4 and A6). In the jet colormap covers a range of z-scores from -2 to 86 with blue corresponding to the lowest values and red to the highest. Each pair of rest/movement blocks corresponds to a particular location along a trajectory that ends at the GPi. Blocks A3-A6 correspond to GPi locations while A1 and A2 to the most distal areas from the GPi. The strong coupling seen at A5 (rest) is denoted by a z-score of 148 while at A6 (movement) of 104 in the bipolar electrode configuration. Similar results (z-score 95 and 79 respectively) are revealed using the monopolar configuration (not shown). B) beta-gamma PACFC magnitude for all subjects along a trajectory ending at the GPi. Locations 10-12 were considered to be at the GPi through stereotactic mapping. To summarize the magnitude of coupling, the area that covers the frequencies of interest was used to derive the center of gravity of the z-scores, which in turn specified a location most likely to contain the peak magnitude. Those magnitudes can be seen in B, with each line representing one subject. C) Beta - very high gamma PACFC in right (C1-C3) and left (C4-C6) GPi of subject 11. The colormap's range is -2 to 16 (C1 - C3) and -2 to 35 (C4 - C6). In each hemisphere two rest blocks (C1, C3 and C4, C6) as well as one contralateral movement block (C2 and C5) with a duration of about 60 seconds were analysed. Both sides revealed beta - very high gamma PACFC that was stronger during rest (right GPi: 16.34 vs 4.35, left GPi: 9.21 vs 5.27 in BIP, similar results in MON). D) Beta - very high gamma PACFC magnitude along trajectory to GPi (locations 10-12).

The angle at which the IAS had higher values with respect to IPS was found to have widely distributed values among subjects at the GPi sites of maximal PACFC for both the beta – gamma and beta – vh gamma band pairs. However, when only subjects with the higher z-scores were considered they varied within about quadrant centered at about 100 degrees (Figure 14), possibly indicating a causal relation between IPS and IAS, in which IPS leads any changes in IAS.

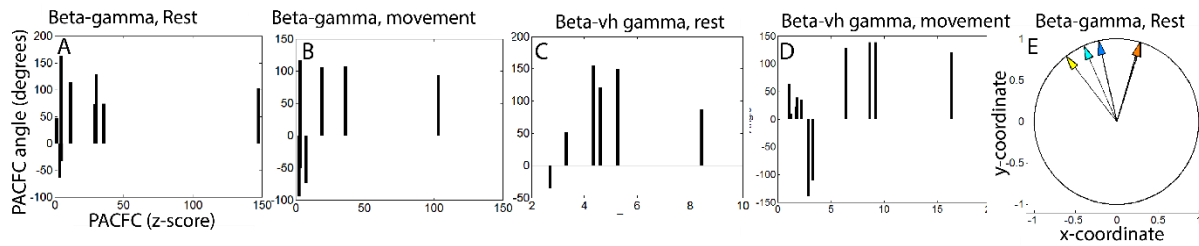


Figure 14.

Angle of modulated component in beta-gamma (A, B, E) and beta-vh gamma (C, D) PACFC. Each vertical line represents a different subject except for subjects 9, 10 and 11 for which both left and right GPi data were available. The angles were taken from GPi sites in which PACFC was maximal. The associated PACFC magnitudes show that in cases of strong coupling the range of the angles and their standard deviation are far smaller than for weak coupling. A) Angle over beta - gamma PACFC magnitude during rest in the bipolar configuration. If one were to look at angles of only those subjects with z-scores greater than 5.24, the result would be that shown in E. B) Same as in A but during movement. Despite significant reductions of beta - gamma PACFC in some subjects, coupling remained present in most cases and thus it was possible to extract meaningful angles of modulation. C) Angle over beta - very high gamma PACFC during rest in BIP. D) Same as in C but for the movement condition.

The analysis of the relation between PACFC and band power or coherence was limited by the small number of samples available for GPi locations ( $n = 7 - 10$ ) as well as low average z-scores across the frequency ranges involved in PACFC. Here we report correlations with beta-gamma PACFC only, since it was the strongest, and only for subjects 2, 3, 4, 5 and 7. In the case of coherence, motor cortex data was not available for subject 2 and subject 4 lacked high coherence in the beta band. For power, subject 3 had low correlations (maximum magnitude of  $\text{cor.} < 0.3$ ) (not shown). For the other subjects, correlations as high as 0.65 were found between GPi PACFC and either power or GPi – motor cortex coherence during either rest or movement (Figure 15).

Time series of PACFC and power or coherence (Figure 15, C1-C4) reveal similarities in their fluctuations for  $r > 0.4$ . Notably, every subject's PACFC seemed to be most correlated with a different band or set of bands. Another observation was that the power of the very high gamma band had the smallest average correlation with the beta-gamma band PACFC across subjects (cor. = -0.077) and did not exceed 0.17 for any of the subjects as opposed to all other bands. The correlation to the low beta band power was smaller than the high beta band power, signifying the importance of considering them separately.

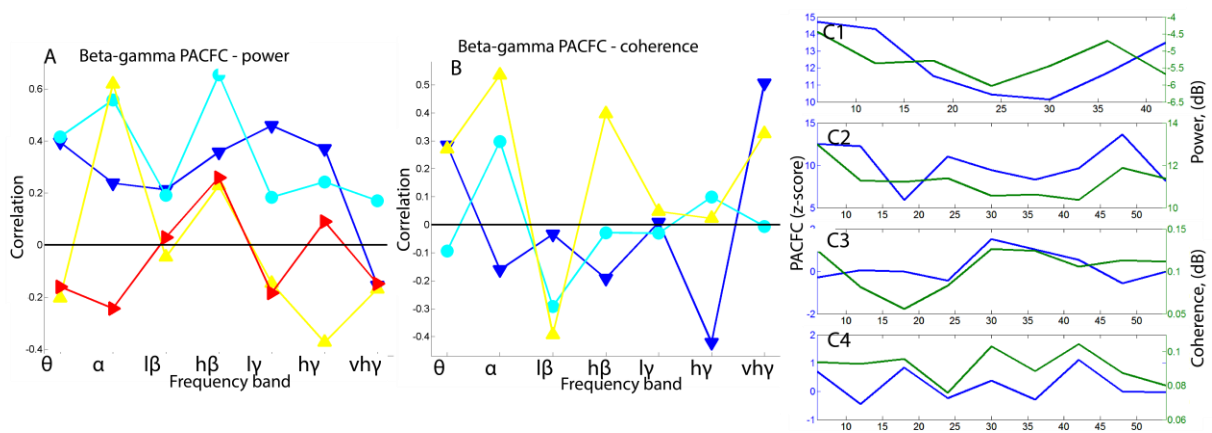


Figure 15.

Temporal correlation between beta-gamma PACFC and band power in the GPi or coherence between motor cortex and GPi. The time series for beta-gamma PACFC at GPi sites in which it was maximal (mostly location 12 in bipolar configuration) was used in the calculations. The time series for power was selected from the same sites that had maximal PACFC. However, for coherence they were selected from GPi - Motor cortex pairs with maximal coherence in the high-beta band. All correlation observations were limited by the fact that the time series were very short ( $n = 7$  to  $10$ ) since for every GPi location a block about 60 seconds long provided approximately 10 nonoverlapping 6 second segments. A) Correlation between PACFC and band power. In two of the four subjects the correlation was high ( $r > 0.4$ ) at either the high beta or low gamma band, which are contained in beta-gamma PACFC. Both rest and movement showed correlations with power. C1 shows a similar reduction in the magnitude of low gamma power and PACFC towards the middle of a 42 second period ( $r = 0.46$ ) during rest. For the same subject but during movement, correlation with the low gamma band was almost zero, but with the very high gamma band 0.51 (C2). B) Correlation between PACFC and coherence. Subject 2 was not included as motor cortex data were not available. Subjects 3, 5 and 7 had high enough PACFC and coherence at the sites of interest to use the windowed analysis. Negative correlations with high magnitude might not simply reflect an inverse relation between PACFC and coherence at particular bands, but a delay that would cause fluctuations in the two time series to look shifted by half a period. High correlations were detected for both rest and movement but in different bands. For subject 7 (yellow) the time series of PACFC (blue) and of coherence in the high beta band (green) during rest are shown in C3 ( $r = 0.40$ ). During movement, and for coherence in the high gamma band the series are shown in C4 ( $r = 0.68$ ). In both cases, the two series appear to be related.

### *3.2.2) Spectral power in the motor cortex*

The theta, alpha, low/high beta, and low/high/very high gamma bands from signals in the motor cortex and GPi were examined but the most notable and significant changes in power with finger movement occurred in the high beta band. That band was used to determine movement-responsive sites (MRSs).

The seven subjects for which LFP data from the motor cortex was available showed a significant reduction in the beta band in at least one contact (Figure 16A) with finger movements. Sites with maximal and significant high beta band suppression (MRSs) were chosen to be the 5<sup>th</sup> 3<sup>rd</sup> 2<sup>nd</sup> 5<sup>th</sup> 3<sup>rd</sup> 4<sup>th</sup> and 4<sup>th</sup> contact for the subjects 1, 3, 4, 5, 7, 10 and 11 respectively in MON. MRSs for BIP are shown in Table 3. With the exception of the first subject, there was a high gamma power increase during movement (Figure 16B) that was significant (  $p\text{-value} < 0.05$  ) at most sites. Significant peaks of the high gamma power were at contacts 3, 4, 3, 6, 8, 1 and 5 (MON) for each of the subjects. Thus, for five subjects the distance between contacts with maximal beta suppression and high gamma increase was not more than two neighboring contacts. The low and very high gamma bands behaved similarly to the high gamma band, all of which displayed broadband changes, rather than distinct peaks.

Temporal correlations between the seven bands revealed strong dependencies between them. The low and high beta bands were highly correlated in rest (  $\text{cor.} > 0.54$  except for subject 7 with  $\text{cor} = 0.2$ ). During movement, temporal correlations between the beta sub-bands decreased except for subject 4 ( $\text{cor. difference} = 0.11$ ) and subject 7 ( $\text{cor. difference} = 0.17$ ). The three gamma sub-bands were positively correlated for all subjects in both the rest and movement conditions.

The high beta band was negatively correlated to high and very high gamma (max. cor. = 0.49) except for subject 4 (cor = 0.43) and subjects 3, 10 (cor. < 0.18) during rest. During movement, all subjects except for subject 4 showed negative correlations.

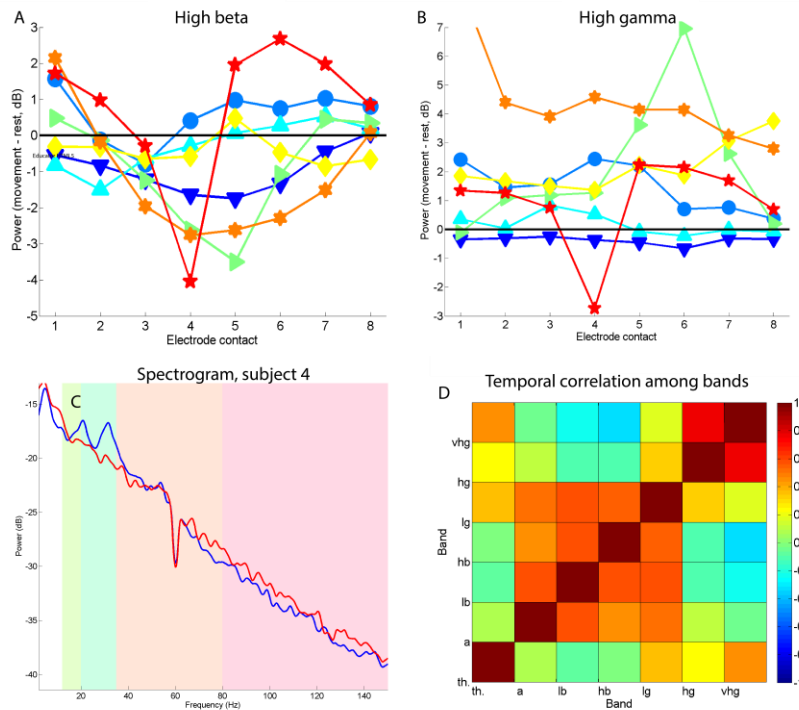


Figure 16.

Band power in movement and rest. Power spectra were estimated using Welch's periodogram and the multitapering method (not shown) using windows 6 second long without overlap. In each window, the average band power for the theta (4 - 8 Hz), alpha (8 - 12 Hz), low beta (12 - 20 Hz), high beta (20 - 35 Hz), low gamma (20 - 80 Hz), high gamma (80 - 150 Hz) and very high gamma (150 - 350 Hz) was extracted for each electrode contact in the monopolar and bipolar configurations. This led to as many estimates of band power as the number of windows in the rest and the movement condition. A) Change in high beta band power from rest to movement as an average of all the window values. Each line represents one subject. Some subjects, show a reduction in power that is better centralized in the middle of the electrode strip. B) Change in high gamma band power. Overall, the low, high and very high gamma bands increased during movement. In most of the subjects, the contact with the peak reduction in beta band was the same as or close to the contact with a peak increase in gamma band. C) An example of average spectra across windows of the third contact in the bipolar configuration of subject 4. With movement (red line) there was a reduction in low and high beta power (green) and increase in low and high gamma (orange and pink) compared to rest (blue line). D) Temporal correlation among the powers of the seven bands during rest for subject 5. For this subject the beta band was negatively correlated to the high and very high gamma bands (-0.33 for h. beta - vh. gamma). A similar observation was made for another three subjects during rest and movement with a correlation reaching as low as -0.5 (subject 1, l.beta - vh. gamma). The rest of the subjects had weak positive correlations with the prominent exception of subject 4 (0.46 l.beta - h. gamma).

### *3.2.3) PACFC within the motor cortex*

PACFC was observed in the ECoG strip placed over the motor cortex at or near MRSs. Among the three pairs of frequency bands examined (beta – low gamma, beta – high gamma, and theta – beta) only the first and the third were found to have PACFC. For all subjects, PACFC analysis of entire blocks (about 60 seconds long) yielded much higher coupling, about one order of magnitude higher, compared to the windowed analysis ( 6 second, non-overlapping windows). However the increased number of samples (about 40 for subjects 1,3,4,5, and 7) from windowing allowed for statistical tests with higher certainty about the standard deviation and also provided the opportunity to find temporal correlations with spectral power and coherence. Areas of maximal PACFC were largely the same between the windowed and non-windowed analyses. However, when PACFC was weak (z-score at peak < 4), the results in the windowed analysis most often could not detect PACFC at levels higher than the baseline.

During resting periods, beta-gamma PACFC was found to be present in all subjects (  $2.22 < z\text{-score} < 24.26$  ), although it was weak in subject 3 (z-score = 1.023). The sites of maximal coupling had either a one-to-one correspondence with movement-responsive sites, or were in close vicinity to them (Table 3, rows labeled Loc. Max PACFC and MRS). Considering as baseline PACFC values from locations separated by at least two contacts from the MRSs, and comparing them to PACFC from MRS sites (Table 3, row labeled “MRS”, and not neighboring sites that might have had higher PACFC as in Table 3, row labeled “Loc. Max PACFC” to avoid bias) the difference was found to be significant ( p-value = 0.023 )



Table 3. Locations of maximal beta-gamma PACFC and reductions in high-beta band power

Subject	1	3	4	5	7	10	11
Loc. Max PACFC	4	3	2	6	2	4	5
PACFC reduction in movement (z-score)	-2.6	-1	-5.9	-24	-12	-2.3	-8.5
MRS	4	3	1	4	3	5	3
Power reduction in movement (dB)	-2	0	-1.6	-3.3	-1.6	-3.5	-5.3

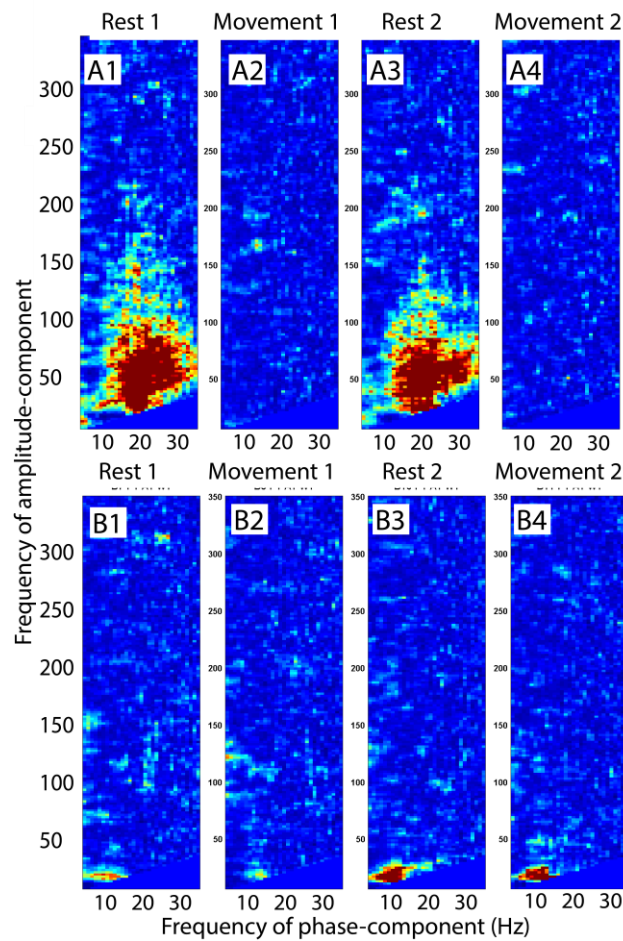


Figure 17.

Movement dependent phase-amplitude cross frequency coupling (PACFC) in the motor cortex. A) PACFC between the phase of the beta band and amplitude of the gamma band in subject 5, contact 6 (BIP, jet colormap with range -2 to 16). The x-axis represents center frequencies of the phase components, while the y-axis center frequencies of the amplitude components. During sessions of one minute of rest (A1, and A3) the coupling was much stronger than during movement (A2 and A4). A similar pattern was revealed for all subjects in at least one of the ECoG contacts that was at or near movement responsive sites, but with a smaller magnitude. The smallest score among subjects was 2.6. B) As in A, but for subject 3 at the first ECoG contact (not a movement responsive site). During sessions that lasted about one minute each (B1 and B3 for rest, B2 and B4 for movement), alpha - low beta PACFC can be seen at the bottom left of the figures. (Theta, alpha) - beta PACFC appeared in subjects 3, 4, 5, 7, 10 and 11, but only seemed to decrease in magnitude in subjects 10 and 11. Coupling between beta and very high gamma (200-300Hz) was not detected in any of the subjects, consistent with the absence of any spectral peaks in the very high gamma range in the motor cortex.

The angle of the modulating component (e.g. the beta band phase from beta-gamma coupling) was limited within a quadrant centered at 0 degrees ( $-4 \pm 32.0$  degrees collectively, Figure 18) for beta-gamma PACFC. This observation was also true for theta-beta PACFC in five subjects. One of the other subjects is shown to have a large lead (-114.6 degrees) while the other

one a large lag (140 degrees), but the periodicity of the beta band means that both of these values could correspond to either a lead or a lag.

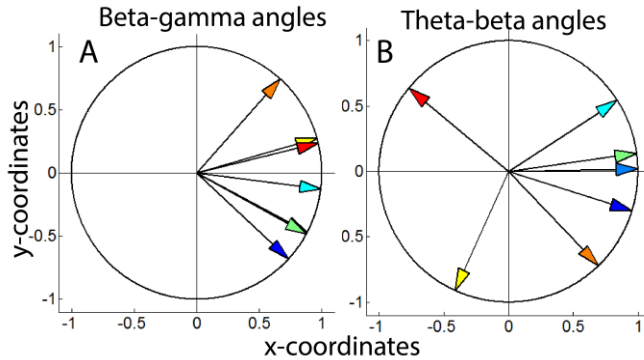


Figure 18.

PACFC angles in motor cortex. Using a small number of frequency pairs centered at the center of gravity of z-score maps from electrode sites with the highest z-scores, average modulating angles were extracted for each subject, which are represented by arrows. A) Beta-gamma band PACFC angles. Collectively the arrows are centered at -4 degrees and dispersed within one quadrant. The arrow from subject 3 is behind that for subject 4. The close proximity to 0 degrees indicates that the gamma band amplitude tended to be higher close to the peak of the beta band components. B) Theta-beta band PACFC angles. For five out of seven subjects the distribution of angles was similar to the beta-gamma coupling, while for the other two these was a large lag and lead compared to the peak of theta band.

Analysis of concurrent band power at ECoG sites with maximal PACFC z-scores (also at or near MRSs) performed on subjects 4, 5 and 7 revealed a high correlation between the low as well as the high beta band and PACFC for the last two subjects ( $\text{cor.} > 0.37$ , Figure 19, A, C1). Z-scores for subjects 1 and 3 were too low in the windowed analysis to derive any correlations. (Theta & alpha) - beta PACFC, which was strong in subject 3 was highly correlated with the alpha band power ( $\text{cor.} = 0.68$ ) as well as low beta ( $\text{cor.} = 0.46$ ).

Coherence between motor cortex and GPi sites with maximal PACFC was also shown to be highly correlated to the beta band ( $\text{cor.} > 0.42$ , in either low or high beta band, Figure 19, B, C2-C4). Due to the lower number of samples available for concurrent recording between a

particular GPi site and the ECoG strip, there was a significant chance of correlations below 0.38 (expected standard deviation for 8 samples from random distribution) to not indicate a link between the two series. However, as shown in Figure 19, C2-C4, correlations greater than 0.49 revealed a consistent fluctuation between the two time series. For subject 3, which had high (theta and alpha) – beta PACFC, its correlation with coherence was 0.40 during rest and 0.68 during finger movement, consistent with the insensitivity of PACFC to movement for that band pair (as opposed to beta-gamma PACFC). The lack of beta-gamma PACFC in the motor cortex during movement led to much lower correlations with either power or coherence (not shown).

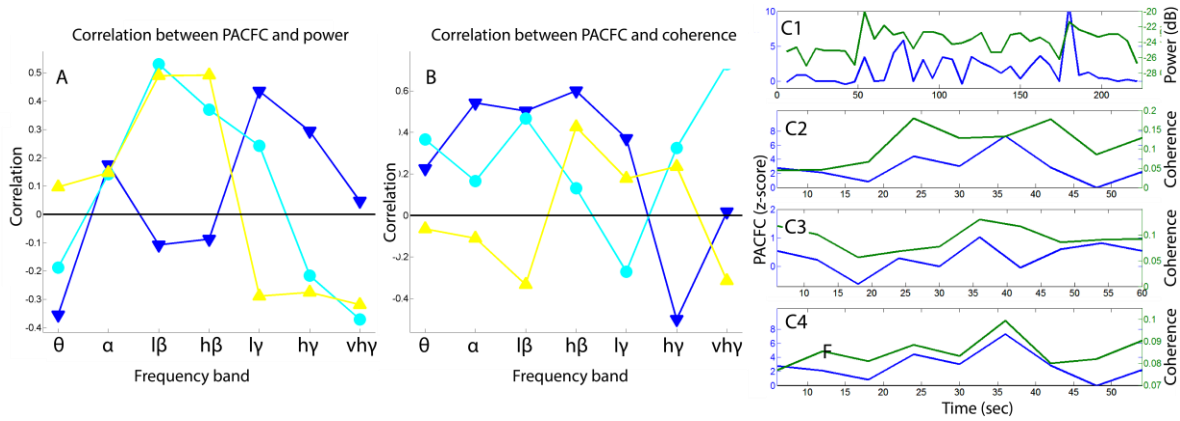


Figure 19.

Correlation between beta-gamma PACFC and band power or coherence. Data for subjects 4, 5 and 7 from ECoG sites with maximal beta-gamma PACFC are shown. A) Correlation between PACFC and band power. Frequencies of the modulating component contain the low and high beta bands, while those of the modulated component of the low gamma band. The three subjects showed a high correlation ( $r > 0.4$ ) with at least one of those bands. If the same number of samples ( $n = 40$  or  $44$ ) came from a uniform distribution the expected standard deviation would be 0.16. Thus the negative correlations shown for the  $\theta$  and  $\gamma$  ranges are potentially significant. B) Correlation between PACFC and coherence. The coherence time series was selected to be between the same ECoG site used for the beta-gamma PACFC time series and the GPi site that was maximally coherent with the motor cortex. Subjects 4, 5 and 7 displayed a high correlation ( $r > 0.4$ ) in the frequency ranges present in the coupling. However, the number of samples available for coherence was much smaller ( $n \geq 8$ ) as only one block of data ( $\sim 60$  seconds) corresponded concurrent recording between motor cortex and GPi. That implies the expected standard deviation of data randomly selected from a uniform distribution is very high ( $r = 0.378$ ), and the corresponding uncertainty with the actual data. Nevertheless, time series revealed that correlations within 0.4 - 0.7 range corresponded to similarly fluctuating values between PACFC and some bands. C) Time series between beta-gamma PACFC (blue) and power (C1) or coherence (C2-C4) (green). The time series of PACFC during rest is shown for the bipolar site with maximal PACFC (C1, contact 2). This series was highly correlated ( $r = 0.49$ ) with the power of the low beta (not shown) and high beta band (C1, green). Despite the difficulty of determining high correlations between PACFC and coherence due to the low number of samples, a correlation coefficient of 0.47 (C1), 0.60 (C2), and 0.73 (C4) was found against the low beta band of subject 5, high beta band of subject 4 and very high gamma band of subject 5 respectively. Among these, it is noteworthy that a band not involved in the PACFC and also showing weak coherence values had the highest correlation with PACFC. This suggests that the clear peaks in the 200 - 300 Hz range might be directly affected by the motor cortex during rest. The equivalent result during movement is  $r = 0.21$ , a very low value with  $n = 9$ .

### 3.2.4) Coherence and Bidirectional PA-CFC between GPi and motor cortex

Coherence between the GPi and motor cortex was observed in differing amounts from the theta to very high gamma bands with baseline levels at about 0.1 for most subjects. Of particular interest was coherence in the beta and gamma ranges as those were mostly involved in PACFC. All subjects except for subject 4 had coherence in the high beta range that exceeded 0.12 ( $0.17 \pm 0.04$ ) at or near MRSs and typically smaller levels at other sites. Low and high gamma coherence was weaker (0.09) but for those bands the baseline was also smaller. The correlation analysis between PACFC and coherence mentioned earlier was done for ECoG sites that were both near MRSs and had maximal coherence in the high beta range.

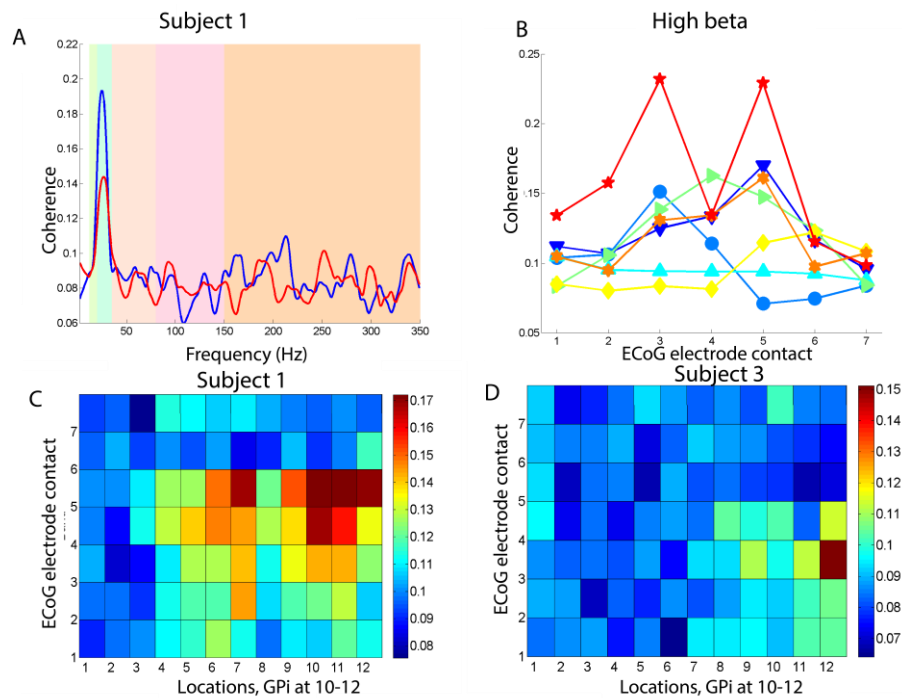


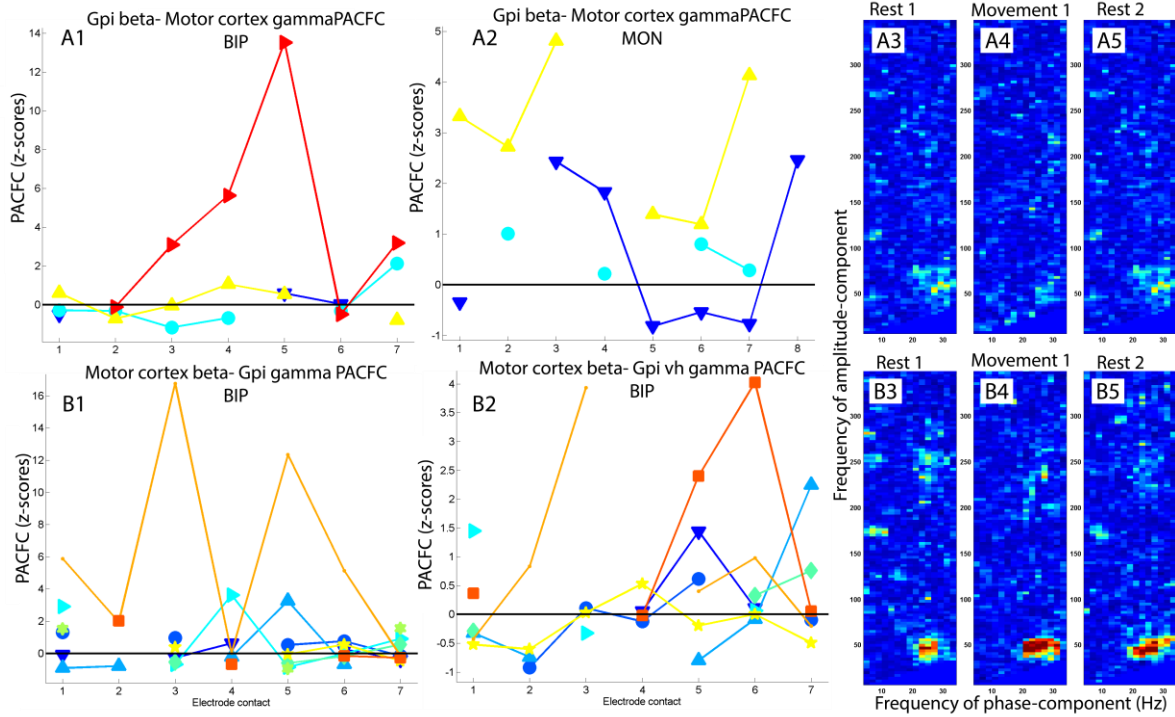
Figure 20.

Coherence between motor cortex and GPi. A) Coherence for first subject between a GPi location and a movement-responsive site (MRS) in the motor cortex in rest (blue line) and movement (red line). B) High beta band coherence between a Gpi location and all ECoG contacts of each subject in the BIP configuration. GPi – EcoG location pairs with maximal beta band coherence tended to correspond well with MRSs in the motor cortex, showing that the strength of the cortical beta band is important for this dependency between the two structures. C, D) High beta band coherence between all possible pairs of locations from the DBS leads and ECoG strip in a bipolar electrode configuration during rest. The GPi is at location 12. D corresponds to subject 1, while E to subject 3.

PACFC across the GPi and motor cortex was present in observable amounts only in a small minority of the subjects. Among them, the most notable was subject 11, which contained strong coupling (z-score = 13.53, Figure 21-A1) between the phase in the beta band of the motor cortex and the amplitude of the gamma band in the GPi, and vice-versa (z-score = 16.76, Figure 21-B1), with the sites reversing roles. In addition, for that subject beta-very high gamma PACFC had a z-score of 4.03 indicating a relation between the previously detected very high frequency oscillations in the GPi and beta band of the motor cortex. Similar observations did not reveal a difference in the coupling parameters between rest and movement, as coupling was present in either of them or both depending on the subject. For most observations the analysis was made in the BIP configuration to minimize the possibility of cross-talk. Nevertheless, at GPi sites local PACFC did not reveal cross-talk in MON.

Figure 21.

Bidirectional PACFC between GPi and motor cortex. Measurements of beta-gamma and beta-vh gamma PACFC between the GPi and the motor cortex revealed that only a small minority of subjects showed coupling that could be observed throughout 60 second blocks. The absence of coupling for that duration, however, should not be interpreted as a complete absence of coupling, since PACFC is dynamic and if it appears scarcely it might not be detectable for long windows of time. Missing values in the figures suggest that the z-scores indicating PACFC are very close to zero. The colomap values range from -2 to 16. The x-axis in A1, A2, B1 and B2 represents a BIP location in the motor cortex. For the GPi, location 12 was selected. A1-2) Beta-gamma PACFC magnitude between GPi (beta band) and motor cortex (gamma band) for subjects 1, 7, 10 and 11 in BIP (A1), and 3, 4, 5 in MON (A2). Only two subjects showed z-scores greater than 4. Subject 11, notably had a relatively high coupling (z-score = 13.53) between the phase of the beta band in the GPi and the gamma band in the motor cortex in the rest (A3, A5) and movement (A4) conditions. B1) Beta-gamma PACFC magnitude between motor cortex (beta band) and GPi (gamma band) for subjects 1, 3, 4, 5, 7, 10 and 11 in BIP. For subjects 10 and 11, in addition to the ipsilateral motor cortex and GPi data, contralateral (left GPi - right motor cortex) were available and are displayed. Only subject 11 had strong PACFC with a z-score of 16.77 in rest and 12.30 in movement (not shown). Notably, the strong coupling seen in subject 11 did not exist between contralateral GPi and motor cortex. Contralateral coupling was also not seen in subject 10, although that was also lacking ipsilateral coupling. B2) As in B1, but for beta-very high gamma PACFC. Coupling was weak but for subject 10 and 11 z-scores exceeded 3.9. The upper portions in B3-B5 show in both rest and movement the phase of the beta band from the motor cortex has influenced the amplitude of the very high gamma band in the GPi. B3-B5) PACFC z-scores for all frequency pairs between motor cortex and GPi for subject 11. The beta-gamma PACFC seen regardless of which of the GPi and motor cortex contains the phase-components suggests a bi-directional PACFC relation between the two



### 3.2.5) PACFC within the GPI during movement

Despite an overall increased power for all the bands at the GPI compared to distant locations, only the beta band and very high gamma band increases were observed for all subjects. The faster oscillating band was better localized to the GPI compared to the more spatially diffused beta band. The effect of finger movement had been studied previously and shown to cause an amplification of the fast oscillation centered at about 235 Hz (Tsiokos, et al. 2013). However, even though movement related changes in beta band power were significant for some subjects, the change was not consistently positive or negative in the population.

The intra-subject significance was determined using samples from the windowed analysis. The beta-gamma band pairs showed significant movement related reductions ( $p < 0.05$ ) only in a subset of subjects while the beta-very high gamma pair even for less. The theta-beta pair did not seem to be related to movement for any subject. Finger movement had a variable effect on beta –

gamma PACFC depending not only on the subject but also the particular location of the GPi (Figure 22A). Interestingly, significance, was established only for cases in which movement caused a reduction and not an increase of PACFC. For example, subject 11 (Figure 13C) showed a reduction during blocks of movement (C2 and C5 for left and right GPi respectively) compared to rest (C1, C3 and C4, C6 for the two hemispheres respectively). Beta – very high gamma PACFC modulation by movement could not be examined carefully, because even though this band pair had a presence when considering the entire experimental blocks (~60 sec.) it was very weak in the windowed analysis and indiscernible from baseline levels.

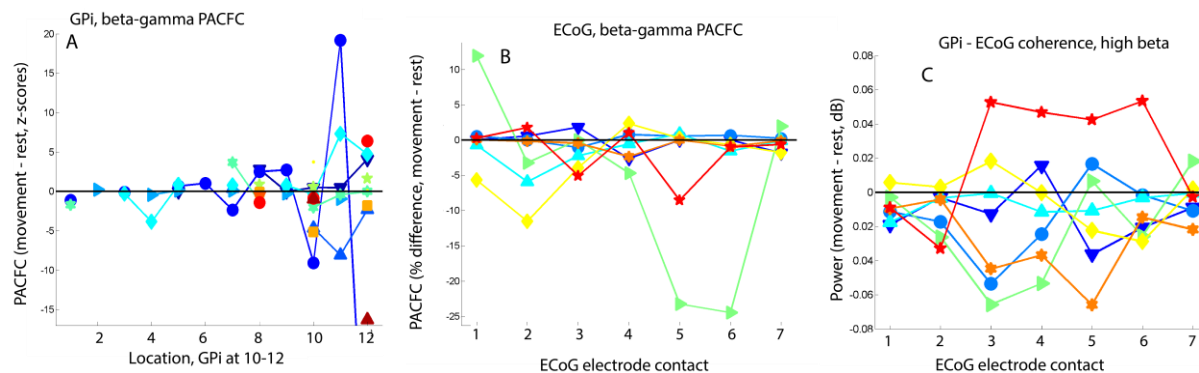


Figure 22.

Effect of movement on beta-gamma PACFC. A) Magnitude of beta-gamma PACFC in the GPi during movement compared to rest. Negative values indicate a reduction in coupling strength during movement while positive values an increase. For the overall population, there is not a significant trend towards positive or negative values. However, the windowed analysis revealed that for some subjects the difference was significant (subject 1: reduction with  $p = 0.001$  in MON configuration, and  $p = 0.056$  in BIP, subject 3: reduction with  $p = 0.024$  in BIP, subject 7:  $p = 0.014$  in BIP. All other results did not show significant changes in movement. Only a reduction in beta-gamma PACFC with movement was significant and not the observed increases. B) Similar to A but for the ECoG strip. During movement all subjects showed a decrease in PACFC z-scores by at least 2.0 except for subject 3. However, in the monopolar configuration even that subject had a drop of 2.8. C) Movement also had a significant effect in the high beta band coherence between GPi and ECoG locations. Except for subject 11, high beta coherence decreased across multiple ECoG contacts. Coherence in other bands did not change significantly.



### *3.2.6) PACFC within the motor cortex during movement*

The sites with maximal beta – low gamma PACFC showed significant reductions in magnitude with movement (  $p < 0.05$ ), while the theta – beta PA-CFC appeared to either stay the same or change in either direction depending on the subject. In addition, the theta – beta pair was not always near MRSs.

Beta-gamma PACFC decreased (Table 3) by approximately the magnitude of PACFC during rest, indicating that coupling was abolished. In cases in which PACFC was very high (subjects 5, and 7) the reduction could also be determined to be significant through the intra-subject windowed analysis ( $p\text{-value} < 0.00012$ ).

In addition to its weak PACFC, the 3<sup>rd</sup> subject also had the lowest amount of power changes with movement. The 3<sup>rd</sup> site displayed a change of zero, although using the magnitude squared method, which yielded the most significant results in this case ( $p\text{value} = 0.00054$ ), there was a 22% decrease in power with movement. The weak PACFC and power changes in that subject could be indicative of a poor overlap of the ECoG strip over the motor area for finger movements.

## 4. Discussion

### 4.1. 200 – 300 Hz oscillations in the GPi

Our findings indicate there is increased high  $\gamma$  (200-300 Hz) activity in the GPi of patients undergoing DBS for PD that is movement-modulated. We characterized the peak in that range, which had an average center frequency of  $234 \pm 17$  Hz, and FWHM  $60 \pm 8$  Hz. The peak height was pro-kinetic in most subjects.

The results also confirmed the presence of increased  $\beta$  band in the GPi of patients with PD (Priori et al., 2002). The same study showed movement-dependent decreases in  $\beta$  band power in the STN and GPi, which contrasts with our findings. The anti-kinetic character of the  $\beta$  band has largely emerged from studies of the STN (Levy et al., 2002; Kuhn et al., 2004; Kuhn et al. 2006) with only a single report in GPi. As discussed below, the two nuclei form distinct neuronal networks for which oscillatory activity can have different neurophysiological roles.

The  $\beta$  band could have a widespread regulatory role in the signal processing cascade of the basal ganglia. As is the case with the STN and motor cortex, at the GPi it has been shown (Silverstein et al. 2003) that  $\beta$  power decreases with medication. However, unlike the STN and motor cortex, the relative position of GPi in the basal ganglia circuits as a common output for both the indirect and direct pathways may in part account for the lack of modulation by activity. Another explanation is that since  $\beta$  power is often considered as “inhibitory”, the failure to suppress it in the GPi with movement in the dopamine depleted state (MED OFF) may in fact be part of the pathophysiology of PD.

#### *4.1.1. Movement-dependent 200-300 Hz power in GPi*

Although very high  $\gamma$  power activity in the GPi has not been previously described, others have described dopamine and movement-modulated very high gamma power (300 Hz or 150-200 Hz) in the STN of PD patients (Foffani et al., 2003; Kane et al., 2009; López-Azcárate et al., 2010). Foffani et al. (2003) and López-Azcárate et al. (2010) reported movement-modulation of very high frequency rhythms (200-350 Hz, central frequency 319 Hz and 323 Hz) in the STN in the “on” state (after administration of dopaminergic therapy) with contralateral self-paced movement of a finger or wrist. Interestingly, our findings resemble a similar pattern to these findings with a comparable task. While both studies indicate a “pro-kinetic” nature of very high gamma band activity, the STN studies showed that in the “off” medication state there was little to no change in the fast rhythms with movement, in contrast to our results. One possibility is that movement-modulated very fast oscillations are present in the GPi of healthy subjects to accommodate temporal integration from the large input from the striatum and external part of the Globus Pallidus. In PD patients, the neuronal circuits in the GPi might partially or fully retain their ability to oscillate in a movement dependent manner, unlike the STN. Moreover, in the “off” state the peak center at the GPi is 235 Hz, considerably lower than the 319 Hz oscillations in the STN found by (Foffani et al. 2003) but closer to the  $265 \pm 33$  Hz STN rhythm reported by López-Azcárate et al. (2010). While both nuclei are targets for therapeutic neuromodulation, they comprise distinct neuronal circuits in the BG. Patterns of activity might have similarities among BG nuclei, but may not be easily extrapolated from one nucleus to another. To shed more light on the unique properties of the GPi further studies could compare the effect of “on” and “off” medication conditions on very fast oscillations.

#### *4.1.2. Role of high frequency activity in basal ganglia function*

GPI projections to thalamic nuclei constitutes the primary output from the BG, with the substantia nigra pars reticulata (SNpr) also being an output structure. Thalamocortical coupling has been detected in the theta and  $\beta$  band (Llinas et al., 1999; Paradiso et al., 2004; Sarnthein and Jeanmonod, 2007) and has been implicated in the preparation of voluntary movements (Paradiso et al., 2004). A possible role of high frequency oscillations in GPI could be to encode information before it is relayed to thalamic nuclei. Higher frequencies could theoretically carry more information than slower ones if they reflect an increased rate of spiking activity and the statistical characteristics of spike trains represent units of information. As explained by Theunissen and Miller (1995), with an approximate duration of 1 msec for one action potential, a 100 msec window could encode a staggering  $2^{100}$  symbols in a deterministic sense. Despite our uncertainty about the functional significance of the 200-300 Hz rhythms, it is noteworthy that they afford processing in a decreased temporal scale and that high  $\gamma$  band activity has been found in the striatum (Masimore et al., 2005; van der Meer and Redish, 2009) and STN (Cassidy et al., 2002). A similar argument that higher frequencies can process more information was also made by Foffani et al. (2003). However, the oscillatory activity might not be involved in the delivery of “messages” to the thalamo-cortical network, but rather in providing a dynamic background for cortical signal processing (Shi et al., 2004). In this scenario neuronal activity between GPI and motor cortex are likely to be coherent. Coupling between the two structures has already been demonstrated for low frequency rhythms at  $\sim 1$  Hz (Magill et al., 2000) and the alpha band (Salih et al. 2009).

Another possibility for the role of 200-300 Hz rhythms is that the temporal encoding capability might accommodate the integration of the vast input received by the basal ganglia that comes from most areas of the neocortex and the intralaminar nuclei of the thalamus (DeLong and Georgopoulos, 2011). The output nuclei of the BG (GPI, SNpr) are considerably smaller in size

and have less neurons than the main input structures (putamen and caudate nucleus). The reduction in size is accompanied by a convergence of neuronal projections, with an estimated 31 million projections in the striatum and only 229000 in the GPi (Tisch et al., 2004). This anatomical substrate seems appropriate for integration or selection of information from the input to the output structures and the result of this process could be encoded in time by the 200-300 Hz rhythms. This working model is consistent with findings that fast oscillations in the  $\gamma$  band can be observed in the GPi during movement (Cassidy et al., 2002, Brown and Williams, 2005), which possibly requires extensive integration of input from the sensorimotor cortex. It is likely that temporal coding is necessary for proper communication with the thalamus whereas the choice of neural circuits that are being activated is determined primarily by the specific intended action according to the topographic representation that can be found throughout the cortico-basal ganglia thalamo-cortical circuit (DeLong and Georgopoulos, 2011).

While considering a possible significance of the 200-300 Hz rhythms for basal ganglia coding capacity it is important to consider the possibility of increased synchronization in that frequency range being detrimental to normal function of the network. Considering the monosynaptic interactions between the GPi and the thalamus, GPi 200-300 Hz activity might contribute to motor deficits by 1) dominating over signals or other oscillations, such as  $\gamma$ , that encode information for movement execution, or 2) modulating thalamic oscillatory activity and preventing the thalamocortical network from organizing parallel cortical activities prior to onset of movement. Nevertheless, our finding that the 235 Hz rhythm is pro-kinetic suggests it might be present in the normally functioning GPi.

## 4.2. PACFC in GPi and motor cortex

PACFC in cortical areas has been observed in the human frontal (Schack, et al. 2002) and temporal lobes (Canolty, et al. 2006), the visual cortex of monkeys (Lakatos, et al 2008), and the motor cortex (Hemptonne, et al. 2013). In our study we verified the presence of beta – gamma PACFC and its strong dependence on movement in the motor cortex. In addition, cortical sites other than MRSs revealed theta – beta PACFC, which has also been previously observed (Canolty, et al. 2006, Figure 1D).

Most importantly, our findings indicate previously unreported PACFC in the GPi between three distinguishing band pairs, beta – gamma, beta – very high gamma, and theta – beta, in order of decreasing strength of modulation. A small subset of subjects indicated significant decreases in PACFC strength with movement, a high temporal correlation with coherence between GPi and motor cortex, as well as bidirectional cross-site PACFC between the two structures. The results also revealed the highly dynamic nature of PACFC in both GPi and motor cortex, and indicate that PACFC is capable of engaging most frequency bands from theta to 300 Hz. This work complements a prior animal study in the GPi (Dejean, et al. 2011) showing PACFC between 3Hz oscillations and the beta (~14Hz) and gamma (~60Hz) bands as well as human studies on the STN.

### *4.2.1) PACFC within the GPi*

The spectral analysis of GPi LFP signals revealed peaks in the power of the same bands as the motor cortex, including the beta and gamma ranges most prominently involved in PACFC of that nucleus. Those two bands were significantly higher than locations distant to the GPi in all subjects. A stark difference from the motor cortex was the presence of a 200-300 Hz component

which has been characterized in more detail previously (Tsiokos, et al. 2013). They determined that a peak centered at around 235 Hz showed increases in magnitude during finger movement. In addition, temporal correlations could be observed between PACFC and the power of bands participating in the coupling. However, a substantially lower sensitivity of PACFC detection in the windowed analysis meant that those correlations could not be derived for all subjects and conditions.

Hemptinne, et al. (2013) identified PACFC within the STN, which has also been reported by Azcarate, et al. (2010). Notably, in both studies, in the off-medication and pathological state, movement had a small effect on coupling. Such observation could underlie an inability of the diseased basal ganglia to suppress PACFC regardless of their functional state. We found that in the GPi only a few patients had significant decreases in PACFC during movement, and even for them, z-scores for PACFC were at times relatively high. In that respect, the human GPi acted similar to the STN.

Interestingly, movement has been shown to increase the peak's magnitude in the 200-300 Hz range (Tsiokos, et al. 2013) in subjects that were included in the present study, while the current results showed that for some of those subjects the extent of PACFC between the beta band and 200-300 Hz was significantly reduced ( $p < 0.05$ ). The two observations suggest a possible pro-kinetic role of the very high gamma band in the GPi, in which a release of those oscillations from the influence of anti-kinetic slower components in the beta range is essential for letting the very high gamma oscillations function normally and carry movement related tasks. The fact that the movement condition did not abolish beta-very high gamma or beta-gamma PACFC completely and in some cases even increased it, although non-significantly, could indicate an effect or cause

of PD related dysfunction. The STN results mentioned earlier are also amenable to a similar interpretation.

In contrast to the motor cortex, the angle of modulation in the beta-gamma and beta-very high gamma PACFC of the GPi was not near zero. It varied without revealing an area of the circle in which the preferred angles of modulation would cluster for the subjects. However, when only subjects with the strongest coupling were considered ( $z$ -scores  $> 5.0$ ) their angles of modulation remained within a quadrant centered at around  $100^\circ$ . This observation suggests either that the amplitude of the fast frequency was highest at  $0.28 * T$  seconds after the peak of the slow oscillation occurring at 0 degrees, where  $T$  is the period of the slow oscillation, or that the amplitude of the fast oscillations was highest prior to the peak of the slow ones by  $0.72 * T$  seconds. It is tempting to consider the first one as more likely, since, if one assumes a causal relationship between the phase and amplitude, the effect of the phase must precede the impact on the amplitude. However, it remains important to consider as a possible modulator the slow oscillations in a different site (e.g. the motor cortex) that are coherent to the slow oscillations of the GPi thereby making it appear as if the coupling is caused locally in the GPi.

#### *4.2.2) PACFC within the motor cortex*

A spectral analysis of the ECoG signals revealed those electrode contacts that were maximally responsive to movement for all subjects, as seen by reductions in the power of the high beta band with movement. Those contacts were shown to overlap with sites of maximal beta – gamma PACFC or be in close proximity (Table 3). In the latter case, it was shown that maximal beta – gamma PACFC always corresponded to sites whose high beta band was reduced with



movement. The spectral analysis also verified the presence of oscillations that were seen to be involved in PACFC of the motor cortex, of which the most prevalent were low and high beta, and low and high gamma bands. Unlike the GPi, the motor cortex displayed neither any peaks in the 200-300 Hz range nor any coupling with that band.

A recent report (Hemptinne, et al. 2013) examined the motor cortex and subthalamic nucleus (STN) for PACFC in three pathological conditions, PD, dystonia and epilepsy. It was suggested that the strong beta-gamma coupling for PD, but not for epilepsy patients, is a sign of a pathophysiological role of the coupling. Similarly, the movement dependent beta – gamma coupling seen in the present study for all PD subjects, although in varying degrees, could be the result, or an agent of the pathological condition. However, we did not have non-PD patients to use as controls, as our main focus was a characterization of the GPi that was only accessible for PD patients undergoing DBS surgery.

The angle of modulation in beta – gamma PACFC for all subjects was approximately within a quadrant centered at zero, which meant the faster oscillations assumed their highest values during the peak of the slower oscillations with only a small lag or lead. Assuming higher amplitudes of the slow frequency network cause a neuronal membrane depolarization that favors excitation of the fast frequency network, the small lead or lag in the modulating angle could mean the two oscillators are occupying highly overlapping volumes in space. Such co-existence would facilitate an immediate impact of the phase of the beta band on the amplitude of the gamma band through a short synaptic pathway or diffusion of depolarization in the extracellular space.

Results discussed next indicate the presence of bidirectional beta-gamma coupling between the motor cortex and GPi, although at much lower magnitudes in comparison to the local coupling of either site.

#### *4.2.3) Bidirectional PA-CFC between GPi and motor cortex*

The involvement of PACFC in the communication between the motor cortex and the GPi was first examined by measuring the temporal correlation between coherence of the two areas and local PACFC for motor cortex and GPi, which was made possible using non-overlapping 6 second windows to create a time series for the two metrics. Necessarily, several subjects had to be excluded from that analysis when the presence of PACFC was very weak during the 6 second periods, effectively yielding z-scores close to 0 for which fluctuations were random, and also because coherence required both ECoG and DBS simultaneous recordings.

However, in three subjects examined, coherence for at least one band from low beta to high gamma had a correlation greater than 0.4 with the beta-gamma PACFC from the motor cortex (Figure 19B). The same was true between that coherence and beta-gamma PACFC from the GPi in three out of four subjects examined, although in one of those subjects the strong correlation was for coherence in the alpha band (Figure 15B). A concern was that the small number of samples ( $7 \leq n \leq 11$ ) could yield high correlation even between random time series. However, it was unusual to observe a correlation of 0.4 or above that did not indicate a pattern of positive influence between the two time series (Figure 15 and 19, C1-C4 in each). Overall the results suggested that when beta-gamma PACFC in either nucleus was observable in a smaller time scale it influenced or was influenced by concurrent oscillations in the two sites. This observation implicates local coupling into the network dynamics and cross-site communication.

PACFC between the motor cortex and GPi with either one providing the slow oscillations and the other the faster oscillations was appreciably weaker than local coupling and observable

only in a few subjects (Figure 21). Among them, subject 11 was the most interesting as its cross-site beta-gamma PACFC scores were high in both directions (z-score for motor cortex – GPi: 16.77, Figure 21 B1, B3-B5, and for GPi – motor cortex: 13.53, Figure 21 A1, A3-5). The bidirectional relation between the two sites could indicate a state of strong functional integration of network components in which oscillations are coherent among the structures and nested within each other.

## 5. Future directions

### 5.1. GPi features in a broader context of tasks and brain nuclei

LFP recordings in the GPi were made only in the MED OFF state and without deep brain stimulation (STIM OFF), two factors that might modulate the 200-300 Hz band power. Consequently our findings are amenable mostly to interpretation of how the GPi functions in the MED OFF and STIM OFF conditions in PD patients. Future efforts should evaluate differences between the OFF and ON states. Rouse et al. (2011) and Stanslaski et al. (2011) have implemented implantable devices capable of concurrent sensing and stimulation. While interpreting results from these experiments it is important to consider the differential effect that acute and chronic dopamine (DA) depletion can have on the presence of oscillations. Some animal studies (Mallet et al., 2008; Degos et al., 2009) have shown that pathological oscillations appear mostly in chronic DA depletion and that PD symptoms can precede any observable disturbances in oscillatory activity. A link between DA medication or DBS stimulation and 200-300 Hz oscillations could implicate the latter with PD dysfunction and comprise a physiological characteristic of the disease that should be included in models of BG functionality.

Further suggestions include an examination of the GPi fast rhythms in the broader context of the cortico-basal ganglia-thalamocortical network. An appealing reason for looking at directional coupling between the GPi and thalamo-cortical network in the form of nested frequency components is that the 200-300 Hz rhythms of the former might be coherent to very high oscillations (600-1000 Hz) that have been observed in the latter as somatosensory evoked potentials (Gobbelé et al., 2008). Finally, as it has been done in studies testing for coherence between unit recordings and LFP in the  $\beta$  band (Goldberg et al., 2004), similar experiments but

focused on the 200-300 Hz rhythms could elucidate how closely network activity can be predicted from spike discharges.

## 5.2 Basal ganglia modeling for closed-loop DBS

Despite the relative success of DBS more could be done in terms of treatment if there was a deeper understanding of spectral content and extent of CFC in the BG. Currently, the selection of the site of stimulation and the stimulation parameters are empiric. Moreover, once the stimulation parameters (e.g. frequency, pulse width/amplitude) have been selected, they remain constant until a reassessment of the patient is made. Not only does the treatment lose its effect over time, but it might not have an optimal short term outcome due to the fact that brain dynamics are being disregarded. Brain function, including that of the BG is influenced by a multitude of time-dependent factors such as mood, movement, and its prior state, which might require a configuration of DBS that adapts to changes in brain dynamics. Such system has to be closed-loop.

In this discussion we only consider closed-loop systems that incorporate a setpoint, that is, a reference value corresponding to a therapeutic state. We first discuss the simpler case of a single reference point with a compensator having fixed parameters.

High frequency stimulation can be viewed as an electrophysiological lesion that “shuts down” the deleterious synchronized activity of a nucleus. After the stimulation waveform parameters have been set, DBS acts as an on/off switch. However, it might be possible to restore the lost functionality by stimulating the target nucleus based on a state-space model of the basal ganglia in order to force a feature to attain a value believed to be present only in a therapeutic state. This value would constitute a desirable reference point the compensator attempts to bring

the controlled variable closer to. Two limitations are the assumption that the disease manifestation can be attributed to a feature that used to be constant at a reference level in a normal state, and that restoring the value of that feature is sufficient to restore basal ganglia functionality. This suggestion seems less plausible if the effect of the disease is not limited to exaggerated oscillations, but has its roots in the loss of neuronal organization which prevents proper information processing.

A model for a closed-loop system that contains multiple modes of operation of the basal ganglia can be utilized to partially account for the non-linear characteristics of the system and in order to reflect the fact that the subcortical motor network has to facilitate a wide range of motor tasks. That model could be used to address the need for generating a variety of patterns depending on the context of what needs to be accomplished. For example, prior to movement initiation, the reference point could constitute high suppression of beta power, while during continuous execution of movement might call for concurrent beta suppression and gamma power increase. The advantage compared to the single setpoint closed-loop compensation is that it opens the door for treatment even when the functionality to be replaced varies widely depending on motor goals. A significant limitation is that the need for multiple desirable setpoints requires a mechanism to obtain some indication of the overall goal of cortico-basal ganglia activity in order to dynamically adjust the setpoint. Those indications could be obtainable from motor-planning cortical areas or sites in the basal ganglia, including those at the stimulation site.

The two closed-loop DBS models described so far contain compensators with fixed parameters. However, those scenarios leave out the possibility that the neurophysiological counterpart of the compensator that is being “replaced” itself is undergoing dynamic changes in order to accommodate differing goals. In that case, in a similar manner to how the overall goal of the motor circuits is determined to decide on a setpoint, the compensator parameters could be

updated to reflect the engagement of the proper neuronal network. Essentially, those changes could take place based on parameters that are predetermined and stereotyped from information gained through subjects without motor deficits such as epilepsy patients.

### 5.3 Incorporating PACFC into closed-loop DBS

PA-CFC as a possible mechanism of information processing in the basal ganglia would be expected to be highly dynamic in order to accommodate the time-varying goals of the cortico-basal ganglia circuits. We discuss two ways in which a measure of PA-CFC could be used in closed-loop DBS such that it might confer an advantage to current practices.

In closed-loop DBS architectures with a fixed compensator or a finite number of compensators, as mentioned earlier, the goal is to discover one or more reference points that if a controlled variable converges to it provides the patient with optimal motor capability. A PA-CFC metric obtained from one or more nuclei could be used in order to i) select the compensator and reference point that best describe the task the BG are attempting to carry out, and ii) as a reference point itself.

PA-CFC as a metric that points to a mode of operation might exist in the motor planning areas of the cortico-basal ganglia network. Possible target areas could be the prefrontal cortex due to its executive control over behavior and the anterior cingulate cortex as it can detect when actions have been made in error (M.F.S. Rushworth, et al. 2004). However, it is worth emphasizing that the exact contribution of distinct network nodes such as the striatum or premotor cortex in carrying out motor tasks is still under debate, partly due to interconnected and closed-loop circuits involved in those processes.

PA-CFC as a reference point in a closed-loop DBS system would be most useful if there exists a one-to-one relation between that metric and the pathological state of the patient. Studies discussed earlier have revealed a link between PA-CFC and motor dysfunction in the STN and motor cortex. Currently, it is not known whether this type of coupling causes PD symptoms. In a similar manner that aberrant oscillations have been shown to be present in chronic but not in early stages of dopaminergic depletion (B. Degos, et al. 2009), it could be the case that nonlinear interactions between oscillations do not appear before pronounced synchronization sets in. This scenario would lend credence to the hypothesis that coupling is a mere consequence of plastic changes in the BG networks that take place over time, and reducing the presence of oscillations would not, in turn, benefit the patient. This subject is under debate due to very well established correlations between synchronized activity and the pathological state in Parkinson's disease at the cellular and systems level in multiple species.

If we accept that late symptoms of PD are accounted for by different mechanisms compared to early symptoms and that pronounced rhythms are the root cause of BG dysfunction, it is more likely that coupling between the oscillations can give us some information about the state of the patient. Discovering PA-CFC patterns that are beneficial to patients would be a key milestone on the way towards closed-loop DBS. Such patterns could be stereotypic and cover a large proportion of the affected population, or patient-specific, in which case off-line or real-time calibrations steps would be needed. The case of real-time adjustments would fall under the category of closed-loop DBS with a continuously updated reference point to reflect a desired goal of the motor system as discussed earlier. After desirable reference points or methods to obtain them in real-time have been established the next logical step would be determining whether they are controllable. This task requires a state space representation of BG functionality, possibly with multiple inputs to reflect



the distributed effects of dopamine depletion in BG nuclei. The operation of the closed-loop DBS would be to deliver excitatory or inhibitory electric pulses at a particular rate, pattern and shape to one or more nodes such that the desirable PA-CFC at the same or different nodes can be obtained.

## 6. Conclusion

Movement-dependent 200-300 Hz power in the GPi of patients with PD has been identified, providing additional material to consider in the complex model of BG physiology and pathophysiology. It is unknown how the 110-150Hz stimulation frequency of DBS in the GPi or STN of PD patients has a therapeutic outcome. It is noteworthy that the second harmonic of typical choices for stimulation frequency is included in the 200-300Hz range and (Foffani et al., 2003) notes a possible link between them. If the high frequency oscillations are strongly correlated with PD symptoms they might be a good choice for a controlled variable in closed-loop DBS. Moreover, the peak at 235 Hz could serve as intraoperative confirmation of the correct placement of an electrode.

Our study identified the presence of three distinct types of PACFC in the human GPi: beta - gamma, beta – very high gamma and theta – beta. Of those beta-gamma PACFC was the strongest. Movement seemed to have an effect on beta-gamma as well as beta – very high gamma and at times it caused significant reductions in coupling. Coupling was highly dynamic, as revealed by time series in which PACFC was computed in 6 second intervals. Strong PACFC (mostly beta-gamma) was also shown to be a part of mechanisms transcending the local sites, as evidenced by its correlation to coherence between the GPi and motor cortex and bidirectional cross-site coupling.

All results are pertinent to PD patients and the extent to which PACFC in the GPi is responsible for or an outcome of pathology remains an open question. Suggested goals for the near future are a close examination on dynamic features of PACFC and their relation to the pathological state either by administration of L-dopa or by measuring a concurrent index of pathology, such as amount of trembling during rest. In addition, research on animal counterparts presents the

opportunity to study healthy subjects as well as models of the disease, and has already shown delta-beta or delta-gamma coupling during rest (Dejean, et al. 2011). The findings can also be incorporated into computational models to account for the differences between basal ganglia nuclei in terms of oscillatory activity.

## 7. Appendices

### 7.1 PACFC algorithm

Three algorithms are shown here that share the common goal of detecting PACFC. They were used in preliminary stages of our study. All the experimental results presented in the main text of the manuscript are based on the first of these algorithms. The frequency components of a signal sometimes interact with each other and one type of those interactions is called phase-amplitude modulation or phase-amplitude CFC (PACFC). We use the abbreviations CFC and PACFC interchangeably since we only consider phase-amplitude coupling. During CFC, the coupling of frequencies occurs when the instantaneous amplitude of one frequency (IAF) is dependent on the instantaneous phase of another frequency (IPF). In other words, for certain values of an IPF there is a tendency of an IAF to be higher or lower than baseline values.

The first algorithm makes use of relative entropy between two distributions (Tort, 2010). The second one combines the time series of an IPF and an IAF together to form the composite signal  $Ae^{i\varphi}$  in which  $A = IAF$  and  $\varphi = IPF$ . This signal estimates the CFC by measuring the divergence of the resulting plot from circular symmetry (Canolty, 2006). The provided references contain detailed information on both algorithms. The third algorithm is based on conditional entropy and measures the strength of dependence between the random variables IPF and IAF. In particular, what is being estimated is the dependence of the instantaneous amplitude of one frequency on the instantaneous phase of another.

### 7.1.1) Method of relative entropy

Shannon entropy is defined as the expected value of the information content of a random variable  $X$ . The information content,  $I(X)$  is a measure of the uncertainty that is associated with an event  $X=x_i$ .

$$I(X) = -\log_n(p(x_i))$$

$$H(x) = E(I(X))$$

$$H(X) = \sum_{i=1}^n p(x_i) I(x_i) = -\sum_{i=1}^n p(x_i) \log_n(p(x_i))$$

For the base of the logarithm  $n$  frequently used values are 2,  $e$  (Euler's number) or 10. However, if the entropy is normalized by its maximum value  $\log(N)$ , where  $N$  is the number of elements in the probability distribution  $p(X)$ , the choice of base does not make a difference.

For two probability mass functions  $p(X)$  and  $q(X)$ , the relative entropy of  $q$  with respect to  $p$  is defined by

$$H(p; q) = -\sum_{i=1}^n p(x_i) \log_n(q(x_i)) + \sum_{i=1}^n p(x_i) \log_n(p(x_i)) = \sum_{i=1}^n p(x_i) \log_n\left(\frac{p(x_i)}{q(x_i)}\right)$$

If  $p$  and  $q$  are equal, their relative entropy is zero. The CFC algorithm calculates the divergence of a distribution that will be described shortly from the uniform distribution with pmf  $q(X) = 1/N$ .

Therefore the relative entropy of  $q$  with respect to  $p$  is

$$H(p; q) = \sum_{i=1}^n p(x_i) \log_n\left(\frac{p(x_i)}{1/N}\right)$$

In this case the relative entropy attains its maximum value when  $p$  is a pmf with 0 entropy. In other words  $p(x_i) = 0$  except for one value of  $X$ , say  $x_k$  for which  $p(x_k) = 1$ . Therefore the maximum value is

$$\max(H(p; q)) = \log_n(N)$$

Since during CFC detection we will be comparing a distribution always to the uniform distribution we can obtain the normalized relative entropy by

$$H(p; q) = \sum_{i=1}^n p(x_i) \log_n \left( \frac{p(x_i)}{1/N} \right) / \log(N)$$

We examined relative entropy as a metric for the ‘distance’ between two distributions. However, this is only one step in the CFC detection process. All of them together are listed as follows

1. The LFP signal is filtered to extract its individual frequency components. The type of filter that can be used is either FIR or IIR and is called a resonator.
2. Looking at two different frequency components at a time, we obtain the instantaneous phase time series of one (IPF) and the instantaneous amplitude time series of the other (IAF). The extraction of the instantaneous phase and amplitude is accomplished by the Hilbert transform.
3. A number of bins are assigned to the range  $-\pi$  to  $\pi$  (the range of the IPF). Then in each individual bin we add the values of all the amplitude points from IAF that occurred while IPF was within the range of that bin. For example, if we create 20 bins the first one has range  $-\pi$  to  $-\pi + 2\pi/20$ .

4. After finding the sum of the amplitude values within each bin, we divide all of them by the total sum of amplitudes, thereby creating a probability mass function. Therefore, adding up all the bin amplitudes yields the value one. This distribution is then compared to the uniform distribution using the relative entropy metric that was explained earlier.
5. The obtained relative entropy is normalized by  $\log(N)$ , where  $N$  is the number of bins that were used.
6. Finally to determine the level of significance of the result we calculate a z-score for the measured level of coupling against a population of surrogate data that differs only by a random circular shift in time between the IAF and IPF. For those surrogates CFC is computed and is considered to reflect a baseline value for which coupling does not exist. This poses an important limitation on how small the time series is, as smaller amounts of shifting are more likely not to lose coupling between IAF and IPF if it is present. In the windowed analysis in which each time segment lasted only 6 seconds, we circumvented that problem by keeping the IAF constant and selecting the IPF from distant time points (e.g. 20 seconds lag or lead) when generating surrogates.
7. This process is repeated for all the IPF-IAF pairs we were interested in and finally a matrix of CFC values was obtained.

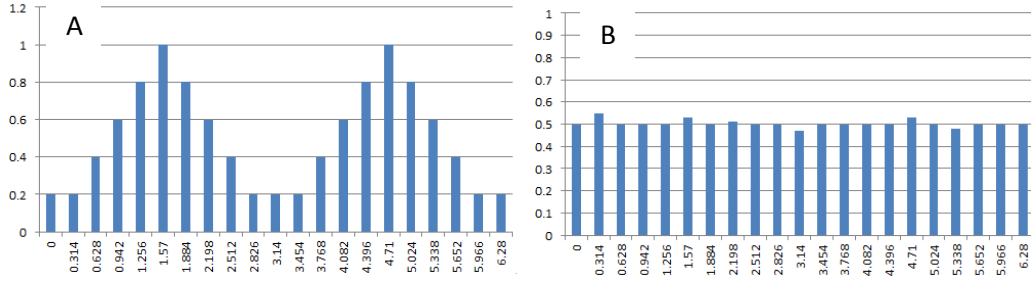


Figure 23.

A) Coupling between the phase of a frequency and the amplitude of another. The amplitude (y axis) depends on the value of the phase (x axis). B) Lack of phase-to-amplitude coupling. The amplitude (y axis) is about the same regardless of the value of the phase (x axis).

### 7.1.2) PACFC using a composite signal

Another method of CFC detection is to combine the two time series IAF and IPF in order to form the composite signal  $C = IAF \times e^{-j \cdot IPF}$ . If this signal is plotted in a coordinate system with the x axis corresponding to the real part  $\text{Re}\{C\}$ , and the y axis to the imaginary part  $\text{Im}\{C\}$ , as the time index increases the vector  $C$  rotates around the origin in a counter-clockwise direction. The phase of that vector is the value of the IPF at a specific time point, while its amplitude is the value of IAF. Suppose that all the points of  $C$  are plotted for several full rotations of the composite signal. If the amplitude is not modulated by the phase we would expect the distribution of points to be nearly circularly symmetrical. If, on the other hand, the IAF tends to have higher values at specific phase intervals, the vectors of  $C$  at those values will have a larger magnitude. This would result in a deviation from the circular symmetry. An example of a coupled IPF-IAF pair is shown in Figure 24A.



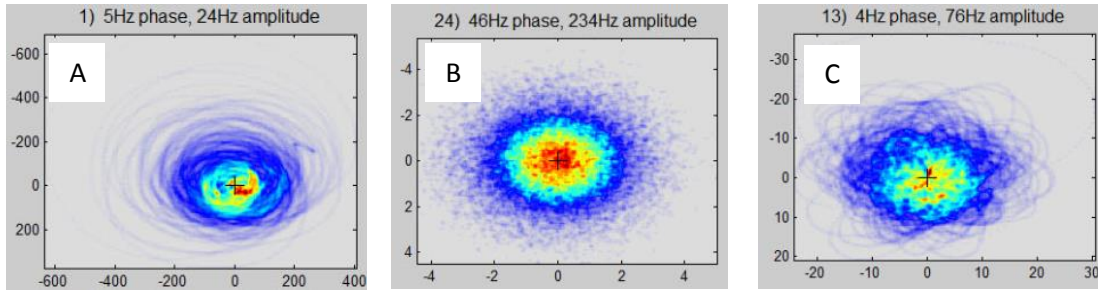


Figure 24.

Circularly symmetric and asymmetric composite signals. For the plot on the left, the magnitude of the composite signal vectors is higher in the second quadrant than in the fourth quadrant. The second appears to be symmetric. A possible coupling in the third plot cannot easily be seen by visual inspection.

Using the composite signal we can obtain a numerical measure of the degree of coupling. When all the vectors are added up we would see a relatively small magnitude for the resulting vector if there is circular symmetry. If, however, there is a tendency towards higher amplitudes in a particular phase interval, the resulting vector will have a larger magnitude. However, this method will not detect CFC if increases in the amplitude happens in equidistant phase values in such a way that the vectors cancel each other out. For example, high modulation at  $\pi$  and  $-\pi$  would be cancelled out due to the opposite sign of the large vectors. Therefore, when constructing a composite signal caution should be exercised and one needs to be aware of the number of peaks present in one period of the slow oscillation.

### 7.1.3) PACFC using conditional entropy

Conditional entropy is defined as the entropy of a random variable  $Y$  given that we know the random variable  $X$  has a particular value, i.e.  $X=x_i$

$$\begin{aligned} H(Y | X) &= \sum_{x \in X} p(x) H(Y | X = x) = \\ &= - \sum_{x \in X} p(x) \sum_{y \in Y} p(y | x) \log(p(y | x)) \\ &= - \sum_{x \in X} \sum_{y \in Y} p(x) p(y | x) \log(p(y | x)) \\ &= - \sum_{x \in X} \sum_{y \in Y} p(x, y) \log \left( \frac{p(x, y)}{p(x)} \right) \\ &= \sum_{x \in X} \sum_{y \in Y} p(x, y) \log \left( \frac{p(x)}{p(x, y)} \right) \end{aligned}$$

This entropy is calculated as the expected value of the entropy of  $Y$  given  $X = x$ . The entropy of  $Y$  given  $X = x$  is the expected value of  $-\log(Y|x)$  for all  $y$ , given  $X = x$ . Therefore the calculation involves finding entropies associated with certain values of  $X$  and then averaging these values using  $p(x)$  as a weighting function.

It can also be shown that

$$H(Y | X) = H(Y, X) - H(X)$$

If  $Y$  does not depend on  $X$ , then  $H(Y|X) = H(Y)$ . Therefore the conditional entropy simply reduces to the entropy of  $Y$ . In that case we also note that  $H(Y, X) - H(X) = H(Y)$ . Therefore this difference has a maximum value  $H(Y)$ , which it attains when  $Y$  is independent of  $X$ .

If, on the other hand, Y is completely dependent on X, (X defines Y deterministically), then  $H(Y|X) = 0$  since for given values of X there is absolute certainty about the values Y will take. For any degree of dependence of Y on X we have

$$\begin{aligned} 0 &\leq H(Y | X) \leq H(Y) \\ 0 &\leq H(Y, X) - H(X) \leq H(Y) \\ 0 &\leq \frac{H(Y, X) - H(X)}{H(Y)} \leq 1 \end{aligned}$$

Also, to find  $H(Y, X)$  we use the formula of Shannon entropy

$$H(Y, X) = -\sum_{x \in X} \sum_{y \in Y} p(y, x) \log(p(y, x))$$

One way to describe how much Y depends on X is by finding the difference  $H(Y, X) - H(x)$  and then normalizing the result in order to obtain values from zero to one.

To return to the discussion on CFC detection, let the random variable X be the IPF value at a time point and the random variable Y be the IAF value at the same time point. Since we are interested in the dependence of IAF values on IPF values, we need to calculate the dependence of Y on X. First we need to construct the joint probability distribution  $p(Y, X)$  by making several simultaneous observations from the two signals, assigning them to quantized values and then dividing the entire matrix of those values with the total sum in order to satisfy the definition of a probability distribution. The resulting matrix is a joint probability mass function of Y and X as shown in the picture below. After calculating the Shannon entropy of the joint distribution  $H(Y, X)$  and the entropy of the marginal probabilities of Y and X,  $H(X)$  and  $H(Y)$  respectively, the formula on the right side is used the result.

$$0 \leq H(Y | X) \leq H(Y) \quad \Leftrightarrow \quad 0 \leq \frac{H(Y, X) - H(X)}{H(Y)} \leq 1$$

Values close to one indicate that Y is independent of X while values close to zero indicate that they are dependent. Therefore, this can give us information about the dependence of IAF on IPF. It tells that to what extent knowledge of a phase value affects the probability mass function of the amplitude.

An example of a joint probability mass function in which the amplitude distribution appears to be less concentrated at the phase interval  $-\pi$  to 0 is shown in Figure 25A. The y axis contains quantized values of the IAF (0V to amplitude at 4 standard deviations) and the x axis quantized values of the IPF ( $-\pi$  to  $\pi$ ). The signal traces can be seen due to the relatively small number of full cycles of the IPF. Figure 25B is similar, but this time the amplitude distributions (columns) have been normalized by the baseline amplitude distribution. This baseline was selected to be the marginal probability of IAF,  $p(\text{IAF})$ . The plotting functions can help us visualize the data, but in order to obtain a numerical result about CFC we can use the conditional entropy.

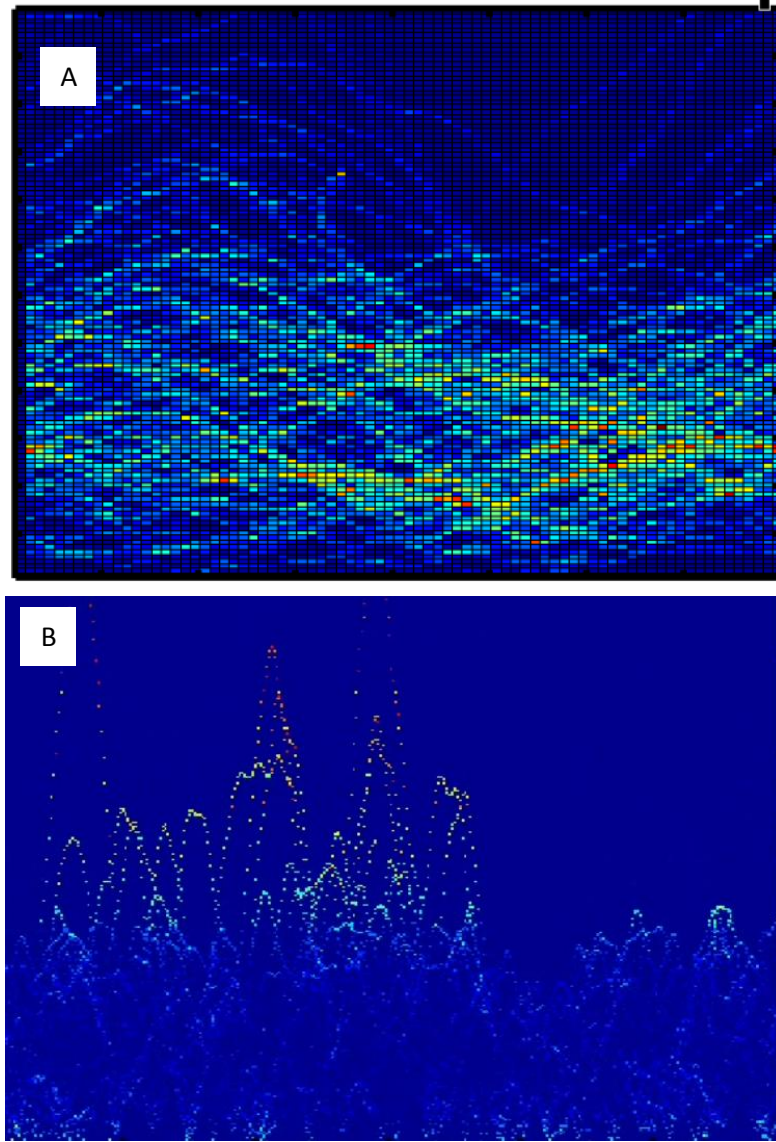


Figure 25.

A) Joint probability mass function of the random variables IAF (y axis) and IPF (x axis). In the right half of the figure the IAF has more concentrated values around the mean as opposed to the left half. 80 quantization levels were used for the IPF ( $-\pi$  to  $\pi$ ) and 120 for the IAF (y-axis from 0 volts to amplitude at 4 standard deviations of observed values). B) Normalized joint pmf of IPF (x axis) and IAF (y axis). This plot is similar to (A) but this time the IAF has been normalized by dividing it by the marginal probability for IAF. This normalization was done for all IPF values

## 7.2 PACFC algorithm implementation

Written in the Matlab language.

```
function out = pacfc(phase_signals, amplitude_signals, settings)
% This function is used to compute phase-to-amplitude cross frequency
% coupling
%
% Input variables -----
%
% phase_signals      -> (m x n double) The signals (one per column) from which
%                        the phase will be extracted
% amplitude_signals -> (m x n double) The signals (one per column) from which
%                        the amplitude will be extracted
%
% NOTE: For any of the settings enter [] to select default value.
% settings.SamplingFrequency -> The sampling frequency of all the signals
% settings.FilterOrder       -> Filter order. The effective filter order
%                               is twice this value since the signals are
%                               filtered once and then again backwards to
%                               ensure zero phase distortion.
%
% settings.PhaseFrequencies  -> Centers of the frequency components/bands
%                               to extract from the signals to be used in
%                               phase extraction.
% settings.AmplitudeFrequencies -> Centers of the amplitude components/bands
%                               to extract from the signals to be used in
%                               amplitude extraction.
% settings.PhaseBandwidths   -> Bandwidths for the phase components. If a
%                               scalar is entered it applies to all
%                               frequencies.
% settings.AmplitudeBandwidths -> Bandwidths for the amplitude components.
% settings.PhaseLocations    -> The column index of the settings.phase
%                               variable.
% settings.LocationsMask     -> In a matrix whose elements correspond to
%                               pairs of 'PhaseLocations' (rows) and
%                               'AmplitudeLocations' (columns) use 1 to
%                               include the pair into the computations and
%                               0 otherwise.
% settings.AmplitudeLocations -> The column index of the settings.amplitude
%                               variable.
% settings.Blocks            -> (m x 2 double) The indices (in samples)
%                               with the beginning (left column) and end
%                               (right column) of each block of analysis.
% settings.BlocksMask        -> In an array use 1 for the blocks you wish
%                               to analyse and 0 otherwise.
% settings.WindowLength      -> The window length to be used when the data
%                               is windowed
% settings.WindowStep        -> The number of samples to move the window
%                               after the first segment is analysed. Set
%                               this step to a number longer than your
%                               signal length to run only the first
%                               segment.
% settings.UseTruncation      -> (bool) Truncate signals after filtering.
%                               The signal is truncated before windowing
%                               and therefore only the segments at the
```

```

% edges are affected.
% settings.Truncation -> (double [0 - 0.5]) Amount of truncation
% at each edge given as a proportion of the
% entire signal length.
% settings.NumberOfBins -> How many bins to create in the interval
% [-pi pi] to hold the mean amplitude values
% . Use smaller numbers, e.g. 8, 12, when
% windows tend to be too short or the phase
% frequencies are too high.
% settings.UseModifiedRelativeEntropy -> (bool) Set this to obtain a modified
% version of the relative entropy that
% considers how many peaks are in the
% distribution. The more peaks in the
% distribution the more the relative
% entropies are attenuated. Also, if the
% distribution is monotonous maximum
% attenuation is applied since it indicates
% no coupling yet yields high relative
% entropy. This setting does not affect the
% reported relative entropy; it just adds a
% new output.
% settings.ModifiedRelativeEntropyStrenght -> How much to attenuate relative
% entropies when the peak number exceeds
% one.
% settings.UseSurrogates -> Use this to recompute relative entropy for
% 'de-coupled' phase-amplitude pairs. This
% is achieved by taking a different phase
% but NOT AMPLITUDE. The phase is shifted by
% a random number
% settings.NumberOfSurrogates -> How many de-coupled pairs to compute.
% settings.UseCircularShifting -> When creating surrogates circularly shift
% the phase. Not recommended because it
% exaggerates z-scores significantly in some
% cases. This can happen the amplitude
% oscillates at the same frequency as the
% phase very regularly. Even without
% coupling this can yield a sinusoidal
% distribution. The shorter the segments and
% the smaller the phase frequency the more
% this effect takes place. The surrogates,
% on the other, will not be affected as much
% since their left and right segments after
% the circular shift are out of phase. An
% artificially high z-score is generated.
% settings.MinimumShift -> The minimum shift that should be performed
% for the phase as a proportion of its
% length when circular shifting is used.
% In small segments shifting might not
% generate "uncoupled" signals to use as
% surrogates.
% settings.SaveData -> Save the output and settings into a matlab
% variable. Data can be saved manually of
% course, but because this script can easily
% take hours or days to complete you might
% want to output the data to a folder you
% can access online when you are away (e.g.
% google drive or dropbox folder).
% settings.Title -> Name to be used to save all the data.

```

```

% settings.Directory          -> The directory in which to save the file.
%                             Do not use \ in the end
%                             (e.g C:\myfiles\matlab). It can also be
%                             relative to the current workspace. If an
%                             error occurs a file named as the error
%                             message will be written here.
% settings.UseProgressBar    -> Enable the progressbar (for this to work
%                             you need Steve Hoelzer's routine (http://www.mathworks.com/matlabcentral/fileexchange/6922-progressbar)).
%
% Ouput variables -----
%
% out.rls                    -> ( phase_signal x amp_signal x block x window ) x
%                             ( phase_freq x amp_freq ) Relative entropy values
% out.zscores                -> Z-scores when surrogates data analysis has been done.
% out.ne                     -> Number of extrema in distribution.
% out.rcoef                  -> Modification coefficient. A metric with range [1 0) that
%                             relates to the number of extrema in the generated
%                             distributions from -pi to pi. Decrease is exponential
% out.dis                    -> The distributions corresponding to out.rls
% out.srls                   -> The relative entropy of the surrogate that ended up having
%                             the highest relative entropy value
% out.sdis                   -> The distributions corresponding to out.srls
% out.time                   -> Total time of execution.

% Example 1
if 0
    Fs = 2400;
    t = 0:1/Fs:60;
    PS = cos(2*pi*20*t)';
    AS = PS.*cos(2*pi*100*t)' + rand(length(t),1); % amplitude modulation
    myblocks = [1/Fs 62; 68 122; 128 182; 188 242; 248 310] * Fs;
    myblocks = [1118353 1263193; 1263193 1390032]; %R4, M4 110714mon
    myblocks = [1170801 1315641; 1315641 1452081]; %R4, M4 110714car
    myblocks = [1170732 1315572; 1315572 1451873]; %R4, M4 110714bip
    myblocks = [1347000 1466160; 1466160 1603199]; %R4, M4 110811mon
    myblocks = [1290239 1447079; 1447079 1596478]; %R4, M4 11120mon
    settings = struct ( ...
        'SamplingFrequency', Fs, ...
        'FilterOrder', 2, ...
        'PhaseFrequencies', [4:1:60]', ...
        'AmplitudeFrequencies', [6:1:200]', ...
        'PhaseBandwidths', 4, ...
        'AmplitudeBandwidths', 6, ...
        'PhaseLocations', [1 2 3 4], ...
        'AmplitudeLocations', [1 2 3 4], ...
        'LocationsMask', eye(4), ...
        'Blocks', myblocks, ...
        'BlocksMask', [1 1 1 1 1], ...
        'WindowLength', Fs * 5, ...
        'WindowStep', Fs * 5, ...
        'UseTruncation', true, ...
        'Truncation', 0.05, ...
        'NumberOfBins', 18, ...
        'UseModifiedRelativeEntropy', true, ...

```



```

'ModifiedRelativeEntropyStrength', 10, ...
'UseSurrogates', true, ...
'NumberOfSurrogates', 80, ...
'MinimumShift', 0.3, ...
'UseCircularShifting', false, ...
'SaveData', true, ...
'Title', 'lhm120921mon, rdbs1-1,2-2,3-3,4-4, R1,FM', ...
'Directory', 'Dropbox\0 CHRISTOS - CHRISTOS\TRANSFER\BOFA-06', ...
'UseProgressBar', true ...
);
out = pacfc(PS, AS, settings)

% Relative entropy
figure; pcolor( settings.PhaseFrequencies, ...
               settings.AmplitudeFrequencies, ...
               squeeze(out.rls(1,1,1,:,:1))');
colorbar;
set(gcf, 'Color', 'white');
xlabel('Phase frequency (Hz)');
ylabel('Amplitude frequency (Hz)');

% Modified relative entropy
figure; pcolor( settings.PhaseFrequencies, ...
               settings.AmplitudeFrequencies, ...
               squeeze(out.rcoef(1,1,1,:,:1))');
colorbar;
set(gcf, 'Color', 'white');
xlabel('Phase frequency (Hz)');
ylabel('Amplitude frequency (Hz)');

end

% -----

tic;

% Default settings if value not provided
defaultSettings = struct ( ...
    'FilterOrder', 2, ...
    'PhaseFrequencies', [2:20]', ...
    'AmplitudeFrequencies', [12 35]', ...
    'PhaseBandwidths', 1, ...
    'AmplitudeBandwidths', 2, ...
    'UseTruncation', true, ...
    'Truncation', 0.05, ...
    'NumberOfBins', 14, ...
    'UseModifiedRelativeEntropy', true, ...
    'ModifiedRelativeEntropyStrength', 10, ...
    'UseSurrogates', true, ...
    'NumberOfSurrogates', 60, ...
    'MinimumShift', 0.2, ...
    'UseCircularShifting', false, ...
    'SaveData', false, ...
    'Title', 'pacfc_results', ...
    'Directory', 'pacfc_directory', ...

```

```

    'UseProgressBar',          false ...
);
% Set default values when empty or '' -----
if isempty(settings.FilterOrder)          settings.FilterOrder          = ...
    defaultSettings.FilterOrder;           end
if isempty(settings.PhaseFrequencies)      settings.PhaseFrequencies      = ...
    defaultSettings.PhaseFrequencies;      end
if isempty(settings.AmplitudeFrequencies)  settings.AmplitudeFrequencies = ...
    defaultSettings.AmplitudeFrequencies; end
if isempty(settings.PhaseBandwidths)       settings.PhaseBandwidths      = ...
    defaultSettings.PhaseBandwidths;       end
if isempty(settings.AmplitudeBandwidths)   settings.AmplitudeBandwidths = ...
    defaultSettings.AmplitudeBandwidths;   end
if isempty(settings.UseTruncation)         settings.UseTruncation        = ...
    defaultSettings.UseTruncation;         end
if isempty(settings.Truncation)            settings.Truncation           = ...
    defaultSettings.Truncation;            end
if isempty(settings.NumberOfBins)         settings.NumberOfBins        = ...
    defaultSettings.NumberOfBins;         end
if isempty(settings.UseModifiedRelativeEntropy) ...
    settings.UseModifiedRelativeEntropy = ...
    defaultSettings.UseModifiedRelativeEntropy; end
if isempty(settings.ModifiedRelativeEntropyStrength) ...
    settings.ModifiedRelativeEntropyStrength = ...
    defaultSettings.ModifiedRelativeEntropyStrength; end
if isempty(settings.UseSurrogates)         settings.UseSurrogates        = ...
    defaultSettings.UseSurrogates;         end
if isempty(settings.NumberOfSurrogates)    settings.NumberOfSurrogates   = ...
    defaultSettings.NumberOfSurrogates;    end
if isempty(settings.MinimumShift)         settings.MinimumShift        = ...
    defaultSettings.MinimumShift;          end
if isempty(settings.UseCircularShifting)  settings.UseCircularShifting = ...
    defaultSettings.UseCircularShifting;   end
if isempty(settings.SaveData)             settings.SaveData            = ...
    defaultSettings.SaveData;              end
if isempty(settings.Title)               settings.Title               = ...
    defaultSettings.Title;                 end
if isempty(settings.Directory)            settings.Directory           = ...
    defaultSettings.Directory;             end
if isempty(settings.UseProgressBar)       settings.UseProgressBar       = ...
    defaultSettings.UseProgressBar;        end

% Length variables -----

% Lengths
np = length(settings.PhaseLocations);      % Number of contacts for phase
                                           % component.
na = length(settings.AmplitudeLocations);  % Number of contacts for amplitude
                                           % component.
nb = size( settings.Blocks,1);             % Number of blocks.
npf = length(settings.PhaseFrequencies);   % Number of center frequencies
                                           % for each phase component.
naf = length(settings.AmplitudeFrequencies); % Number of center frequencies
                                           % for each amplitude component

% if bandwidths are scalars convert them to vectors

```

```

if ( length(settings.PhaseBandwidths) == 1 ),
    settings.PhaseBandwidths = settings.PhaseBandwidths * ones(npf,1);
end
if ( length(settings.AmplitudeBandwidths) == 1 ),
    settings.AmplitudeBandwidths = settings.AmplitudeBandwidths * ones(naf,1);
end

% Windowing -----
% Estimating number of windows for preallocation of results based on the
% first block. Used to show progress and preallocate result arrays
% If the user provided a window size larger than a block, it is adjusted
% internally to not exceed the block size.
win_step = round(settings.WindowStep);
idx = min( find(settings.BlocksMask) ); % Index of first included block
first_block_length = settings.Blocks(idx, 2) - settings.Blocks(idx,1);
nWinEst = numberOfWindows(first_block_length, ...
    settings.WindowLength, ...
    win_step);

% Distributions -----
n_bin = settings.NumberOfBins; % Number of bins.
uni_dis = ( ones(n_bin,1) / n_bin ); % Uniform distribution.
dis = zeros(n_bin,1); % Distribution.

% Surrogates -----
n_sur = settings.NumberOfSurrogates; % Number of surrogates.
re_surs = zeros(n_sur,1); % Relative entropies of surrogates.
dis_surs = zeros(n_bin,n_sur); % Distributions of surrogates (to be used
    % for selecting a sample with high
    % relative entropy).
binIdxs = cell(n_bin,1); % Holds the locations of the phase signal
    % for each bin. Overwritten every time the
    % phase changes.

% Grid of bin values in range [-pi pi)
% Last index used only as a right border for the last bin and does not
% correspond to a bin unlike all other indexes
binGrid = zeros(n_bin,1);
interBinLength = 2*pi/n_bin;
for n = 1:n_bin+1 % + 1 to contain the rightmost border.
    binGrid(n) = -pi + ( (n-1)*interBinLength);
end

% Preallocate space -----

% (phase_location x amp_location x block x window x phase_freq x amp_freq)
out.rls = cell(np, na, nb, nWinEst);
out.zscores = cell(np, na, nb, nWinEst);
out.ne = cell(np, na, nb, nWinEst);
out.dis = cell(np, na, nb, nWinEst);
out.rcoef = cell(np, na, nb, nWinEst);
out.srls = cell(np, na, nb, nWinEst);
out.sdis = cell(np, na, nb, nWinEst);

```

```

for ip = 1:np
    for ia = 1:na
        if settings.LocationsMask(ip,ia) == 0, continue; end
        for ib = 1:nb
            if settings.BlocksMask(ib) == 0, continue, end
            for iw = 1:nWinEst
                out.rls{ ip, ia, ib, iw} = zeros(npf, naf);
                out.zscores{ ip, ia, ib, iw} = zeros(npf, naf);
                out.ne{ ip, ia, ib, iw} = zeros(npf, naf);
                out.dis{ ip, ia, ib, iw} = zeros(npf, naf, n_bin);
                out.rcoef{ ip, ia, ib, iw} = zeros(npf, naf);
                out.srls{ ip, ia, ib, iw} = zeros(npf, naf);
                out.sdis{ ip, ia, ib, iw} = zeros(npf, naf, n_bin);
            end
        end
    end
end
end

% --- COMPUTE CFC -----

pbr = settings.UseProgressBar;

if pbr; progressbar('Phase Electrode','Amplitude Electrode',...
    'Block','Freq. of phase', 'Freq. of amplitude',...
    'Window segment'); end
for ip = 1:np % Electrode location of phase source.
    for ia = 1:na % Electrode location of amplitude source.
        % Skip locations according to mask.
        if settings.LocationsMask(ip,ia) == 0, continue, end
        for ib = 1:size(settings.Blocks,1); % Experimental block.
            % Skip blocks according to mask.
            if settings.BlocksMask(ib) == 0, continue, end
            for ifp = 1:npf %Phase frequency -----

                ticPhaseFrequency = tic;

                %Design and implement filter
                hpeak = fdesign.peak('N,F0,BW', settings.FilterOrder, ...
                    settings.PhaseFrequencies(ifp), ...
                    settings.PhaseBandwidths(ifp), ...
                    settings.SamplingFrequency);
                flt_p = design(hpeak, 'butter','SOSScaleNorm', 'Linf');
                warning('off','signal:filtfilt:ParseSOS');

                %Apply filter to data.
                phase_signal = phase_signals( settings.Blocks(ib, 1) : ...
                    settings.Blocks(ib,2), ...
                    settings.PhaseLocations(ip) );
                filtered_ts_p = filtfilt(flt_p.sosMatrix, flt_p.Scalevalues, ...
                    phase_signal );
                phase = angle( hilbert( filtered_ts_p ) ); % Phase of slow osc.

                % Optional truncation.
                if settings.UseTruncation

```

```

    % Length of truncation.
    lt = round( settings.Truncation * length(phase) );
    phase = phase( lt : end-lt);
end

% Window length for this series.
if settings.WindowLength > length(phase),
    iWinLength = length(phase); % Prevent overshooting.
else
    iWinLength = settings.WindowLength; end % No change.
n_win = numberOfWindows( length(phase), iWinLength, win_step);

for ifa = 1:naf %Amplitude frequency -----
    % Skip frequencies for amplitude less than frequencies for phase.
    if settings.AmplitudeFrequencies(ifa) <= ...
        settings.PhaseFrequencies(ifp), continue;
    end

    %Design and implement filter
    hpeak = fdesign.peak('N,F0,BW', settings.FilterOrder, ...
        settings.AmplitudeFrequencies(ifa), ...
        settings.AmplitudeBandwidths(ifa), ...
        settings.SamplingFrequency);
    flt_a = design(hpeak, 'butter','SOSScaleNorm', 'Linf');

    %Apply filter to data
    amplitude_signal = amplitude_signals(settings.Blocks(ib,1) : ...
        settings.Blocks(ib,2), ...
        settings.AmplitudeLocations(ia) );
    filtered_ts_a = filtfilt(flt_a.sosMatrix, flt_a.Scalevalues, ...
        amplitude_signal );
    amplitude = abs( hilbert( filtered_ts_a ) );

    % Optional truncation ( length of truncation was computed earlier
    % for phase, which should have the same length as amplitude).
    if settings.UseTruncation,
        amplitude = amplitude( lt : end-lt);
    end

    for iw = 1:n_win % Window -----

        left = 1 + (iw-1) * win_step; % Left limit index.
        right = iWinLength + (iw-1) * win_step; % Right limit index
        iphase = phase( left : right ); % Phase segment.
        iamp = amplitude( left : right ); % amplitude segment.

        for ibin = 1:n_bin
            iii = find((iphase > binGrid(ibin) ) & ...
                (iphase <= binGrid(ibin+1)) );
            binIdxs{ibin} = iii; % *** NOTE *** Indexes are saved so they
            % do not need to be recalculated when
            % using surrogates.
            dis(ibin) = mean( iamp( iii ) );
        end
        % Normalizing distribution such that its values add up to one.
        dis = dis ./ sum(dis);
    end
end

```

```

% Relative entropy (Kullback-Leibler divergence of current
% distribution from uniform distribution).
re = sum( uni_dis .* log( uni_dis ./ dis ) );
% Relative entropy (Kullback-Leibler divergence of uniform
% distribution from current distribution.
% re = sum( dis .* log( dis ./ uni_dis ) );

% (block x frequency_of_phase x
% frequency_of_amplitude x bin_number)
out.dis{ip, ia , ib, iw}{ifp, ifa, :} = dis;
out.rls{ip, ia , ib, iw}{ifp, ifa} = re;

% optional search for extrema
if (settings.UseModifiedRelativeEntropy == true)
    nExt = numberOfExtrema(dis);
    out.ne{ip, ia, ib, iw}{ifp, ifa} = nExt;
    if nExt == 0
        warning(['The series is monotonic. If this series is a '...
            'distribution for computation of relative entropy '...
            'in cross-frequency coupling it will yield a high '...
            'relative entropy value without coupling actually '...
            'being present']);
        out.mrls{ ip, ia, ib, iw}{ifp, ifa} = 0;
    else
        % The cases of having 1 or 2 extrema are treated the same
        % since they reflect a sinusoid, peak or valley in the
        % distribution.
        if nExt == 1
            nExt = 2;
        end
        % The more extrema, the more relative entropy is reduced to
        % reflect that with more than 2 extrema it is less likely
        % to have frequency nesting.
        % Reduction coefficient.
        out.rcoef{ ip, ia, ib, iw}{ifp, ifa} = ...
            ( 1 - ( (nExt-2) ./ (n_bin - 2 - 2) ) ) ...
            ^(settings.ModifiedRelativeEntropyStrength);
    end
end

%
% /// SURROGATE DATA ANALYSIS //////////////////////////////////////
if settings.UseSurrogates
    if settings.UseCircularShifting
        % Length of segment stretch at the center of the segment
        % where new start locations can come from to satisfy the
        % requirement for minimum shift
        tmpLength = round( iWinLength * ...
            (1 - 2*settings.MinimumShift) );
        % Random locations.
        rnd_locs = round( iWinLength * settings.MinimumShift + ...
            tmpLength * rand(n_sur, 1) );
        for is = 1:n_sur % Surrogate.
            % *** ATTENTION *** Shifting the amplitude, not the
            % phase to avoid finding phase indexes for each bin again
            iamp_shifted = [ iamp( rnd_locs(is) : end);

```

```

        iamp( 1 : rnd_locs(is)-1 ) ];
    for ibin = 1 : n_bin % Bin.
        iii = binIdxs{ ibin };
        dis_surs(ibin,is) = mean( iamp_shifted( iii ) );
    end
    dis_surs(:,is) = dis_surs(:,is) ./ sum(dis_surs(:,is));
    % Relative entropy of surrogate
    re_surs(is) = sum( uni_dis .* ...
        log( uni_dis ./ dis_surs(:,is) ) );
end
else
    % Non-circular shifting utilizes the time series the
    % segment comes from to extract surrogates by obtaining a
    % shifted segment without connecting the start and end
    % points of any original segments. Of course the shifted
    % segment has to be smaller than the available time series
    if iWinLength > 0.9*length(phase)
        warning(['The window length is larger than 90% of '...
            'the time series length. Surrogates can be '...
            'selected only from (at most) the other 10% '...
            'depending on the desirable shift amount. '...
            'Circular shifting might be preferred in this '...
            'case.']);
    end
    % 1st step in constructing a vector with indexes to choose
    % from as start locations. Removing locations at the right
    % limit within a window's length to make sure all start
    % locations will allow segments to have the right length.
    allowedIndexes = (1 : ( length(phase) - iWinLength )).';
    % How many samples to shift away (to the left or right)
    % from start of window.
    nshift = ceil( settings.MinimumShift * ...
        iWinLength );
    % Left means the left limit of the current segment. No
    % start locations allowed in this range.
    offLimitsRange = [ left - nshift, left + nshift ];
    % Do not allow the range to fall into negative values.
    % Needed for the first few windows. 0 is used instead of 1
    % to avoid selecting location 1 in the next step. 1:0
    % returns an empty matrix as opposed to 1:1.
    offLimitsRange( offLimitsRange < 0 ) = 0;
    % Remove a segment from inside the allowedIndexes vector.
    allowedIndexes = [allowedIndexes(1:offLimitsRange(1)); ...
        allowedIndexes(offLimitsRange(2):end)];
    % Select random location within the allowedIndexes vector.
    tmpRndLocs = ceil( length(allowedIndexes) .* ...
        rand(n_sur,1) );
    % Obtain the final random locations.
    rnd_locs = allowedIndexes( tmpRndLocs );
    for is = 1:n_sur %surrogate
        % *** NOTE *** To obtain more realistic measures of
        % PACFC, the amplitude series should be preserved.
        % Without windowing (using circular shifting) it didn't
        % make a difference whether the phase or amplitude was
        % shifted. Now, however, it should be the phase that is
        % shifted. A random segment is chosen.
        iphase_shifted = phase( rnd_locs(is) : rnd_locs(is) +...
            iWinLength - 1 );

```

```

        for ibin = 1 : n_bin % Bin.
            iii = (iphase_shifted > binGrid(ibin)) &...
                (iphase_shifted <= binGrid(ibin+1));
            dis_surs(ibin,is) = mean( iamp( iii ) );
        end
        dis_surs(:,is) = dis_surs(:,is) ./ sum(dis_surs(:,is));
        re_surs(is) = sum( uni_dis .* ...
            log( uni_dis ./ dis_surs(:,is) ) );
    end
end
out.zscores{ip, ia, ib, iw}{ifp, ifa) = ...
    (re - mean(re_surs)) ./ std(re_surs) ;
out.srls{ ip, ia, ib, iw}{ifp, ifa) = max(re_surs);
tmp = find( re_surs == max(re_surs) );
out.sdis{ ip, ia, ib, iw}{ifp, ifa, :) = ...
    dis_surs(:, tmp(1) );
end
%
    if pbr; progressBar([],[],[],[],[],iw/n_win); end
end % Window
    if pbr; progressBar([],[],[],[],ifa/naf); end
end % Frequency for amplitude
    if pbr; progressBar([],[],[],ifp/npf); end
    disp(['PF-' num2str(ifp) ' B-' num2str(ib) ' A-' num2str(ia) ...
        ' P-' num2str(ip) ' ' num2str(toc(ticPhaseFrequency)) ]);
end % Frequency for phase
    if pbr; progressBar([],[],ib/nb); end
end % Experimental block
    if pbr; progressBar([],ia/na); end
end % Electrode location of amplitude source
    if pbr; progressBar(ip/np); end
end % Electrode location of phase source

if settings.SaveData == true
    save([settings.Directory '\\' settings.Title], 'settings', 'out');
end

out.time = toc;

% -----
% Nested functions

%
function nWin = numberOfWindows(signalSize, windowSize, stepSize)
    if length(signalSize)~=1 || length(windowSize)~=1 || length(stepSize)~=1
        error('All inputs should be scalar')
    end
    if (windowSize < signalSize)
        nWin = 1 + floor( (signalSize - windowSize) ./ stepSize);
    else
        nWin = 1;
    end
end
end

```



```

% -----
function nExt = numberOfExtrema( series )
    % Given a series of samples this function returns the number of times
    % the series reverses sign in the difference from one sample to the
    % previous one. In essence this provides the number of extrema in a
    % discrete series. The matlab function findpeaks() finds only peak.
    % series -> (n x 1 double)

    tmp = diff(series); % Change
    tmp = tmp./abs(tmp); % Direction of change ( turns everything into 1 or -
1)
    tmp = diff(tmp); % Change of direction of change
    nExt = sum( tmp ~= 0 ); % Number of times the pattern of increase or
    % decrease changes (similar to but not the same
    % as 2nd derivative)

end

% -----

end % EOF

```

## 5.2. PACFC grid features

Written in the Matlab language.

```

function [average center_of_gravity center_average standard_deviation...
center_mask] = computeAreaFeatures( map, xValues, yValues, ...
center_rectangle_size)

% average -> (double) The average value in the area
% center_of_gravity -> (1 x 2 double) X and Y coordinates of the center of
% gravity within the xlim and ylim ranges
% center_average -> (double) The average value from samples at the center
% of gravity that fall into a circle with radius x Hz.
% standard_deviation -> (1 x 2 double) Std across the X and Y slice at the
% center of gravity

% map -> (n x m double) The map
% xlim -> (1 x 2 double) The range to consider along the x axis
% ylim -> (1 x 2 double) The range to consider along the y axis
% center_rectangle_size -> (1 x 2 double) The widths for the x and y
% coordinates with center the center_of_gravity that
% will be used to take samples in order to calculate the
% average value at that location; center_average
% center_mask -> (n x m double) A mask over the map that selects only
% the points centered at the center of gravity within an
n% area covered by a center rectangle

```

```

% Example
if 0
    map = round(20*randn(40,10));
    xValues = linspace(1,10,10)'; yValues = linspace(1,200,40)';
    center_rectangle_size = [1 10]; %Hz
    [average center_of_gravity standard_deviation] = ...
        computeAreaFeatures( map, xValues, yValues, center_radius)
end

% average -----
average = mean(map(:));

% centroid -----
xHist = sum( map,1 )';
yHist = sum( map,2 );
center_of_gravity(1) = sum( xHist .* xValues ) / sum(xHist);
center_of_gravity(2) = sum( yHist .* yValues ) / sum(yHist);

% Vector location that best matches center of gravity
if isnan( center_of_gravity )
    location = [NaN NaN]';
else
    df = abs( center_of_gravity(1) - xValues );
    location(1) = find( df == min(df) );
    df = abs( center_of_gravity(2) - yValues );
    location(2) = find( df == min(df) );
end

% centroid average
xMask = ( xValues >= center_of_gravity(1) - center_rectangle_size(1)/2 )...
    & ( xValues <= center_of_gravity(1) + center_rectangle_size(1)/2 );
yMask = ( yValues >= center_of_gravity(2) - center_rectangle_size(2)/2 )...
    & ( yValues <= center_of_gravity(2) + center_rectangle_size(2)/2 );
center_mask = { xMask, yMask };
% Locations for x and y swapped when using it in the map matrix
samples = map( yMask, xMask );
center_average = mean( samples(:) );

% standard deviation -----

% Map slices at that location
if isnan( center_of_gravity )
    standard_deviation = [NaN NaN]';
else
    xSlice = map( location(2) ,: )'; % Row slice using the right y coordinate.
    ySlice = map(:,location(1)); % Column slice using the right x coordinate.

    %Take absolute values of slices
    xSlice = abs(xSlice);
    ySlice = abs(ySlice);

```

```

        standard_deviation(1) = stdFromHistogram( xSlice, xValues );
        standard_deviation(2) = stdFromHistogram( ySlice, yValues );
end

end % EOF

```

## 7.3. Windowed spectra and signal power

Written in the Matlab language.

```

function out = serialPower( SIG, settings )
% *** ATTENTION *** If using this with normalization of signals make sure
% line noise has been removed.
% Finds the power of a signal as an average spectral power or mean squared
% value using a variety of settings that allow for windowing.
%
% Dependencies
% matlab signal processing toolbox
%
% Input variables -----
%
% SIG                                -> (n1 x m double) Column-wise signals.
%                                Coherence is taken between these signals
%                                and SIG2 according to settings.SignalsMask
% settings.SignalsMask                -> (n1 x n2 boolean) Indicates the pairs
%                                between the two signal sets to calculate
%                                coherence for.
% settings.Blocks                    -> (n x 2 double) Blocks that indicate the
%                                first and last sample of a segment to
%                                analyse in the first and second columns
%                                respectively
% settings.Fs                        -> (double) Sampling frequency
% settings.FilterOrder                -> (double) When calculating RMS, filter the
%                                data using this filter order
% settings.NotchFilterOrder          -> (double) When calculating RMS, remove
%                                ranges in settings.NoiseBandToExclude with
%                                a filter of this order
% settings.NortchFilterQFactor        -> (double) The Q factor of the notch filters.
% settings.NW                        -> (double) The more tapers the less variance
%                                in the data but freq. resolution decreases.
% settings.PWelchWindowLength        -> (double) In number of samples. Don't
%                                confuse with settings.WindowLength.
%                                PWelchWindowLength is for the windows that
%                                will be taken within the other windows to
%                                estimate the FFT. For example, if n is 2^11
%                                it yields fft of size 2048/2 + 1 = 1025.
%                                Thus for Fs range is [0 Fs/2] = [0 1200]
%                                the sampling resolution is 1200/1025 =

```

```

% 1.17 Hz.
% settings.PWelchWindowOverlap -> (double) In number of samples. Overlap of
%                               PWelch windows. By default Matlab uses half
%                               the window length.
% settings.NormalizeBlocks      -> (boolean) Whether to normalize each block.
% settings.NormalizeSignals     -> (boolean) Each signal's average becomes 0
%                               and standard deviation 1.
% settings.ShowProgress         -> (boolean) Choose to output progress
%                               information in the command line.
% settings.WindowLength        -> (double) The number of samples in each
%                               windowed segment
% settings.WindowStep           -> (double) The number of samples between two
%                               consecutive windows
% settings.UseTruncation        -> (boolean) Whether to allow truncatio of
%                               signals
% settings.Truncation           -> (double) Amount of truncation of the
%                               signals at their beginning and end before
%                               any windowing or coherence calculations
%                               take place as a proportion of the signal
%                               length
% settings.Bands                -> (n x 2 double) Contains the band ranges to
%                               use when extracting average coherence
%                               across frequency ranges.
% settings.NoiseBandToExclude   -> (n x 2 double) These frequency bands will
%                               be excluded from the analysis even if they
%                               are contained within settings.Bands
% settings.SaveData             -> (boolean) Whether to save the results
% settings.Title                -> (n x 1 char) The title of the file in which
%                               the results are to be saved
% settings.Directory            -> (n x 1 char) The directory in which to save
%                               the file (do not include '/' or '\' in the
%                               end)
% settings.Preallocate         -> (boolean) When true, the output is
%                               prepopulated with zeros. However, this can
%                               lead to extra zeros when blocks have
%                               different number of windows
% settings.KeepSpectra         -> (boolean) When true, the spectra are put in
%                               the output. This vastly increases the data
%                               returned.
% settings.KeepAveSpectra      -> (boolean) When true, for each block the
%                               average spectrum across windows is returned
%                               in out.AveSpectrumPmtm/PWelch. Do not
%                               confuse this with
%                               out.AveSpectralPowerPmtm/PWelch which
%                               averages across frequency ranges and not
%                               windows
%
% Hidden settings - set in the script -----
% settings.PmtmNfft             -> (double) The length of the fft, should be a
%                               power of 2. Leave empty to let matlab
%                               decide based on PWelchWindowLength.
% settings.PWelchNfft           -> (double) Length of fft when using PWelch.
%                               If empty, matlab sets this to a power of 2
%                               at least as long as the PWelch window
%                               length. Don't set this to avoid datawrap
%                               when nfft is smaller than the data
%

```

```

% Input variables -----
%
% out.MS          -> (is x ib x iw cell) x (m x 1 double)
%                  (SIG x SIG2 x block x window ) (coherence)
%                  Contains the main results
% out.AveSpectralPowerPmtm -> (is x ib x iw cell) x (power)
%                  (SIG x block x window ) (average band
%                  coherence) Instead of coherence values for
%                  each frequency it contains only the average
%                  band values. There are as many values in
%                  each windows as there are band ranges
%                  defined in settings.Bands
% out.AveSpectralPowerPWelch -> (is x ib x iw cell) x (power) ( SIG x block
%                  x window) (average band power)
% out.PWelchFreq    -> (n x 1 double) Frequencies for each power
%                  value in each window using the pwelch()
%                  method for spectra
% out.PmtmFreq      -> (n x 1 double) Frequencies for each power
%                  value in each window using the pmtm()
%                  method to get the spectra
% out.SpectraPmtm   -> (is x ib x iw cell) x (n x 1 double) The
%                  computed spectra. These are never
%                  preallocated to ensure there are not any
%                  spectra with zeros.
% out.SpectraPWelch -> (is x ib x iw cell)
% out.AveSpectraPmtm -> (is x ib cell) x (n x 1 double) Average
%                  spectrum for each block across windows.
%                  *** ATTENTION *** Not an average across
%                  frequencies as in out.AveSpectralPowerPmtm
% out.AveSpectraPWelch -> (is x ib cell) x (n x 1 double)

% Example
if 0
    Fs = 2400; %in Hz
    SIG = randn(3*60*Fs,5); % Random signals 3 minutes long with 5 channels
    B = [1/Fs 30; 30 60; 60 120] * Fs; % Three blocks
    settings = struct( ...
        'Fs', Fs,...
        'FilterOrder', 8,...
        'NotchFilterOrder', 6,...
        'NotchFilterQFactor', 60,...
        'SignalsMask', ones(1,5),...
        'Blocks', B,...
        'BlocksMask', [1 1 0],...
        'NW', 5,...
        'PWelchWindowLength', 2^11,...
        'PWelchWindowOverlap', (2^11)/2,...
        'NormalizeBlocks', false,...
        'NormalizeSignals', true,...
        'ShowProgress', true,...
        'WindowLength', Fs * 6,...
        'WindowStep', Fs * 6,...
        'UseTruncation', true,...
        'Truncation', 0.02,...
        'Bands', [4 12; 12 20; 20 35; 35 80; 80 150],...
        'NoiseBandsToExclude', [60-3, 60+3; 120-3, 120+3; 180-3, 180+3; ],...
        'SaveData', true,...

```

```

        'Title',                'signal_power',...
        'Directory',            pwd,...
        'Preallocate',          false,...
        'KeepSpectra',          false,...
        'KeepAveSpectra',       false    );
    out = serialPower( SIG, settings );
end

% -----
% -----

% Private settings
settings.PmtmNfft    = []; % Default value
settings.PWelchNfft = [];

% Default settings if value not provided
defaultSettings = struct ( ...
    'FilterOrder',        8,...
    'NotchFilterOrder',   6,...
    'NotchFilterQFactor', 60,...
    'PWelchNfft',         [],...
    'PmtmNfft',           [],...
    'PWelchWindowLength', [],... % 8 windows
    'PWelchWindowOverlap', [],... % 50% overlap
    'NormalizeBlocks',    false,...
    'NormalizeSignals',   true,...
    'ShowProgress',       true,...
    'UseTruncation',       true,...
    'Truncation',          0.2,...
    'SaveData',            true,...
    'Title',               'coh_example',...
    'Directory',            pwd,...
    'Preallocate',          false,...
    'KeepSpectra',          false,...
    'KeepAveSpectra',       false    );

% Set default values when empty or '' -----
% -----
if (~isfield(settings, 'FilterOrder') || ...
    isempty(settings.FilterOrder)), settings.FilterOrder =...
    defaultSettings.FilterOrder; end
if (~isfield(settings, 'NotchFilterOrder') || ...
    isempty(settings.NotchFilterOrder)), settings.NotchFilterOrder =...
    defaultSettings.NotchFilterOrder; end
if (~isfield(settings, 'NotchFilterQFactor') || ...
    isempty(settings.NotchFilterQFactor)), settings.NotchFilterQFactor =...
    defaultSettings.NotchFilterQFactor; end
if (~isfield(settings, 'PmtmNfft') || ...
    isempty(settings.PmtmNfft)), settings.PmtmNfft =...
    defaultSettings.PmtmNfft; end
if (~isfield(settings, 'PWelchNfft') || ...
    isempty(settings.PWelchNfft)), settings.PWelchNfft =...
    defaultSettings.PWelchNfft; end
if (~isfield(settings, 'PWelchWindowLength') || ...
    isempty(settings.PWelchWindowLength)), settings.PWelchWindowLength =...
    defaultSettings.PWelchWindowLength; end
if (~isfield(settings, 'PWelchWindowOverlap') || ...
    isempty(settings.PWelchWindowOverlap)), settings.PWelchWindowOverlap =...
    defaultSettings.PWelchWindowOverlap; end

```

```

        isempty(settings.PWelchWindowOverlap)), settings.PWelchWindowOverlap =...
        defaultSettings.PWelchWindowOverlap; end
if (~isfield(settings, 'NormalizeBlocks') || ...
    isempty(settings.NormalizeBlocks)), settings.NormalizeBlocks =...
    defaultSettings.NormalizeBlocks; end
if (~isfield(settings, 'NormalizeSignals') || ...
    isempty(settings.NormalizeSignals)), settings.NormalizeSignals =...
    defaultSettings.NormalizeSignals; end
if (~isfield(settings, 'ShowProgress') || ...
    isempty(settings.ShowProgress)), settings.ShowProgress =...
    defaultSettings.ShowProgress; end
if (~isfield(settings, 'UseTruncation') || ...
    isempty(settings.UseTruncation)), settings.UseTruncation =...
    defaultSettings.UseTruncation; end
if (~isfield(settings, 'Truncation') || ...
    isempty(settings.Truncation)), settings.Truncation =...
    defaultSettings.Truncation; end
if (~isfield(settings, 'SaveData') || ...
    isempty(settings.SaveData)), settings.SaveData =...
    defaultSettings.SaveData; end
if (~isfield(settings, 'Title') || ...
    isempty(settings.Title)), settings.Title =...
    defaultSettings.Title; end
if (~isfield(settings, 'Directory') || ...
    isempty(settings.Directory)), settings.Directory =...
    defaultSettings.Directory; end
if (~isfield(settings, 'Preallocate') || ...
    isempty(settings.Preallocate)), settings.Preallocate =...
    defaultSettings.Preallocate; end
if (~isfield(settings, 'KeepSpectra') || ...
    isempty(settings.KeepSpectra)), settings.KeepSpectra =...
    defaultSettings.KeepSpectra; end
if (~isfield(settings, 'KeepAveSpectra') || ...
    isempty(settings.KeepAveSpectra)), settings.KeepAveSpectra =...
    defaultSettings.KeepAveSpectra; end

```

% Length variables -----

```

ns1      = size( SIG, 2 ); % Number of contacts.
nb       = size( settings.Blocks,1); % Number of blocks.
nIncBands = size( settings.Bands,1); % Number of included frequency bands
nExcBands = size( settings.NoiseBandsToExclude,1);

```

% Windowing -----

```

% Estimating number of windows for preallocation of results based
% on the first block.
win_step      = round(settings.WindowStep);
idx           = min( find(settings.BlocksMask) );
first_block_length = settings.Blocks(idx, 2) - settings.Blocks(idx,1) + 1;
nWinEst       = numberOfWindows(first_block_length, ...
                                settings.WindowLength, win_step);

```

% PWelchNfft / Power values / Band indexes -----

```

% Nfft is the greatest of 256 or the next power of 2 greater than the length
% of the segment. For example, if the segment length is 2^11 = 2048 then
% nfft = 2048, if length is 2047, nfft = 2048, but if length = 2049, then
% nfft = 2^12 = 4096
% The number of power values is (nfft/2+1) for even nfft, and (nfft+1)/2 for
% odd nfft.
% pmtm() and pwelch() do not segment the data to get a time-frequency
% representation (tfr). Thus we set nfft to be at least as high as the
% segment length. Don't confuse top level windowing to get a TFR with
% windowing involved in Welch's periodogram or the multitapering method.
power = nextpow2(settings.PWelchWindowLength);
if power <= 8, nfft = 2^8; else nfft = 2^power; end
nPow      = nfftToNumOfValues( nfft ); % Number of power values.
freq      = linspace(0,settings.Fs/2,nPow)';
% Locates the indexes of the freq vector that belong to each band. Those are
% used to extract the right power values
% In addition, ensure noise bands are excluded.
PWelchBandIdxs = cell(nIncBands,1);
for ibd = 1 : nIncBands % band
    PWelchBandIdxs{ ibd } = rangesToIdxs( settings.Bands(ibd,1:2), ...
                                           settings.NoiseBandsToExclude, freq );
end

% pwelch() should output the following frequency vector.
out.PWelchFreq = freq;

% Pmtm Band Indexes -----
power = nextpow2(settings.WindowLength);
if power <= 8, nfft = 2^8; else nfft = 2^power; end
nPow      = nfftToNumOfValues( nfft );
freq      = linspace(0,settings.Fs/2,nPow)';
PmtmBandIdxs = cell(nIncBands,1);
for ibd = 1 : nIncBands % band
    PmtmBandIdxs{ ibd } = rangesToIdxs( settings.Bands(ibd,1:2), ...
                                           settings.NoiseBandsToExclude, freq );
end

% pmtm() should ouput the following frequency vector
out.PmtmFreq = freq;

% Preallocate space -----
if settings.Preallocate
    for is = 1:ns1 % signal
        if settings.SignalsMask(is) == 0, continue; end
        for ib = 1:nb % block
            if settings.BlocksMask(ib) == 0, continue; end
            for iw = 1:nWinEst % window
                out.MS{ is, ib, iw } = zeros( nIncBands, 1 );
                out.AveSpectralPowerPmtm{ is, ib, iw } = zeros( nIncBands, 1 );
                out.AveSpectralPowerPWelch{ is, ib, iw } = zeros( nIncBands, 1 );
            end % window
        end % block
    end % signal
end

```



```

% design includeFilters -----
% Constructs bandpass as well as bandstop filters

includeFilters = cell(nIncBands,1);
for n = 1 : nIncBands % band
    % Input arguments: filter order, first passband freq.,
    % second passband freq., passband ripple (dB), sampling frequency
    h = fdesign.bandpass('n,fp1,fp2,ap', ...
        settings.FilterOrder, ...
        settings.Bands(n,1), ...
        settings.Bands(n,2), ...
        1, ...
        settings.Fs);
    Hbp = design( h, 'cheby1', 'SOSScaleNorm', 'Linf');
    set( Hbp, 'PersistentMemory', true);
    includeFilters{ n } = Hbp;
end % band

excludeFilters = cell(nExcBands,1);
for n = 1 : nExcBands % band
    h = fdesign.notch( 'N,F0,Q', ...
        settings.NotchFilterOrder, ...
        mean(settings.NoiseBandsToExclude(n,1:2)), ...
        settings.NotchFilterQFactor, settings.Fs );
    Hn = design(h, 'butter', 'SOSScaleNorm', 'Linf');
    set( Hn, 'PersistentMemory', true);
    excludeFilters{ n } = Hn;
end % band

% Main computations -----

for is = 1 : ns1 % Signal.
    % Skip signal pairs according to mask.
    if settings.SignalsMask(is) == 0, continue, end
    signal = SIG( :, is );
    if settings.NormalizeSignals
        signal = (signal - mean(signal)) ./ std(signal);
    end
    for ib = 1 : nb; % Experimental block.
        % Skip blocks according to mask.
        if settings.BlocksMask(ib) == 0, continue, end
        ticBlock = tic;
        sigBlock = signal( settings.Blocks(ib, 1) : settings.Blocks(ib,2) );

        if settings.UseTruncation % Optional truncation.
            % Length of truncation.
            lt = round( settings.Truncation * length( sigBlock ) );
            sigBlock = sigBlock( lt : end-lt);
        end

        if settings.NormalizeBlocks % Optional normalization of blocks.
            sigBlock = (sigBlock - mean(sigBlock)) ./ std(sigBlock);
        end

        %Window length for this series.

```

```

if settings.WindowLength > length(sigBlock),
    iWinLength = length(sigBlock);
else
    iWinLength = settings.WindowLength; end
% Number of windows for this sigBlock series.
n_win = numberOfWindows(length(sigBlock), iWinLength, win_step);

for iw = 1:n_win % Window -----

    left = 1 + (iw-1) * win_step; % Left limit index.
    right = iWinLength + (iw-1) * win_step; % Right limit index.
    isBlock = sigBlock( left : right ); % sigBlock segment.

    % Pmtm - average spectrum values -----
    [spectrum, ~] = pmtm( isBlock, settings.NW, ...
        settings.PmtmNfft, settings.Fs);
    spectrum = 10.*log10( spectrum );
    % If only settings.KeepAveSpectra is true we'll keep the spectra
    % temporarily until we can calculate the average spectra
    if settings.KeepSpectra || settings.KeepAveSpectra,
        out.SpectraPmtm{ is, ib}{ iw } = spectrum;
    end
    for ibd = 1:nIncBands % band
        out.AveSpectralPowerPmtm{ is, ib, iw }(ibd) = ...
            mean( spectrum( PmtmBandIdxs{ibd} ) );
    end % band

    % PWelch - average spectrum values -----
    [spectrum, ~] = pwelch( isBlock, ...
        settings.PWelchWindowLength, ...
        settings.PWelchWindowOverlap, ...
        settings.PWelchNfft, ...
        settings.Fs);
    spectrum = 10.*log10( spectrum );
    if settings.KeepSpectra || settings.KeepAveSpectra,
        out.SpectraPWelch{ is, ib }{ iw } = spectrum;
    end
    for ibd = 1:nIncBands % Band
        out.AveSpectralPowerPWelch{ is, ib, iw }(ibd) = ...
            mean( spectrum( PWelchBandIdxs{ibd} ) );
    end % band

    % Mean squared values -----
    -----
    for ibd = 1 : nIncBands % Band.
        output = filter( includeFilters{ibd}, isBlock );
        % Check whether any noise band is contained in the current passband
        % and if yes remove it
        for ibdN = 1 : nExcBands % Noise band.
            % Conditions in which the noiseband overlaps with the passband.
            if areOverlapping( settings.NoiseBandsToExclude(ibdN,:), ...
                settings.Bands(ibd,:) )
                % Remove stopband using the saved notch filters.
                output = filter( excludeFilters{ ibdN }, output );
            end
        end
    end
end

```

```

        end % noise band
        out.MS{ is, ib, iw }(ibd) = mean( output.^2 );
    end % band

    end % Window.
    if settings.ShowProgress, disp(['SIG-' num2str(is) ' B-' num2str(ib)...
        ' ' num2str(toc(ticBlock)) ]); end
end % Block.
end % Signal.

if settings.KeepAveSpectra,
    for is = 1 : ns1 % Signal.
        if settings.SignalsMask(is) == 0, continue, end
        for ib = 1 : nb % block
            if settings.BlocksMask(ib) == 0, continue, end
            nWin = length( out.SpectraPmtm{ is, ib } );
            allPmtm = zeros( length( out.PmtmFreq ), nWin );
            allPWelch = zeros( length( out.PWelchFreq ), nWin );
            for iw = 1 : nWin % Window.
                allPmtm(:,iw) = out.SpectraPmtm{ is, ib }{ iw }(:) ;
                allPWelch(:,iw) = out.SpectraPWelch{ is, ib }{ iw }(:) ;
            end % Window.
            out.AveSpectraPmtm{ is, ib } = mean( allPmtm, 2 );
            out.AveSpectraPWelch{ is, ib } = mean( allPWelch, 2 );
        end % Block.
    end % Signal.
end

% Deleting spectra that were only kept so far to calculate average spectra
% across windows i.e. settings.AveSpectraPmtm/PWelch
if ~settings.KeepSpectra
    out.SpectraPmtm = [];
    out.SpectraPWelch = [];
end

if settings.SaveData
    save([settings.Directory '\\' settings.Title], 'settings', 'out');
end

% -----
% Nested functions

%
function nWin = numberOfWindows(signalSize, windowSize, stepSize)
    if length(signalSize)~=1 || length(windowSize)~=1 || length(stepSize)~=1
        error('All inputs should be scalar')
    end
    if (windowSize < signalSize)
        nWin = 1 + floor( (signalSize - windowSize) ./ stepSize);
    else
        nWin = 1;
    end
end
end % EOF

```

```

%
% Given the nfft of a real signal it returns how many values of power we
% should obtain.
function nPow = nfftToNumOfValues( nfft )
    if mod(nfft,2) == 0, nPow = nfft/2 + 1; % nfft is even
    else nPow = (nfft+1)/2; % nfft is odd
    end
end % EOF

%
% Check whether two ranges overlap
function out = areOverlapping( range1, range2 )
    nonOverlapPatterns = [ 3 4 1 2; 1 2 3 4; ]';
    if (range1(1) > range1(2)) || (range2(1) > range2(2)),
        error(['The ranges should be given with the lower value first and '...
            'the higher value second']);
    end
    edges = [ range1(:); range2(:) ];
    [~, ordering] = sort(edges);
    if all( nonOverlapPatterns(:,1) == ordering ) || ...
        all( nonOverlapPatterns(:,2) == ordering ),
        out = false;
    else
        out = true;
    end
end % EOF

%
% Given ranges of frequency values to include and to exclude it returns the
% indexes of where they can be found in the frequency vector
function idxs = rangesToIdxs( includeRanges, excludeRanges, values )
    % includeRanges -> (n x 2 double) Ranges to include. First step
    % excludeRanges -> (n x 2 double) Ranges to exclude. Second step. Thus
    % whatever overlaps with included ranges is excluded.

    nValues = length(values); % Number of values for possible inclusion.
    nIRanges = size(includeRanges,1);
    nERanges = size(excludeRanges,1);
    incRanges = false( nValues,nIRanges ); % Holds include ranges.
    exRanges = false( nValues,nERanges ); % Holds exclude Ranges.
    for ir = 1 : nIRanges % range
        incRanges(:,ir) = values >= includeRanges(ir,1) & ...
            values <= includeRanges(ir,2) ;
    end % Range.
    incRanges = logical( sum( incRanges, 2 ) ); % OR operator for each row.
    for ir = 1 : nERanges % Range.
        exRanges(:,ir) = values >= excludeRanges(ir,1) & ...
            values <= excludeRanges(ir,2) ;
    end % Range.
    exRanges = logical( sum( exRanges, 2 ) );
    idxs = find( incRanges & (~exRanges) ) ; % Use exRanges as a mask. From
                                            % the incRanges ones keep
                                            % only those that have not been
                                            % excluded

end %EOF
end % EOF

```

## 7.4. Time-frequency representation in real time

A software program was implemented in Visual C++ that interfaces with our recording equipment and can generate time-frequency spectra during a recording session. A variety of settings allow the user to adjust the trade-offs between the length of signal to be used for the spectral estimate and how soon the spectra become available. The program accommodates viewing the dynamically generated time-frequency representation for an arbitrary number of channels and devices that is limited by hardware specifications and the particular settings used. For example, a refresh rate of 10 Hz and buffer size of 15 sec. is expected to allow less channels in the same hardware configuration as a refresh rate of 3 Hz and buffer size of 5 sec.

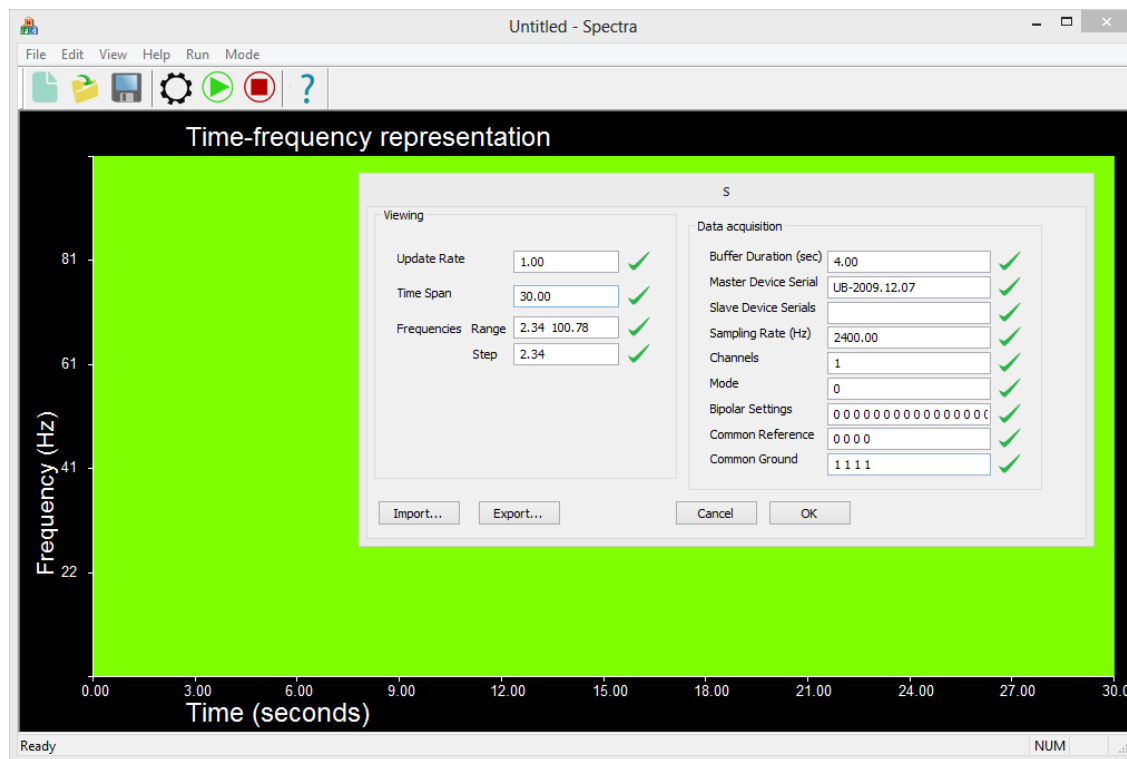


Figure 26.

Figure. Dynamic display of time-frequency representation. Among some of the settings are those that determine the rate at which spectra are computed, the time span to display before spectra start from time 0 again, covering older values are they are generated, the range and resolution of frequencies to display, and the duration of the most recent data provided that is used to find the spectra. The number of channels supported is arbitrary and an equivalent number of axes is provided to support them.

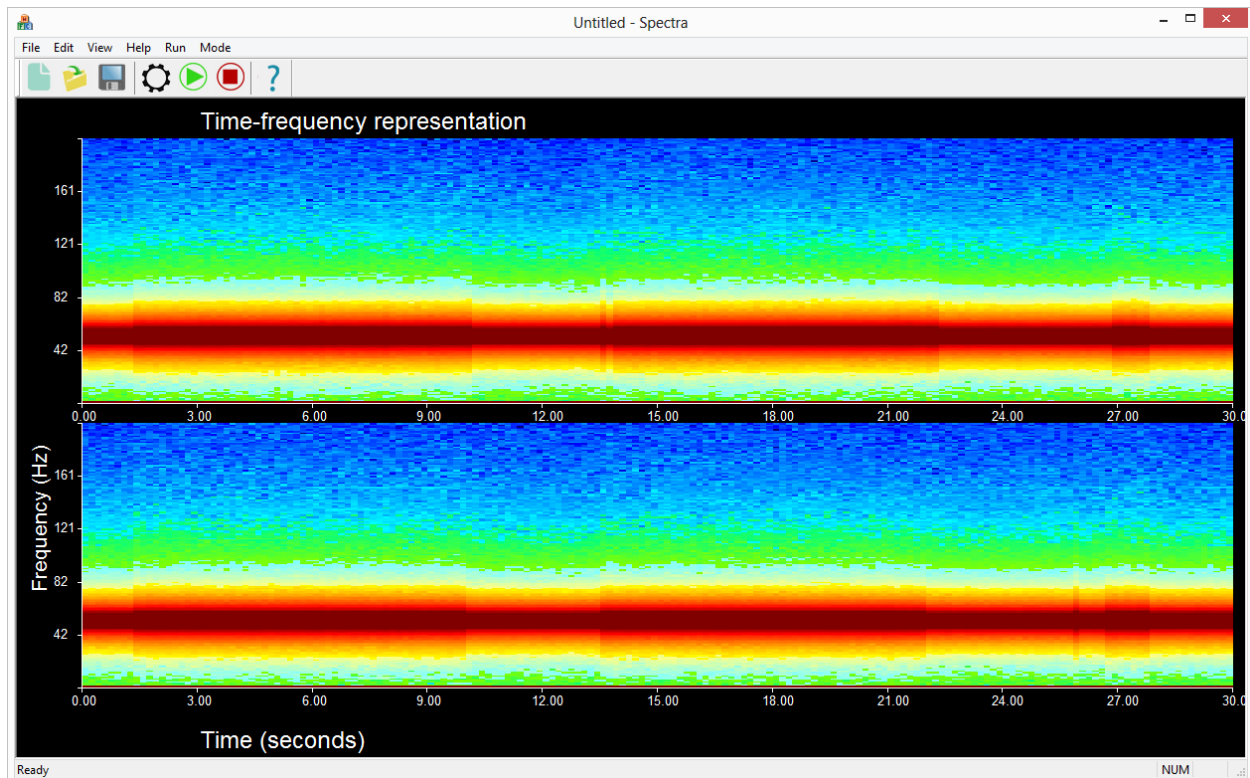


Figure 27.

Time-frequency representation with simulated data. A programmatically generated sinusoid mixed with noise was generated in a separate thread, and fed into the time-frequency generation module to demonstrate the program's use for those without access to the recording equipment. Using our intraoperative recording equipment connected to a sinusoid generator, the program displays the spectra with peaks at the generated frequency and its harmonics. Changing the frequency has almost an immediate effect on the TFR, although it takes as long as the duration of the buffer size to remove the older frequency peak and show the new one, since during that time the buffer contains a fragment of data oscillating in the older frequency and another fragment with the newer frequency.

The time-frequency representation is a collection of objects from a class named CSpectrum. That collection coordinates the time at which each spectrum is computed. The heavily computational part is done by CSpectrum objects. The class's definition and implementation as shown below. It is written using Visual Studio 2005 despite our access to more recent versions in order to comply with requirements of the recording equipment driver.

CSpectrum definition:

```

/*
    CSpectrum class
    Encapsulates a power spectrum. To make this modular it is simply
    associated with a vector of the time series data from which to obtain the
    spectrum and not the TFR.
*/

#pragma once

#include "afx.h"
#include <vector>
#include "math.h"
#include "ffft/FFTReal.h"
using std::vector;
//using std::deque;

template <class T> class CRingBufferODD;
class CTimeFreq;

class CSpectrum {
public: // construct/destruct -----
    CSpectrum( vector<float>* pTimeSeries = &vector<float>(0) ,
               float samplingRate = 0, long nfft = 0);
    virtual ~CSpectrum();

public: // write -----
    void SetTimeSeriesAndCompute(vector<float>* pTimeSeries); //convenience
    function; sets the series and uses all the data in it to compute the spectra
    void SetTimeSeries(vector<float>* timeSeries);
    void SetTimeSeriesRange( UINT* range );
    void SetWindowStep( UINT step );
    void UpdateRange(); //updates the range such that it includes the
    entire time series
    void UpdateNumOfWindows(); //updates m_NumOfWindows in accordance with
    the current range, nfft and window step
    void UpdateFftPowerContainer(); //creates a container that will hold
    fft results; any fft series is used per window
    void UpdateSpectrum(); //computes the spectrum
    void UpdateFft(); //depends on: nfft
    void Update5And95Quantiles(); //updates the 5% and 95% quantiles of
    the average fft powers
    void Update5And95QuantileIdxs(); //update the indices of quantiles;
    depends on nfft

public: // read -----
    vector<float>& GetData() { return m_Data; }
    long GetNfft() { return m_Nfft; }
    float* GetMinMaxData();
    void Get5And95Quantiles( float quantiles[2] );

public: // state -----
    // relations ---
    vector<float>* m_pTimeSeries; //used to compute spectra.
    only values within the range m_TimeSeriesRange are considered
    //composition ---
    UINT m_TimeSeriesRange[2]; //lower and upper
    indices [l,u) of segment to use in computation
    float m_SamplingFrequency;

```

```

        long                m_Nfft;
        long                m_NfftDivBy2;    //simply saves m_Nfft/2
        float*              m_FftSeries;    //will hold fft values; NOT
USED CURRENTLY
        vector< vector<float>*> > m_FftPowersContainer;    //as many power
series in the form of 10log10(abs(fft)) as there are windows;
        UINT                m_NumOfWindows; //according to m_Nfft and
m_TimeSeriesRange
        UINT                m_WinStepSize; //windows are used to estimate
the fft over multiple subregions and then average the result
        fft::FFTReal<float>& m_Fft; //fft object used for computations,
not the result of the transformation
        vector<float>        m_Data;        // values of the spectrum
        float                m_5Quantile;
        UINT                m_5QuantileIdx;
        float                m_95Quantile;
        UINT                m_95QuantileIdx;

protected: // utilities -----
        UINT NumOfWindows(UINT tsSize, UINT winSize, UINT stepSize) {
            if (tsSize >= winSize)
                return 1 + floor( (tsSize - winSize) / (float)stepSize );
            else
                return 0;
        }

};

```

CSpectrum implementation:

```

#include "StdAfx.h"
#include "Spectrum.h"
#include "fftss.h"
#include "TimeFreq.h"
#include <cmath>
#include <algorithm>

// construction/destruction -----
//
CSpectrum::CSpectrum(vector<float>* pTimeSeries,
                    float samplingRate,
                    long nfft ) :
    m_pTimeSeries( pTimeSeries ),
    m_TimeSeriesRange( ),    //updated in body
    m_SamplingFrequency( samplingRate ),
    m_Nfft( nfft ),
    m_NfftDivBy2( nfft/2 ),
    m_FftSeries( new float[nfft] ),
    m_FftPowersContainer( vector< vector<float>*>(0) ),
    //updated in body

```



```

        m_NumOfWindows(    1 ),          //updated in body
        m_WinStepSize(    m_Nfft/2 ),
        m_Fft(             *(new ffft::FFTReal<float>(nfft)) ),
        m_Data(            vector<float>(nfft/2 + 1) ),
        m_5Quantile(       0 ),
        m_5QuantileIdx(    0.15 * (nfft/2) ),
        m_95Quantile(      0 ),
        m_95QuantileIdx(   0.99 * (nfft/2) ) { //each spectrum
will have nfft/2 + 1 frequencies

```

```

        //time series range (indices) - default is that the entire time series
        is included in the range

```

```

        UpdateRange();

```

```

        //window size

```

```

        UpdateNumOfWindows();

```

```

        //a place to save fft powers

```

```

        UpdateFftPowerContainer();      //depends on number of windows

```

```

        /*      //DELETEME - TESTING ONLY

```

```

            float init = 0;

```

```

            for (UINT i = 0; i < m_Data.size(); ++i) {

```

```

                m_Data.at(i) = init;

```

```

                --init;

```

```

            }

```

```

        */

```

```

    }

```

```

    //

```

---

```

    CSpectrum::~CSpectrum() {

```

```

        //

```

```

        delete[] m_FftSeries;

```

```

        m_FftSeries = NULL;

```

```

        //fft power series

```

```

        for (UINT i = 0; i < m_FftPowersContainer.size(); ++i) {

```

```

            delete m_FftPowersContainer.at(i);

```

```

        }

```

```

        m_FftPowersContainer.clear();

```

```

    }

```

```

//write -----

```

```

//

```

---

```

//creates a container that will hold fft results; any fft series is used per
window

```

```

void CSpectrum::UpdateFftPowerContainer() {

```

```

    //delete old

```

```

    for (UINT i = 0; i < m_FftPowersContainer.size(); ++i ) {

```

```

        delete m_FftPowersContainer.at(i);

```

```

    }

```

```

    m_FftPowersContainer.clear();

```

```

    for (UINT i = 0; i < m_NumOfWindows; ++i) {

```

```

        vector<float>* pFftPower = new vector<float>(m_NfftDivBy2 + 1);
        m_FftPowersContainer.push_back( pFftPower ); //didn't use
shared_ptr<float[2048]> because shared_ptr does not call delete[], only
delete
    }
}
//
void CSpectrum::SetTimeSeriesAndCompute( vector<float>* timeSeries ) {
    SetTimeSeries( timeSeries );
    UpdateSpectrum();
}
//
//set a new time series and reset the range to include it all
void CSpectrum::SetTimeSeries( vector<float>* timeSeries) {
    m_pTimeSeries = timeSeries;
    UpdateRange(); //by default range includes all the data
    UpdateNumOfWindows(); //must be called after setting the range
    UpdateFftPowerContainer(); //depends on number of windows
}
//
//set the range and update the number of windows appropriately
void CSpectrum::SetTimeSeriesRange( UINT* range ){
    m_TimeSeriesRange[0] = range[0];
    m_TimeSeriesRange[1] = range[1];
    UpdateNumOfWindows();
}
//
//set the window step and update the number of windows that can fit
void CSpectrum::SetWindowStep( UINT step ) {
    m_WinStepSize = step;
    UpdateNumOfWindows();
}
//
//updates the range such that it includes the entire time series
void CSpectrum::UpdateRange() {
    m_TimeSeriesRange[0] = 0;
    m_TimeSeriesRange[1] = m_pTimeSeries->size();
}
//
//updates m_NumOfWindows in accordance with the current range, nfft and
window step
void CSpectrum::UpdateNumOfWindows() {
    UINT tsSize = m_TimeSeriesRange[1]-m_TimeSeriesRange[0];
    m_NumOfWindows = NumOfWindows( tsSize, m_Nfft, m_WinStepSize );
//number of samples of: time series, window, and window step
}
//
void CSpectrum::UpdateFft() {
    //m_Fft = *( new fft::FFTReal<float>(m_Nfft) );
}
//
// compute the spectrum given the current state of the object
void CSpectrum::UpdateSpectrum() {

    m_Data = vector<float>(m_NfftDivBy2 + 1, 0); // zero out vector;
previous results might exist

```

```

        //Computing average fft  Fft, Powers of fft and vector that holds
multiple fft results (used for averaging ffts to reduce noise)

        vector<float>* pFftPower; //pointer to power series for corresponding
window
        float* f = new float[m_Nfft];

        for (UINT iw = 0; iw < m_NumOfWindows; ++iw) { //window
            float* x = &(m_pTimeSeries->at(0)) + //start of time series
                    m_TimeSeriesRange[0] + //offset by desired
time range
                    iw * m_WinStepSize ; //offset by window step
size

            // *** GETTING FFT ***
            m_Fft.do_fft(f, x);

            //assign into vector to see contents in debugger
            vector<float> deleteme;
            deleteme.assign(f, f + m_Nfft);

            //power of fft
            pFftPower = m_FftPowersContainer[iw];
            (*pFftPower)[0] = f[0];
            (*pFftPower)[m_NfftDivBy2] = f[m_NfftDivBy2];
            //start at 1 since 0 location was set
            for (UINT is = 1; is < m_NfftDivBy2; ++is) {
                (*pFftPower)[is] = 10 * log10( sqrt(
                    pow(f[is],2) +
                    pow(f[m_NfftDivBy2 + is],2
                ) )
            );
        }
    }
    delete f;

    //averaging fft power
    for (UINT is = 0; is < m_Data.size(); ++is) { // sample
        //accumulate
        for (UINT it = 0; it < m_NumOfWindows; ++it) { //temporary fft
            m_Data[is] += m_FftPowersContainer[it]->at(is);
        }
        m_Data[is] /= m_NumOfWindows; // or ... / pAllFft.size()
    }

    Update5And95Quantiles(); //if this is too expensive remove it
}

// read -----
void CSpectrum::Update5And95Quantiles() {
    vector<float> data = m_Data; //copy data to new vector
    std::sort(data.begin(), data.end()); //sort data
    m_5Quantile = data[ m_5QuantileIdx ]; //set 5% quantile
    m_95Quantile = data[ m_95QuantileIdx ]; //set 95% quantile
}

```

```

//return the minimum and maximum values in the current data;
//can be used to determine color ranges when plotting the fft power
float* CSpectrum::GetMinMaxData() {
    float range[2] = { *(min_element(m_Data.begin(), m_Data.end())),
                      *(max_element(m_Data.begin(), m_Data.end()))
    };
    return range;
}
void CSpectrum::Get5And95Quantiles( float quantiles[2] ) {
    quantiles[0] = m_5Quantile;
    quantiles[1] = m_95Quantile;
}

```

## 7.5. Ring buffer optimized for read operations

A custom ring buffer was created to allow for optimal read speeds and was used in the program providing a time-frequency representation in real time. The ring buffer returns a pointer to elements saved sequentially in memory as is a case for a vector, thus it is not necessary to copy data at access time. For this to be possible some restrictions are necessary not present in typical ring buffer implementations.

We show the inner workings by example. Consider a scenario in which the goal is to read up to six elements of most recently added data in a ring buffer but without copying into a new array. Suppose the number of elements that can fit in the buffer is 14, the number of elements that fit in one chunk (chunks can be used for better performance but are not required) is 3 and the maximum number of chunks that can be read sequentially is 2.

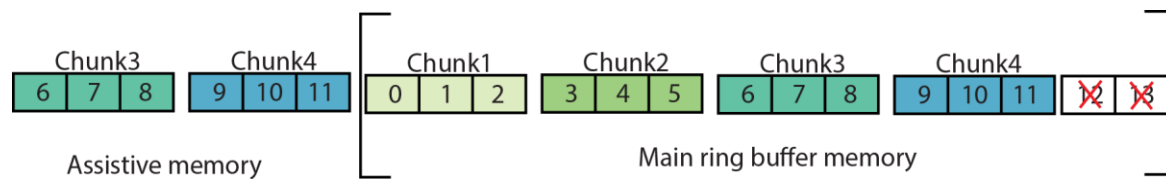


Figure 2811.

A ring buffer that provides access to an uninterrupted sequence of its last received elements. The buffer requires having to use extra memory (the assistive memory segment) and making dual write operations for some elements, both of which depend on the maximum number of last received elements that can be requested. The benefit is being able to simply obtain a pointer to the requested data with the guarantee they are sequential, thus a copy operation at read time is being avoided.

To read data from a typical ring buffer, if the most recent 6 elements were in the first couple chunks (or Chunk2 and Chunk3, or Chunk3 and Chunk4) we would not need to copy that data into a new array but simply return a pointer because the data are guaranteed to be sequential in memory. However if the desired data are in Chunk4 and Chunk1, a pointer is useless; we would need to first

copy it in a new array. The buffer shown resolves this issue by using an assistive memory segment. If the most recent data are in Chunk4 and Chunk1 I simply return a pointer to the beginning of Chunk4 in the assistive memory (on the left). The benefit is reading without making a new array, the penalties is more memory usage and having to write twice into the buffer when reaching the edge of the buffer.

1. Some conditions that could favor the use of the described buffer:  
Sequential memory not too expensive.
2. Read operations request segments relatively small compared to buffer size.
3. Read operations use the data very quickly, otherwise we might as well create a copy of the desired segment to remove the lock on the buffer segment which is needed in multithreading.
4. Read operation are used for copying data into some container. For example, if we want to put it in a vector, we can get the pointer from the buffer and start copying. With a normal ring buffer, we would first copy into an array and copy the array into the container since most containers can't wrap themselves around a pre-existing array (e.g. std:vector).
5. Segments of data have a length that is an integer multiple of some number to allow using chunks for performance increase. This decreases the of processor instructions.

Another example is a scenario in which reading up to six oldest elements added is desired, but without copying into a new array. The concept is the same as explained earlier but this time with the assistive memory segment on the right side of the buffer as shown in the figure.

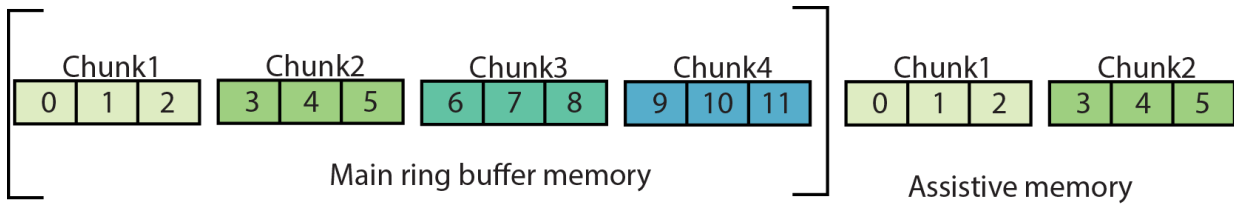


Figure 29.

A ring buffer that provides access to an uninterrupted sequence of its oldest elements. The concept is similar as for the ring buffer optimized for read access of last received elements, with the difference that this one has its assistive memory segment on the right side.

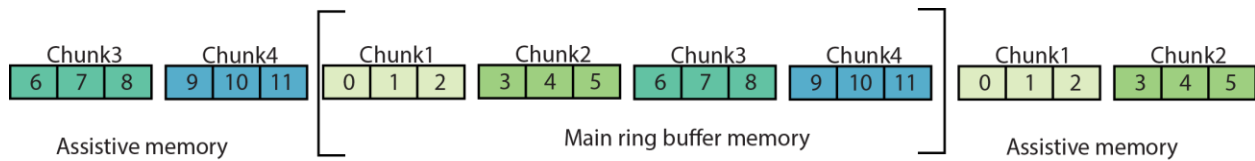


Figure30.

A ring buffer optimized for random access. In this example, retrieval of any two chunks of data can be accomplished simply by providing a pointer to the first element of the first chunk, as they are both guaranteed to be sequential. Note that the extra freedom in selecting segments comes at the cost of having twice as much assistive memory. The assistive memory for this example consists of four chunks.

## 8. Bibliography

Benabid, Alim Louis. "Deep Brain Stimulation for Parkinson's Disease." *Current Opinion in Neurobiology* 13, no. 6 (2003): 696-706.

Bergman, H., A. Feingold, A. Nini, A. Raz, H. Slovin, M. Abeles, and E. Vaadia. "Physiological Aspects of Information Processing in the Basal Ganglia of Normal and Parkinsonian Primates." *Trends in neurosciences* 21, no. 1 (1998): 32-38.

Berke, JD. "Fast Oscillations in Cortical-Striatal Networks Switch Frequency Following Rewarding Events and Stimulant Drugs." *European Journal of Neuroscience* 30, no. 5 (2009): 848-59.

Berns, G.S., and T.J. Sejnowski. "A Computational Model of How the Basal Ganglia Produce Sequences." *Journal of Cognitive Neuroscience* 10, no. 1 (1998): 108-21.

Bernsz, S., and TJ Sejnowskil. "How the Basal Ganglia Make Decisions." (2010).

Brown, P. "Abnormal Oscillatory Synchronisation in the Motor System Leads to Impaired Movement." *Current opinion in neurobiology* 17, no. 6 (2007): 656-64.

Brown, P. "Bad Oscillations in Parkinson's Disease." *Parkinson's Disease and Related Disorders* (2006): 27-30.



Brown, P. "Cortical Drives to Human Muscle: The Piper and Related Rhythms." *Progress in neurobiology* 60, no. 1 (2000): 97-108.

Brown, P. "Oscillatory Nature of Human Basal Ganglia Activity: Relationship to the Pathophysiology of Parkinson's Disease." *Movement disorders* 18, no. 4 (2003): 357-63.

Brown, P., and C.D. Marsden. "Bradykinesia and Impairment of Eeg Desynchronization in Parkinson's Disease." *Movement disorders* 14, no. 3 (1999): 423-29.

Brown, P., P. Mazzone, A. Oliviero, M.G. Altibrandi, F. Pilato, P.A. Tonali, and V. Di Lazzaro. "Effects of Stimulation of the Subthalamic Area on Oscillatory Pallidal Activity in Parkinson's Disease." *Experimental neurology* 188, no. 2 (2004): 480-90.

Brown, P., A. Oliviero, P. Mazzone, A. Insola, P. Tonali, and V. Di Lazzaro. "Dopamine Dependency of Oscillations between Subthalamic Nucleus and Pallidum in Parkinson's Disease." *The Journal of neuroscience* 21, no. 3 (2001): 1033-38.

Brown, P., and D. Williams. "Basal Ganglia Local Field Potential Activity: Character and Functional Significance in the Human." *Clinical Neurophysiology* 116, no. 11 (2005): 2510-19.

Burkhardt, J.M., C. Constantinidis, K.K. Anstrom, D. Roberts, and D.J. Woodward. "Synchronous Oscillations and Phase Reorganization in the Basal Ganglia During Akinesia Induced by High-Dose Haloperidol." *European Journal of Neuroscience* 26, no. 7 (2007): 1912-24.

Canolty, R.T., E. Edwards, S.S. Dalal, M. Soltani, S.S. Nagarajan, H.E. Kirsch, M.S. Berger, N.M. Barbaro, and R.T. Knight. "High Gamma Power Is Phase-Locked to Theta Oscillations in Human Neocortex." *science* 313, no. 5793 (2006): 1626-28.

Canolty, R.T., and R.T. Knight. "The Functional Role of Cross-Frequency Coupling." *Trends in cognitive sciences* 14, no. 11 (2010): 506-15.

Cassidy, M., P. Mazzone, A. Oliviero, A. Insola, P. Tonali, V. Di Lazzaro, and P. Brown. "Movement-Related Changes in Synchronization in the Human Basal Ganglia." *Brain* 125, no. 6 (2002): 1235-46.

Chu Chen, C., A.A. Kühn, T. Trottenberg, A. Kupsch, G.H. Schneider, and P. Brown. "Neuronal Activity in Globus Pallidus Interna Can Be Synchronized to Local Field Potential Activity over 3–12 Hz in Patients with Dystonia." *Experimental neurology* 202, no. 2 (2006): 480-86.

Cruz, A.V., N. Mallet, P.J. Magill, P. Brown, and B.B. Averbeck. "Effects of Dopamine Depletion on Network Entropy in the External Globus Pallidus." *Journal of neurophysiology* 102, no. 2 (2009): 1092-102.

Da Cunha, C., E.C. Wietzikoski, P. Dombrowski, M. Bortolanza, L.M. Santos, S.L. Boschen, and E. Miyoshi. "Learning Processing in the Basal Ganglia: A Mosaic of Broken Mirrors." *Behavioural brain research* 199, no. 1 (2009): 157-70.

de Hemptinne, Coralie, Elena S Ryapolova-Webb, Ellen L Air, Paul A Garcia, Kai J Miller, Jeffrey G Ojemann, Jill L Ostrem, Nicholas B Galifianakis, and Philip A Starr. "Exaggerated Phase–Amplitude Coupling in the Primary Motor Cortex in Parkinson Disease." *Proceedings of the National Academy of Sciences* (2013).

Degos, B., J.M. Deniau, M. Chavez, and N. Maurice. "Chronic but Not Acute Dopaminergic Transmission Interruption Promotes a Progressive Increase in Cortical Beta Frequency Synchronization: Relationships to Vigilance State and Akinesia." *Cerebral Cortex* 19, no. 7 (2009): 1616-30.

Dejean, C., G. Arbuthnott, J.R. Wickens, C. Le Moine, T. Boraud, and B.I. Hyland. "Power Fluctuations in Beta and Gamma Frequencies in Rat Globus Pallidus: Association with Specific Phases of Slow Oscillations and Differential Modulation by Dopamine D1 and D2 Receptors." *The Journal of neuroscience* 31, no. 16 (2011): 6098-107.

Dejean, C., C.E. Gross, B. Bioulac, and T. Boraud. "Dynamic Changes in the Cortex-Basal Ganglia Network after Dopamine Depletion in the Rat." *Journal of neurophysiology* 100, no. 1 (2008): 385-96.

DeLong, M.R., and A.P. Georgopoulos. "Motor Functions of the Basal Ganglia." *Comprehensive Physiology* (2011).

Dostrovsky, J., and H. Bergman. "Oscillatory Activity in the Basal Ganglia—Relationship to Normal Physiology and Pathophysiology." *Brain* 127, no. 4 (2004): 721-22.

Doyle, LMF, AA Kühn, M. Hariz, A. Kupsch, G.H. Schneider, and P. Brown. "Levodopa-Induced Modulation of Subthalamic Beta Oscillations During Self-Paced Movements in Patients with Parkinson's Disease." *European Journal of Neuroscience* 21, no. 5 (2005): 1403-12.

Eusebio, A., and P. Brown. "Synchronisation in the Beta Frequency-Band--the Bad Boy of Parkinsonism or an Innocent Bystander?". *Experimental neurology* 217, no. 1 (2009): 1-3.

Foffani, G., G. Ardolino, M. Egidì, E. Caputo, B. Bossi, and A. Priori. "Subthalamic Oscillatory Activities at Beta or Higher Frequency Do Not Change after High-Frequency Dbs in Parkinson's Disease." *Brain research bulletin* 69, no. 2 (2006): 123-30.

Foffani, G., G. Ardolino, P. Rampini, F. Tamma, E. Caputo, M. Egidì, S. Cerutti, S. Barbieri, and A. Priori. "Physiological Recordings from Electrodes Implanted in the Basal Ganglia for Deep Brain Stimulation in Parkinson's Disease. The Relevance of Fast Subthalamic Rhythms." *Re-Engineering of the Damaged Brain and Spinal Cord* (2005): 97-99.

Foffani, G., A. Priori, M. Egidì, P. Rampini, F. Tamma, E. Caputo, KA Moxon, S. Cerutti, and S. Barbieri. "300-Hz Subthalamic Oscillations in Parkinson's Disease." *Brain* 126, no. 10 (2003): 2153-63.

Frank, M.J. "Hold Your Horses: A Dynamic Computational Role for the Subthalamic Nucleus in Decision Making." *Neural Networks* 19, no. 8 (2006): 1120-36.

Gatev, P. and T. Wichmann (2009). "Interactions between cortical rhythms and spiking activity of single basal ganglia neurons in the normal and parkinsonian state." *Cerebral Cortex* 19(6): 1330-1344.

Gillies, A., and D. Willshaw. "Models of the Subthalamic Nucleus:: The Importance of Intranuclear Connectivity." *Medical engineering & physics* 26, no. 9 (2004): 723-32.

Gobbelé, R., D. Thyerlei, W. Kawohl, H. Buchner, and T.D. Waberski. "Evaluation of Thalamocortical Impulse Propagation in the Akinetic Rigid Type of Parkinson's Disease Using High-Frequency (600 Hz) Sep Oscillations." *Journal of Clinical Neurophysiology* 25, no. 5 (2008): 274.

Goldberg, J.A., U. Rokni, T. Boraud, E. Vaadia, and H. Bergman. "Spike Synchronization in the Cortex-Basal Ganglia Networks of Parkinsonian Primates Reflects Global Dynamics of the Local Field Potentials." *The Journal of neuroscience* 24, no. 26 (2004): 6003-10.

Gustafsson, F. "Determining the Initial States in Forward-Backward Filtering." *Signal Processing, IEEE Transactions on* 44, no. 4 (1996): 988-92.

Hadipour, N.A. "Transmission of the Subthalamic Nucleus Oscillatory Activity to the Cortex: A Computational Approach." *Journal of computational neuroscience* 15, no. 2 (2003): 223.

Hanajima, R., R. Chen, P. Ashby, A.M. Lozano, W.D. Hutchison, K.D. Davis, and J.O. Dostrovsky. "Very Fast Oscillations Evoked by Median Nerve Stimulation in the Human Thalamus and Subthalamic Nucleus." *Journal of neurophysiology* 92, no. 6 (2004): 3171-82.

Humphries, M.D., R.D. Stewart, and K.N. Gurney. "A Physiologically Plausible Model of Action Selection and Oscillatory Activity in the Basal Ganglia." *The Journal of neuroscience* 26, no. 50 (2006): 12921-42.

Hutchison, WD, AM Lozano, RR Tasker, AE Lang, and JO Dostrovsky. "Identification and Characterization of Neurons with Tremor-Frequency Activity in Human Globus Pallidus." *Experimental brain research* 113, no. 3 (1997): 557-63.

Jensen, O., and L.L. Colgin. "Cross-Frequency Coupling between Neuronal Oscillations." *Trends in cognitive sciences* 11, no. 7 (2007): 267-69.

Kane, A., W.D. Hutchison, M. Hodaie, A.M. Lozano, and J.O. Dostrovsky. "Dopamine-Dependent High-Frequency Oscillatory Activity in Thalamus and Subthalamic Nucleus of Patients with Parkinson's Disease." *Neuroreport* 20, no. 17 (2009): 1549.

Kang, G., and MM Lowery. "A Model of Pathological Oscillations in the Basal Ganglia and Deep Brain Stimulation in Parkinson's Disease." 2009.

Klostermann, F., T. Funk, J. Vesper, and G. Curio. "Spatiotemporal Characteristics of Human Intrathalamic High-Frequency (> 400 Hz) Sep Components." *Neuroreport* 10, no. 17 (1999): 3627.

Kühn, A.A., L. Doyle, A. Pogosyan, K. Yarrow, A. Kupsch, G.H. Schneider, M.I. Hariz, T. Trottenberg, and P. Brown. "Modulation of Beta Oscillations in the Subthalamic Area During Motor Imagery in Parkinson's Disease." *Brain* 129, no. 3 (2006): 695-706.

Kühn, A.A., D. Williams, A. Kupsch, P. Limousin, M. Hariz, G.H. Schneider, K. Yarrow, and P. Brown. "Event-Related Beta Desynchronization in Human Subthalamic Nucleus Correlates with Motor Performance." *Brain* 127, no. 4 (2004): 735-46.

Kumar, R., AM Lozano, YJ Kim, WD Hutchison, E. Sime, E. Halket, and AE Lang. "Double-Blind Evaluation of Subthalamic Nucleus Deep Brain Stimulation in Advanced Parkinson's Disease." *Neurology* 51, no. 3 (1998): 850-55.

Lakatos, Peter, George Karmos, Ashesh D Mehta, Istvan Ulbert, and Charles E Schroeder. "Entrainment of Neuronal Oscillations as a Mechanism of Attentional Selection." *science* 320, no. 5872 (2008): 110-13.

Levy, R., W. D. Hutchison, et al. (2002). "Synchronized neuronal discharge in the basal ganglia of parkinsonian patients is limited to oscillatory activity." *The Journal of Neuroscience* 22(7): 2855-2861.

Leblois, A., T. Boraud, W. Meissner, H. Bergman, and D. Hansel. "Competition between Feedback Loops Underlies Normal and Pathological Dynamics in the Basal Ganglia." *The Journal of neuroscience* 26, no. 13 (2006): 3567-83.

Lempka, S.F., S. Miocinovic, M.D. Johnson, J.L. Vitek, and C.C. McIntyre. "In Vivo Impedance Spectroscopy of Deep Brain Stimulation Electrodes." *Journal of neural engineering* 6 (2009): 046001.

Levy, R., P. Ashby, W.D. Hutchison, A.E. Lang, A.M. Lozano, and J.O. Dostrovsky. "Dependence of Subthalamic Nucleus Oscillations on Movement and Dopamine in Parkinson's Disease." *Brain* 125, no. 6 (2002): 1196-209.

Llinás, R.R., U. Ribary, D. Jeanmonod, E. Kronberg, and P.P. Mitra. "Thalamocortical Dysrhythmia: A Neurological and Neuropsychiatric Syndrome Characterized by Magnetoencephalography." *Proceedings of the National Academy of Sciences* 96, no. 26 (1999): 15222.

López-Azcárate, J., M. Tainta, M.C. Rodríguez-Oroz, M. Valencia, R. González, J. Guridi, J. Iriarte, et al. "Coupling between Beta and High-Frequency Activity in the Human Subthalamic Nucleus May Be a Pathophysiological Mechanism in Parkinson's Disease." *The Journal of neuroscience* 30, no. 19 (2010): 6667-77.



Lopiano, L., M. Rizzone, B. Bergamasco, A. Tavella, E. Torre, P. Perozzo, MC Valentini, and M. Lanotte. "Deep Brain Stimulation of the Subthalamic Nucleus: Clinical Effectiveness and Safety." *Neurology* 56, no. 4 (2001): 552-54.

Magill, P.J., J.P. Bolam, and M.D. Bevan. "Relationship of Activity in the Subthalamic Nucleus–Globus Pallidus Network to Cortical Electroencephalogram." *The Journal of neuroscience* 20, no. 2 (2000): 820-33.

Magill, P.J., A. Sharott, J.P. Bolam, and P. Brown. "Delayed Synchronization of Activity in Cortex and Subthalamic Nucleus Following Cortical Stimulation in the Rat." *The Journal of physiology* 574, no. 3 (2006): 929-46.

Mallet, N., A. Pogosyan, L.F. Márton, J.P. Bolam, P. Brown, and P.J. Magill. "Parkinsonian Beta Oscillations in the External Globus Pallidus and Their Relationship with Subthalamic Nucleus Activity." *The Journal of neuroscience* 28, no. 52 (2008): 14245-58.

Mallet, N., A. Pogosyan, A. Sharott, J. Csicsvari, J.P. Bolam, P. Brown, and P.J. Magill. "Disrupted Dopamine Transmission and the Emergence of Exaggerated Beta Oscillations in Subthalamic Nucleus and Cerebral Cortex." *The Journal of neuroscience* 28, no. 18 (2008): 4795-806.

Masimore, B., N.C. Schmitzer-Torbert, J. Kakalios, and A. David Redish. "Transient Striatal [Gamma] Local Field Potentials Signal Movement Initiation in Rats." *Neuroreport* 16, no. 18 (2005): 2021.

McAuley, JH. "The Physiological Basis of Clinical Deficits in Parkinson's Disease." *Progress in neurobiology* 69, no. 1 (2003): 27-48.

Miocinovic, S., J. Zhang, W. Xu, G.S. Russo, J.L. Vitek, and C.C. McIntyre. "Stereotactic Neurosurgical Planning, Recording, and Visualization for Deep Brain Stimulation in Non-Human Primates." *Journal of neuroscience methods* 162, no. 1-2 (2007): 32-41.

Noori, H.R., and W. Jäger. "Neurochemical Oscillations in the Basal Ganglia." *Bulletin of mathematical biology* 72, no. 1 (2010): 133-47.

Paradiso, G., D. Cunic, J.A. Saint-Cyr, T. Hoque, A.M. Lozano, A.E. Lang, and R. Chen. "Involvement of Human Thalamus in the Preparation of Self-Paced Movement." *Brain* 127, no. 12 (2004): 2717-31.

PRIORI, A. "The Effects of Levodopa and Ongoing Deep Brain Stimulation on Subthalamic Beta Oscillations in Parkinson's Disease." *Movement disorders* 26, no. Suppl. 2 (2011): S269-S69.

Priori, A., G. Foffani, A. Pesenti, A. Bianchi, V. Chiesa, G. Baselli, E. Caputo, et al. "Movement-Related Modulation of Neural Activity in Human Basal Ganglia and Its L-Dopa Dependency: Recordings from Deep Brain Stimulation Electrodes in Patients with Parkinson's Disease." *Neurological Sciences* 23 (2002): 101-02.

Ray, NJ, N. Jenkinson, S. Wang, P. Holland, JS Brittain, C. Joint, JF Stein, and T. Aziz. "Local Field Potential Beta Activity in the Subthalamic Nucleus of Patients with Parkinson's Disease Is Associated with Improvements in Bradykinesia after Dopamine and Deep Brain Stimulation." *Experimental neurology* 213, no. 1 (2008): 108-13.

Rivlin-Etzion, Michal, Odeya Marmor, Gali Heimer, Aeyal Raz, Asaph Nini, and Hagai Bergman. "Basal Ganglia Oscillations and Pathophysiology of Movement Disorders." *Current opinion in neurobiology* 16, no. 6 (2006): 629-37.

Rouse, AG, SR Stanslaski, P. Cong, RM Jensen, P. Afshar, D. Ullestad, R. Gupta, et al. "A Chronic Generalized Bi-Directional Brain–Machine Interface." *Journal of neural engineering* 8 (2011): 036018.

Ryan, L.J. "Lesion of the Subthalamic Nucleus or Globus Pallidus Does Not Cause Chaotic Firing Patterns in Basal Ganglia Neurons in Rats." *Brain research* 873, no. 2 (2000): 263-67.

Salih, F., A. Sharott, R. Khatami, T. Trottenberg, G. Schneider, A. Kupsch, P. Brown, and P. Grosse. "Functional Connectivity between Motor Cortex and Globus Pallidus in Human Non-Rem Sleep." *The Journal of physiology* 587, no. 5 (2009): 1071-86.

Sarnthein, J., and D. Jeanmonod. "High Thalamocortical Theta Coherence in Patients with Parkinson's Disease." *The Journal of neuroscience* 27, no. 1 (2007): 124-31.

Schack, B., N. Vath, H. Petsche, and H.G. Geissler. "Phase-Coupling of Theta-Gamma Eeg Rhythms During Short-Term Memory Processing." *International Journal of Psychophysiology* 44, no. 2 (2002): 143-63.

Sharott, A., P.J. Magill, J.P. Bolam, and P. Brown. "Directional Analysis of Coherent Oscillatory Field Potentials in the Cerebral Cortex and Basal Ganglia of the Rat." *The Journal of physiology* 562, no. 3 (2005): 951-63.

Shi, LH, F. Luo, DJ Woodward, and JY Chang. "Neural Responses in Multiple Basal Ganglia Regions During Spontaneous and Treadmill Locomotion Tasks in Rats." *Experimental brain research* 157, no. 3 (2004): 303-14.

Silberstein, P., A.A. Kühn, A. Kupsch, T. Trottenberg, J.K. Krauss, J.C. Wöhrle, P. Mazzone, et al. "Patterning of Globus Pallidus Local Field Potentials Differs between Parkinson's Disease and Dystonia." *Brain* 126, no. 12 (2003): 2597-608.

Soares, J., M. A. Kliem, et al. (2004). "Role of external pallidal segment in primate parkinsonism: comparison of the effects of 1-methyl-4-phenyl-1, 2, 3, 6-tetrahydropyridine-induced parkinsonism and lesions of the external pallidal segment." *The Journal of Neuroscience* 24(29): 6417-6426.

Sridharan, D., PS Prashanth, and VS Chakravarthy. "The Role of the Basal Ganglia in Exploration in a Neural Model Based on Reinforcement Learning." *International journal of neural systems* 16, no. 2 (2006): 111-24.

Stanslaski, S., P. Afshar, P. Cong, J. Giftakis, P. Stypulkowski, D. Carlson, D. Linde, et al. "Design and Validation of a Fully Implantable, Chronic, Closed-Loop Neuromodulation Device with Concurrent Sensing and Stimulation." *Neural Systems and Rehabilitation Engineering, IEEE Transactions on*, no. 99 (2012): 1-1.

Theunissen, F., and J.P. Miller. "Temporal Encoding in Nervous Systems: A Rigorous Definition." *Journal of computational neuroscience* 2, no. 2 (1995): 149-62.

Tisch, S., P. Silberstein, P. Limousin-Dowsey, and M. Jahanshahi. "The Basal Ganglia: Anatomy, Physiology, and Pharmacology." *Psychiatric Clinics of North America* (2004).

Tort, A.B.L., R. Komorowski, H. Eichenbaum, and N. Kopell. "Measuring Phase-Amplitude Coupling between Neuronal Oscillations of Different Frequencies." *Journal of neurophysiology* 104, no. 2 (2010): 1195-210.

Tort, A.B.L., R.W. Komorowski, J.R. Manns, N.J. Kopell, and H. Eichenbaum. "Theta–Gamma Coupling Increases During the Learning of Item–Context Associations." *Proceedings of the National Academy of Sciences* 106, no. 49 (2009): 20942-47.

Tort, A.B.L., M.A. Kramer, C. Thorn, D.J. Gibson, Y. Kubota, A.M. Graybiel, and N.J. Kopell. "Dynamic Cross-Frequency Couplings of Local Field Potential Oscillations in Rat Striatum and Hippocampus During Performance of a T-Maze Task." *Proceedings of the National Academy of Sciences* 105, no. 51 (2008): 20517-22.

Tsiokos, Christos, Xiao Hu, and Nader Pouratian. "200-300 Hz Movement Modulated Oscillations in the Internal Globus Pallidus of Patients with Parkinson's Disease: 200-300 Hz Movement-Dependent Oscillations in Gpi." *Neurobiology of disease* (2013).

van der Meer, M.A.A., and A.D. Redish. "Low and High Gamma Oscillations in Rat Ventral Striatum Have Distinct Relationships to Behavior, Reward, and Spiking Activity on a Learned Spatial Decision Task." *Frontiers in Integrative Neuroscience* 3 (2009).